CATALYTIC REACTION IN THE PROCESS OF CARBON MONOXIDE DISINTEGRATION

by

Ming-Wei Paul Xu

Dissertation submitted to the Faculty of the
Virginia Polytechnic Institute and State University
in partial fulfillment of the requirements for the degree of

Doctor of Philosophy

in

Materials Engineering Science

APPROVED:

J. J. Brown, Jr., Chairman

G. V. Gibbs

G. Sanzone

J. L. Lytton

J. P. Wightman

May, 1984

Blacksburg, Virginia

CATALYTIC REACTION IN THE PROCESS OF CARBON MONOXIDE DISINTEGRATION

by

Ming-Wei Paul Xu

(ABSTRACT)

The catalytic effects of selected iron phases (metal, oxides, sulfides, and carbides) on the Boudouard reaction ($2\ CO = CO_2 + C$) were studied, in an effort to more fully understand the disintegration of refractories when exposed to CO for long periods of time.

Based on computer generated equilibrium phase maps (SOLGASMIX program), experimental kinetic data including activation energies and x-ray diffraction data of iron phases, the following conclusions were reached:

(1) Ferric oxide (Fe_2O_3) is most catalytic;

(2) Active iron atom generated by the reduction of Fe_2O_3 is a catalyst for carbon monoxide disintegration;

(3) The catalytic process consists of the adsorption of CO, the formation of intermediates FeC, Fe_2C, and Fe_3C, and the decomposition of these intermediates.

ACKNOWLEDGEMENTS

The author wishes to express his sincere appreciation and respect to the chairman of his Graduate Committee, Dr. J. J. Brown, Jr. for his support and invaluable guidance, which is the key to the completion of the author's M.S. and Ph.D. programs within two and one-half years. He also appreciates Dr. , Head of Department of Materials Engineering, Virginia Polytechnic Institute and State University for his support and concern.

The author wishes to express thanks to his members of Graduate Committe, Dr. G. V. Gibbs, Dr. J. L. Lytton, Dr. G. Sanzone and Dr. J. P. Wightman for their careful correction of his dissertation and giving valuable advice.

The author would also like to acknowledge:

(1) Dr. , Oakridge National Laboratory, for sending SOLGASMIX program and giving some instructions.

(2) Dr. , Medical College of Georgia, for his encouragement, concern and instructions.

(3) Mr. , , Mr. for helping him to run all X-ray diffraction tests.

(4) The secretarial staff of Department of Materials Engineering, especially Mrs. and Mrs.

, for the many favors done for me within these two and one-half years.

Finally, the author would like to thank his wife,

, for giving him various supports from the other side of the Pacific Ocean.

Part of this investigation was sponsored by Department of Energy.

TABLE OF CONTENTS

LIST OF FIGURES

LIST OF FIGURES (cont'd)

LIST OF FIGURES (cont'd)

LIST OF FIGURES (cont'd)

LIST OF TABLES

I. INTRODUCTION

The disintegration of carbon monoxide to carbon and carbon dioxide, the so-called Boudouard reaction, has been studied for more than a century. Ceramists are concerned with this reaction because carbon deposited on iron impurities, primarily in fireclay brick, may crack furnace linings. Such damage usually occurs in blast furnaces, furnaces for coal gasification, etc. Recently, renewed interest in carbon deposition on catalytic metals has arisen in the petroleum/petrochemical industry and nuclear industry.[1] In the systhesis of hydrocarbons by the Fisher-Tropsch process, carbon deposition may lead to the deactivation of the catalyst. In the nuclear industry where helium is used for cooling the high temperature reactor, carbon deposited on metal components during operation will lower the heat-transfer coefficient of the metal tube heat exchanger (Carbon monoxide and hydrogen are always impurities in helium). Furthermore, in certain cases, carbon deposition may corrode the walls of the heat exchanger.

The basic characteristics of carbon monoxide disintegration follow:

(1) Catalytic reaction. Although the Boudouard reaction is thermodynamically spontaneous, ΔG (cal/mole) =

-39,810 + 40.87 T , carbon is scarcely deposited in the absence of a catalyst. It has been shown that ferromagnetic metals are the most active catalysts for this reaction and the order of activity is in the sequence Fe > Co > Ni.[2] Also, it was reported that supported ferromagnetic metals possess higher activity for catalysis,[3] e.g. Rh/Al_2O_3 and Rh/SiO_2, etc. are more active than Rh for carbon deposition.[4] Furthermore, the rate of carbon deposition depends on the crystallographic face of the catalyst exposed to the gas.[5]

(2) Temperature range. Berry, et al.[6] pointed out that the dissociation of carbon monoxide in contact with iron oxide occurs essentially in the temperature range of 400 - 700°C , and that the rate of carbon monoxide disintegration varies with temperature, with a maximum rate at ~ 550°C.

(3) Partial pressure of carbon monoxide. Haas, et al.[7] studied the effect of partial pressure of carbon monoxide on the reaction rate. A plot of reaction rate vs. partial pressure of carbon monoxide (p_{CO})is shown in Figure 1 (for quasi-steady state).

(4) Activation of the Boudouard reaction. The amount of carbon deposition not only depends on the catalyst present, reaction temperature, partial pressure of carbon

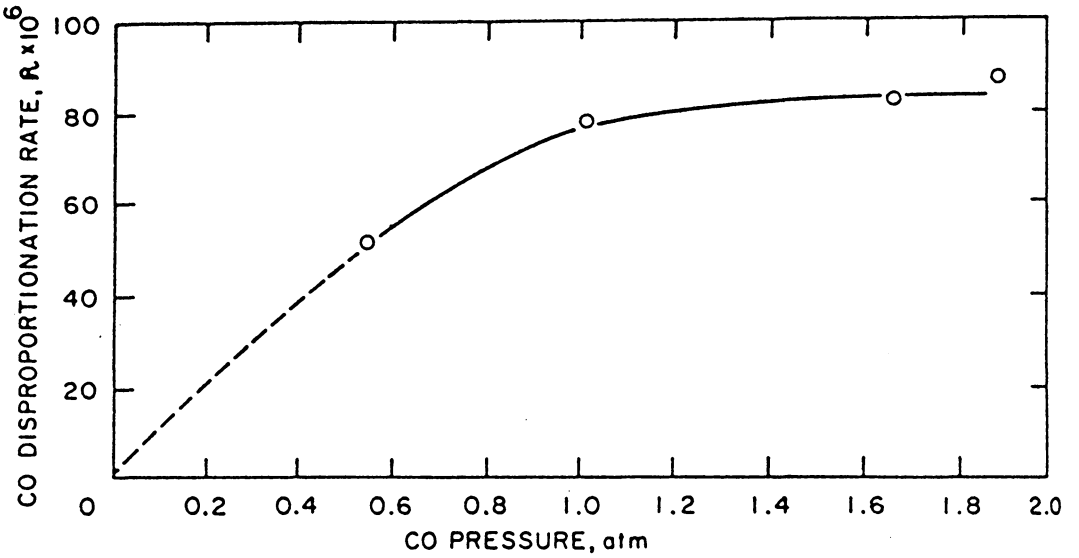

Fig. 1 The Effect of the P_{CO} on the Quasi-Steady State Rate of Carbon Monoxide Dissociation at 500°C (Iron Catalyst)[7]

monoxide, and the flow rate of gas; but also upon the traces of impurities present in either the gas phase or the catalyst. Berry, et al.[6] reported that hydrogen as well as water vapour accelerates carbon deposition. Walker, et al.[8] indicated that the addition of hydrogen to carbon monoxide has a relatively small effect on the maximum deposition rate and the amount of carbon deposit formed at lower temperatures (470 - 528°C). However, at higher temperatures (> 850 K), both rate and amount of carbon deposition increase markedly with increasing hydrogen content to their maximum values, then decreases with further addition.

(5) Poison and reactivation of catalyst. Contrary to the effects of hydrogen and water vapour, the addition of some impurities to either the gas or solid phase inhibits the Boudouard reaction, e.g. a small amount of NH_3 (0.06 vol %) or sulfur in gas suppresses carbon deposition.[6] A poisoned catalyst can be reactivated by adding Zn, ZnO or K_2CO_3 to an iron oxide catalyst.

Despite the presence of much information about carbon monoxide disintegration, the actual physical and chemical nature of this catalytic reaction is still unknown. Probably, the most controversial aspect concerning the reaction is the identity of the actual catalyst.

In 1956, Berry, et al.[6] suggested that iron carbides were the catalyst for carbon monoxide disintegration; for 400 - 565°C, Hägg carbide (Fe_2C) was the catalyst, while for 565 - 700°C cementite (Fe_3C) having an abnormally low Curie temperature range was the catalyst, because X-ray diffraction patterns show that these carbides are always in the sample having carbon deposit. Recently, having studied iron-iron oxide - gas phase diagram, Sacco and Caulmare[9] indicated that carbon deposition could only occur when a carbide was thermodynamically favored.

Emmett, et al.[10] found that Hägg carbide did not chemisorb carbon monoxide at 200°C. As Hagg carbide and cementite have essentially the same ferromagnetic moment, it is expected that their ability for chemisorption should essentially be the same. Therefore, carbon monoxide is not expected to be chemisorbed on Fe_3C at elevated temperature. Walker et al.[8] argued that the loss of catalytic activity of iron was accompanied by a gradual conversion to iron carbides. In addition to Walker's work, Haas, et al.[7] also concluded that metallic iron rather than iron carbides is a catalyst for carbon monoxide disintegration.

Renshaw, et al.[11] suggested that α-Fe_2O_3, a spinel phase, is the catalyst for carbon monoxide disintegration.

Brown and Martin[12] indicated that α-Fe_2O_3 and Fe_3C have the strongest catalytic activity for carbon monoxide disintegration. Other iron compounds and pure α-Fe crystal did not act as catalysts.

All these authors had experimental data to support their viewpoints. Hence, it is probable that these species do have catalytic ability for the Boudouary reaction. Nevertheless, owing to the presence of many simultaneous chemical reactions in the iron phase - carbon monoxide system and the mutual convertions of some species, it is quite difficult to determine which species is the exact catalyst for carbon monoxide dissociation.

The purpose of this work is to explore the catalyst for carbon monoxide disintegration and to study the catalytic process of the reaction. This work consists of the following three parts:

(1) Testing the catalytic effects of selected iron phases (metal, oxides, sulfides, carbides and carbon) on the Boudouard reaction.

(2) Generating the equilibrium phase maps of systems Fe-CO and Fe_2O_3-CO by using SOLGASMIX computer program.

(3) Obtaining the kinetic and X-ray diffraction data from the samples of the most catalytic phases.

II. EXPERIMENTAL PROCEDURES

(1) Sample Preparation.

In this work, two kinds of sample, powder and pellet, were used. Powders were purchased* and pellets were made by the following two different procedures according to the material tested.

(A) Pure α-Fe pellets. Iron pellets (diameter 5.5 mm, thickness 2 mm) were made from iron powder with water as a binder. After being pressed, the pellets were sintered at 1000°C for 6 hours under the protection of flowing nitrogen. X-ray diffraction patterns** showed that the phases present in the sintered smaples were α-Fe and α-Fe_2O_3. In order to secure pure α-Fe, the sintered pellets were further reduced by hydrogen at 450°C for 28 hours in a 1" alumina tube with a hydrogen flow rate of > 50 ml/min. X-ray diffraction patterns showed that the reduced pellets consisted of single phase α-Fe.

---

*Powders were purchased from the following companies:
Fisher Scientific Co. —— ferric oxide (α-Fe_2O_3), ferric-ferrous oxide (Fe_3O_4), granular iron sulfide (FeS) and charcoal;
Cerac. Inc. —— ferrous oxide (FeO, purity > 99.8%);
Alfa Products ——cementite (Fe_3C, -325 mesh).

**All X-ray diffraction patterns were done on Siemens Type F Goniometer.

(B) α-Fe_2O_3 pellets. α-Fe_2O_3 pellets were made from ferric oxide powder with water as a binder. After being pressed, these pellets were sintered in a muffle furnace at 1200°C for 16 hours. X-ray diffraction patterns showed that the phase present in the sintered pellet was single phase α-Fe_2O_3.

(2) Experiments.

(A) Samples were weighed on Mettler AC 100 to an accuracy of 0.1 mg.

(B) Ceramic boats containing sample (either pellet or powder depending on the material used) were placed in a 1¼" tube furnace (Figure 2).

(C) The tube was evacuated to a vacuum higher than 50 millitorr in order to protect the sample from oxidation and fulfill the desorption of adsorbed oxygen and nitrogen on the surface of the sample. For powder samples, Ar was used to protect the sample from oxidation rather than evacuating the tube.

(D) The furnace temperature was raised to the required temperature. Simultaneously, the Vycor tube was evacuated to 20 millitorr.

(E) Carbon monoxide* was introduced at a predetermined flow rate and for a predetermined time.

*Carbon monoxide used is Airco Grade 2.3 (CO > 99.3%).

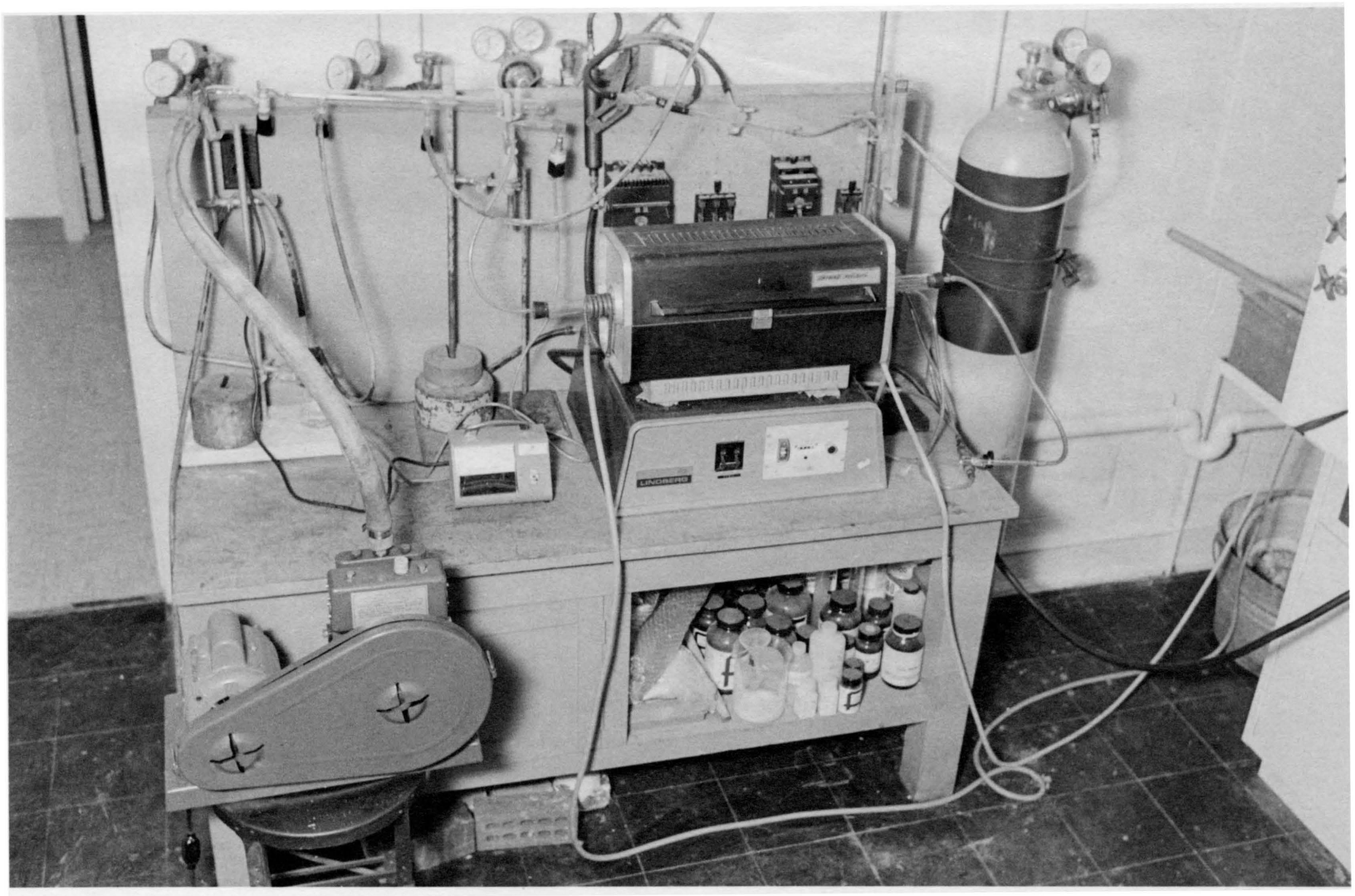

Fig. 2(a) Photograph of the Carbon Deposition Apparatus

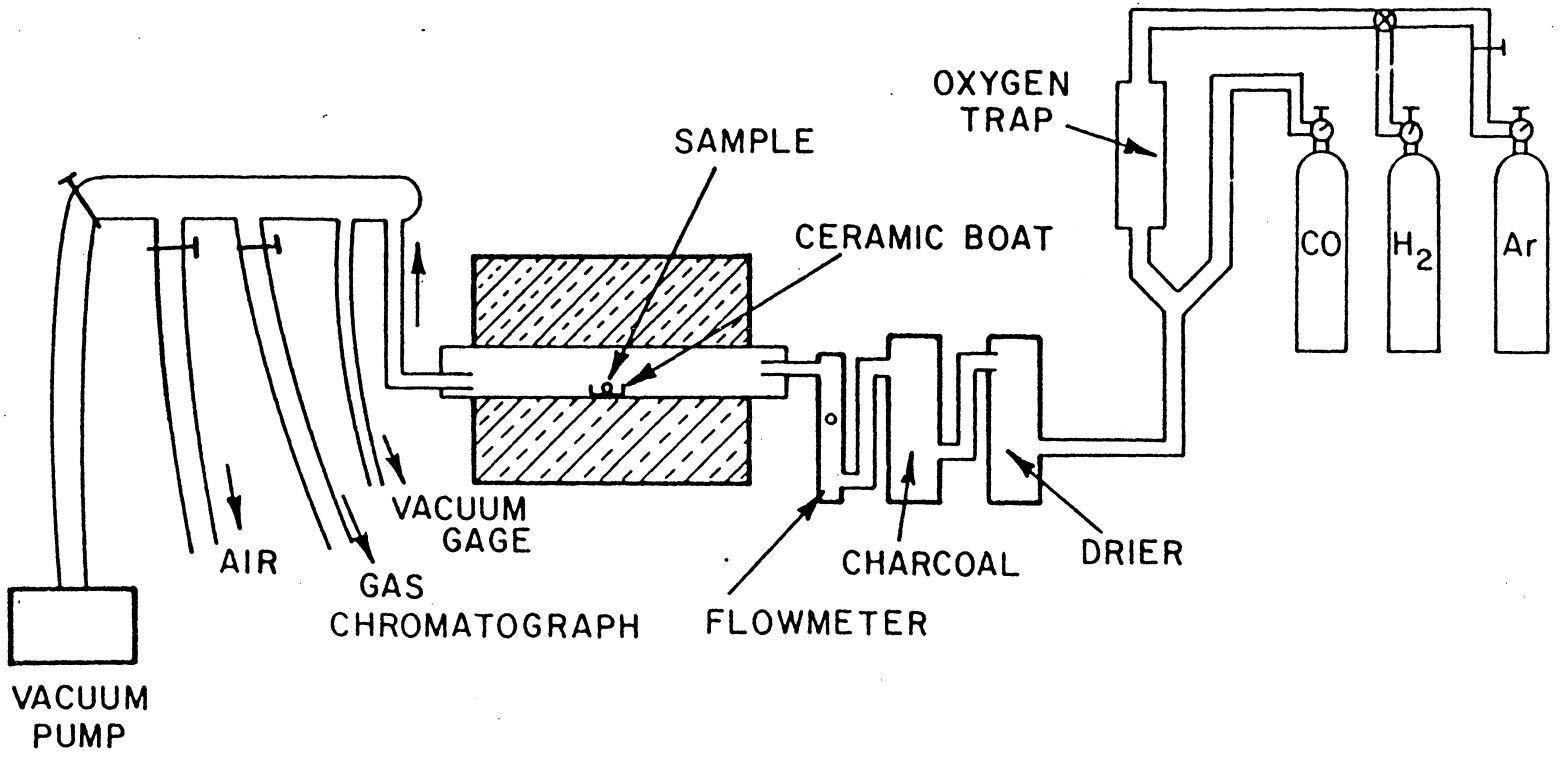

Fig. 2(b) Sketch of Laboratory Equipment for Carbon Deposition

(F) The supply of carbon monoxide was shut off and Vycor tube was flushed with Ar. Meanwhile, the furnace temperature was lowered as fast as possible in order to avoid further reaction.

(G) The sample was reweighed and the weight change was calculated.

(H) X-ray diffraction data were collected, if necessary.

III. RESULTS AND ANALYSIS

(1) The Catalytic Effects of Iron Phases (Pure α-Fe, Iron Oxides, Iron Sulfides, Iron Carbide and Carbon) On Carbon Monoxide Disintegration.

(A) From Table 1, it can be seen that α-Fe_2O_3, Fe_3O_4 and Fe_3C have strong catalytic effects on carbon deposition, while α-Fe crystals, iron sulfides (FeS and FeS_2) and carbon have little catalytic ability.

(B) X-ray diffraction data show that in all samples having graphite, there are FeC, Fe_2C, Fe_3C along with graphite. The appearence of FeC and Fe_2C peaks in these patterns is very important.

(C) There are two possible explanations of the catalytic behavior of α-Fe_2O_3.

(a) CO is directly adsorbed on α-Fe_2O_3 or other iron oxides and disintegrated. It was pointed out[13] that due to the presence of excess oxygen, α-Fe_2O_3 and other oxides (FeO, Fe_3O_4) are p-type semiconductors, which can adsorb carbon monoxide. Also, it was reported[14] that p-type semiconductors can catalyze the oxidation of carbon monoxide according to the following equation

$$CO_{ads} + O_{ads} = CO_2 \qquad (1)$$

Table 1. The Catalytic Effects of Iron Phases on Carbon Deposition.

Sample No.	Specimen	Test Temperature (°C)	Test Time (hr)	Flow Rate of CO (ml/min)	Carbon Deposition	Weight Increment (g/g sample)	Phases Present After Test
1	α-Fe (pellet)	500	5	20	No	0.0005	α-Fe + a little Fe_3O_4
2	α-Fe_2O_3 (pellet)	500	5	20	Yes	1.15	Graphite + Fe(SS) + FeC + Fe_2C + Fe_3C + Fe_3O_4
3	α-Fe_2O_3 (powder) 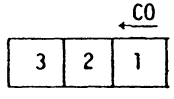 Powder	500	5	35	Yes	0.36824	Part I Graphite + Fe(SS) + FeC + Fe_2C + Fe_3C + Fe_3O_4 + FeO Part II Less G, Fe(SS), Carbide, and more Fe_3O_4 than I Part III Fe_3O_4 + little Fe and Fe_3C

Table 1. The Catalytic Effects of Iron Phases on Carbon Deposition (Continued).

Sample No.	Specimen	Test Temperature (°C)	Test Time (hr)	Flow Rate of CO (ml/min)	Carbon Deposition	Weight Increment (g/g sample)	Phases Present After Test
4	Fe_3O_4 (powder)	500	5	35	Yes	0.3738	Part I Graphite + Fe(SS) + FeC + Fe_2C + Fe_3C + Fe_3O_4 + FeO Part II Less G, Fe(SS), Carbide and more Fe_3O_4 than I Part III Fe_3O_4 + little Fe and Fe_3C
5	FeO (powder)	500	5	35	Yes (a little)		
6	Fe_3C (powder)	500	5	35	Yes	0.2843	Graphite + Fe(SS) + FeC + Fe_2C + Fe_3C
7	FeS (granule)	500	5	35	No	-0.0339	FeS + a little Fe and Fe_3O_4

Table 1. The Catalytic Effects of Iron Phases on Carbon Deposition (Continued).

Sample No.	Specimen	Test Temperature (^{o}C)	Test Time (hr)	Flow Rate of CO (ml/min)	Deposition	Weight Increment (g/g sample)	Phases Present After Test
8	FeS_2 (ore)	500	5	50	No	-0.2561	FeS + β-$Fe_{0.905}$ S
9	charcoal (granule)	500	5	35	No	-0.0664	Graphite

However, there is no report about the catalytic disintegration of carbon monoxide adsorbed on these semiconductors.

(b) Atomic state Fe is a catalyst. Due to the occurrence of Fe and Fe_3O_4 in samples having carbon deposit, another possibility is that α-Fe_2O_3 is first reduced to Fe_3O_4 and Fe, then CO is adsorbed on the reduced Fe and then decomposed. In addition, the reduced iron has a porous structure which has been shown by SEM of reduced Venezuelar ore and sintered Fe_2O_3.[15] The porous surface area of a Venezuelar ore with grain size 2-5 μm diameter after reduction was 14 m^2/g *. The large surface area favors the adsorption of carbon monoxide.

The consecutive processes may be assumed as the following:

$$3Fe_2O_3 + CO = 2Fe_3O_4 + CO_2 \quad (2)$$

$$Fe_3O_4 + 4CO = 3Fe + 4CO_2 \quad (3)$$

$$Fe + CO_{ads} \rightarrow (Fe...CO)^{\ddagger} \quad (4)$$

(activated complex **)

---

*The surface area of this porous structure was measured by BET method from N_2 adsorption at -195°C.

**According to transition state theory, the formation of activated complex is possible. However, there is no experimental evidence to verify the existance of such complexes.

$$(Fe...CO)^{\ddagger} \rightarrow FeC + O \quad (5)$$

$$O \xrightarrow{CO} CO_2$$

$$2FeC \rightarrow Fe_2C + \text{Graphite} \quad (6)$$

$$3Fe_2C \rightarrow 2Fe_3C + \text{Graphite} \quad (7)$$

$$Fe_3C \rightarrow 3Fe + \text{Graphite} \quad (8)$$

By comparing the phases existing in the α-Fe_2O_3 sample (sample No. 2 in Table 1) and the species listed in reactions (2) - (8), it is seen that both have the same phases Fe(ss), Fe_3O_4, FeC, Fe_2C, Fe_3C and G; therefore, it is reasonable that reduced Fe is a catalyst for carbon monoxide disintegration.

(D) The catalytic behavior of Fe_3C can also be explained by using the idea of atomic Fe. Because Fe_3C is a metastable carbide, it may decompose to Fe and C during carbon monoxide dissociation test. This decomposed Fe has the same function of reduced Fe, thus can catalyze carbon deposition.

In order to identify the decomposition of Fe_3C in the condition of carbon monoxide disintegration test, Fe_3C was heated in Ar at 1 atom, 500°C. The results are shown in Table 2. X-ray diffraction patterns showed strong peaks

Table 2. The Results of Heating Fe_3C in Ar Flow.

Sample No.	Specimen	Test Temperature (^oC)	Test Time (hr)	Phases After Test
10	Fe_3C (powder)	500	5	Fe + Fe_3C + Graphite
11	Fe_3C (powder)	500	9	Fe + Fe_3C + Graphite

of α-Fe after heating. The decomposed Fe plays the same role for carbon monoxide disintegration as Fe atom reduced from α-Fe_2O_3 does.

So far by using the idea of atomic state iron, the catalytic effects of iron oxides and cementite Fe_3C can be explained.

(E) From Table 1, it can be seen that α-Fe crystals do not have the catalytic ability for carbon monoxide decomposition. The difference of catalytic ability between α-Fe crystals and atomic state Fe is the following: According to the literature[16], the bond association energy of carbon monoxide is 255.8 Kcal/mole, which is much higher than that of many heteronuclear diatomic molecules. The presence of carbon deposits on the catalyst means that the catalyst (e.g. Fe) must have a strong affinity for carbon, so that the bond energies of Fe-C are large enough to break C-O bonds. In metallic Fe, there is cohesion between metallic atoms, which is assumed to stem from localized dsp hybrid bonds. In other words, some of the d-orbitals participate in hybrid bonds, while others are atomic orbitals, which are responsible for the adsorption of CO. In order to express the degree of d-orbitals participating in dsp hybrid bonds,

d-character* is adopted, e.g. for Fe, d-character is about 40%. The higher d-character indicates a higher participation of electrons in cohesions of metal. Consequently, the higher d-character of -Fe crystal (ca. 40%) indicates a low availability for the formation of covalent bonds between Fe and C. For atomic state Fe, the absence of dsp hybrid bonds means strong covalent Fe-C bond.

The single bond energy of A-B bonds is given by

$$D_{A-B} = (D_{A-A} \cdot D_{B-B})^{\frac{1}{2}} + 30(X_A - X_B)^2 \qquad (9)$$

where D_{A-A}, D_{B-B} —— bond energies of A-A and B-B, respectively.

X_A, X_B —— electronegativities of A and B, respectively.

For Fe-C bond,

$D_{Fe-Fe} = \frac{1}{6}$ x (heat of sublimation) = 16.5 kcal/mole

D_{C-C} = 83.1 kcal/mole

X_{Fe} = 1.83

X_C = 2.55

Substituting all above values into equation (9),

D_{Fe-C} = 53 kcal/mole

---

*d-character defined by Pauling is the ratio of d bonding electrons to total bonding electrons plus metallic orbitals, i.e. d-character = d bonding electrons/(total bonding electrons + metallic orbitals).

Notice these values are single bond energies, the actual bond energy is the combination of these single bond energies. Hence, it is possible to break C-O bond as carbon monoxide is absorbed on atomic state iron having porous structure of large surface area.

(F) If atomic state Fe (so called active Fe atom) is the catalyst for the Boudouard reaction, then the next question is the life-time of these Fe atoms, i.e. whether the catalytic activities of these active atoms decrese with increasing time. The results are listed in Table 3 in which sample No. 12 (after the reduction of Fe pellet by H_2 and flushing with Ar for 10 minutes, CO was immediately introduced) showed carbon deposit, while sample No. 13 (after the reduction of the Fe pellet by H_2, the sample was cooled to room temperature and reheated to 500°C, then CO was introduced) did not have any carbon deposit. This means cooling the sample to room temperature restored the crystal structure of Fe, which is responsible for the loss of catalytic activity.

In the preceding discussion, it has been pointed out that the possible process for carbon monoxide disintegration consists of the generation of active Fe atoms, the adsorption and disintegration of carbon monoxide. In order to

Table 3. Comparison of the Life Time of Active Fe Atoms

($500^{o}C$, Test Time 5 hours, Flow Rate 35 ml/min)

Sample No.	Specimen	Carbon Deposit
12	(a) Reducing Fe pellet (α-Fe + γ-Fe_2O_3) by H_2 at $450^{o}C$ for 28 hrs. (b) Flushing tube with Ar for 10 mins (50 ml/min), Rasing temperature to $500^{o}C$. (c) Introducing CO.	Yes
13	(a) Reducing Fe pellet (α-Fe + γ-Fe_2O_3) by H_2 at $450^{o}C$ for 28 hrs. (b) Cooling to room temperature with Ar flow. (c) Reheating furnace to $500^{o}C$. (d) Introducing CO.	No

confirm this hypothesis, it is necessary to develop substantiating thermodynamical calculations and kinetic experiments.

(2) Thermodynamical Calculations - Phase Maps Plotted by SOLGASMIX Computer Program.

The process of carbon monoxide disintegration in a closed system or flowing system with an extremely low flow rate must approach thermodynamical equilibrium. Therefore, the equilibrium phases and mole fraction of each phase can be calculated thermodynamically. Nevertheless, there are so many reactions in Fe_2O_3-CO or Fe-CO systems that it is difficult to obtain satisfactory results by calculating individual reactions thermodynamically. Fortunately, this problem can be simplified by using the SOLGASMIX computer program (Appendix 1).[17,18,19]

The advantage of the SOLGASMIX program is its simplicity. All we need to run this program is a list of all possible chemical species including reactants and possible products and their basic thermodynamical data $\Delta_f G$ (the Gibbs free energy of formation).[20,21] This makes the calculation much easier even without knowing the actual chemical reactions.

Figure 3 is the phase map of Fe_2O_3-CO system plotted by running SOLGASMIX program. Several points are noteworthy,

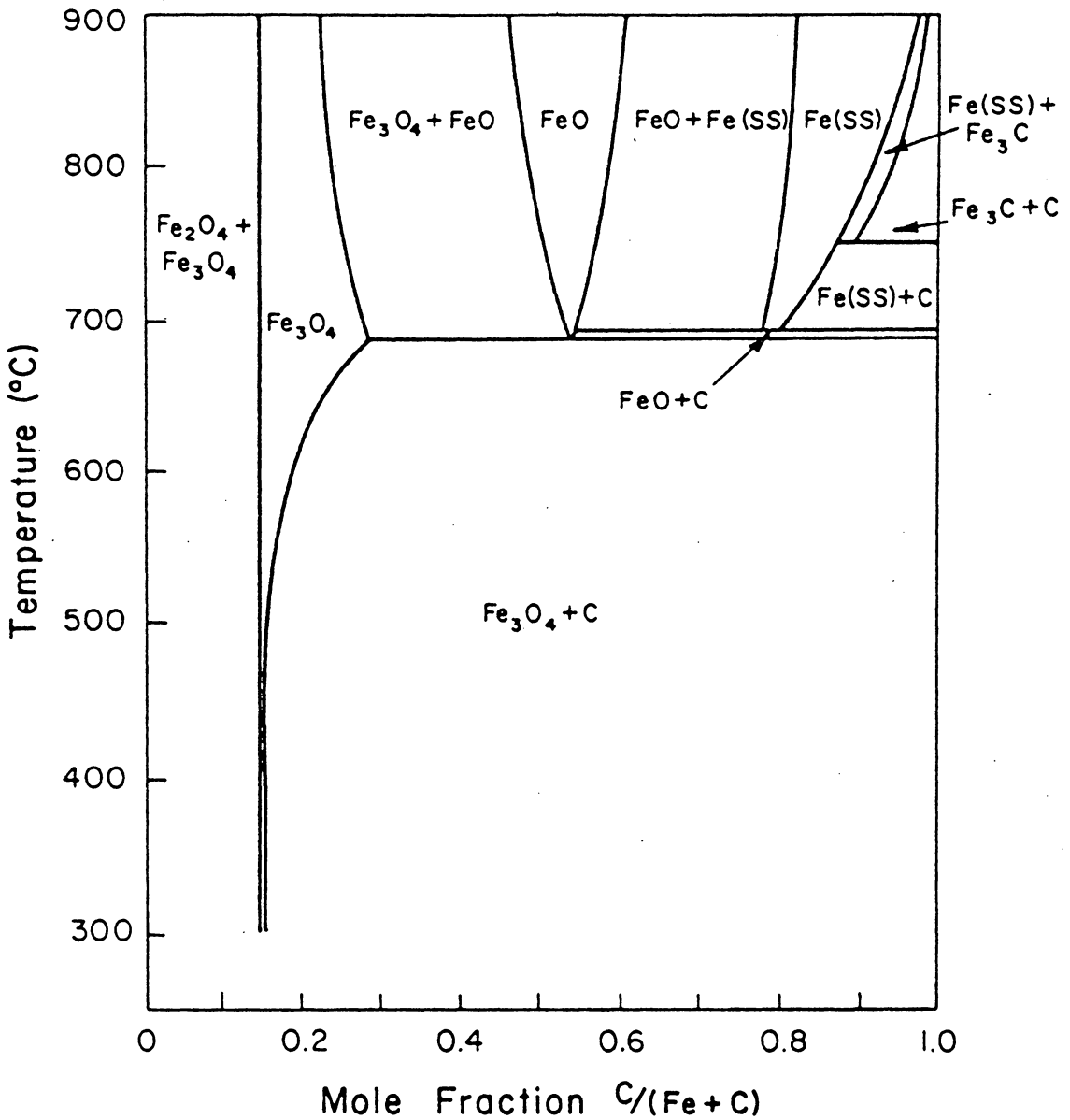

Fig. 3(a) Phase Map of System Fe_2O_3 - CO at 1 atm.

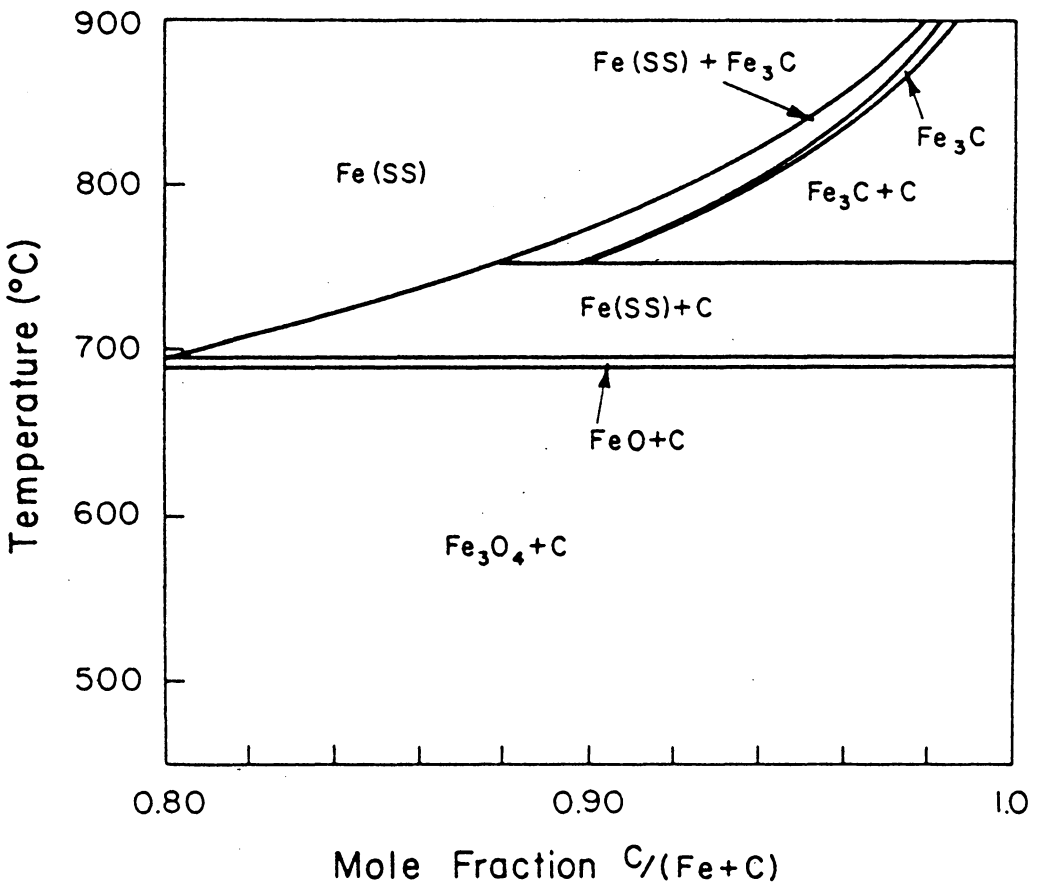

Fig. 3(b) The Upper Right Corner of Fig. 3(a)

(A) Except in the low carbon region, the equilibrium phases* are Fe_3O_4 + C, FeO + C or Fe(SS) + C depending on temperature. Due to the absence of the two phase Fe_2O_3 + C region, it can be concluded that carbon cannot be in equilibrium with Fe_2O_3.

(B) Fe_3C, Fe_2C and FeC, metastable phases at lower temperatures, are not shown on the phase maps because this program is only used to calculate the mole fractions of equilibrium phases.

(C) Although Figure 3 describes the phases existing in a equilibrium system, it can also be used to explain the phases existing in flowing system if some modifications are made. For example, in sample No. 2 (Table 1) the phases present in a sample having carbon deposit are graphite, Fe_3O_4, iron carbides and Fe(SS). The phase difference between closed and flowing systems is the presence of Fe(SS), which can be explained as the following: Fe_3O_4 generated from the reduction of Fe_2O_3 may also be reduced by CO according to reaction (3).

$$Fe_3O_4 + 4\ CO = 3\ Fe + 4\ CO_2 \qquad (3)$$

The change of free energy for this reaction is

$$\Delta G\ (cal/mole) = -5170 + 8.02\ T$$

---

* In this work, all phase maps show only condensed phases in systems.

As $G = -RT \ln \frac{p^4_{CO_2}}{p^4_{CO}}$, reaction (3) reaches equilibrium.

In other words, at T = 773K as long as $\frac{p_{CO_2}}{p_{CO}} < 0.8268$,

Fe_3O_4 can always be reduced. In this work (flowing system), the partial pressure of CO_2 is much lower than that of CO; hence, the presence of α-Fe in sample No. 2 is reasonable. Therefore, the phase maps can be used to explain the phases present in the flowing system if some modifications are made.

(D) Figure 3 shows that carbon deposition occurs in the whole temperature range (300 - 900°C), if C/Fe+C is sufficiently high. Actually, carbon can only be deposited in the temperature range 400 - 760°C. The difference between the results of thermodynamic calculations and experiments illustrates the insufficiency of the thermodynamic calculation. From the view point of thermodynamics, the Boudouard reaction might occur at temperatures < 1100°C,[7] but the absence of adsorption at high temperature makes the upper temperature limit 760°C. On the other hand, thermodynamic calculations show that the lower the temperature, the more the amount of carbon deposit (Table 4). As a matter of fact, carbon deposit can only be measured about > 400°C because the whole process of carbon deposition consists of chemisorption, disintegration of CO and diffusion, etc.

Table 4. The Amount of Carbon Deposit (moles) of Systems Fe_2O_3-CO at Different Temperatures (1 atom).

Temperature (^oC)	Mole Fraction C/Fe + C						
	0.5	1.0	1.5	2.0	2.5	3.0	3.5
300	0.23323	0.48314	0.73305	0.98295	1.2329	1.4828	1.7327
400	0.23199	0.48014	0.72948	0.97822	1.2270	1.4757	1.7245
500	0.22415	0.46554	0.70693	0.94832	1.1897	1.4311	1.6725
600	0.19325	0.40567	0.61809	0.83051	1.0429	1.2553	1.4678
700	0	0.06178	0.20098	0.34017	0.47937	0.61856	0.75776
800	0	0	0	0	0	0	0.03143

which are activated processes. This means that from a kinetic view point low temperature is unfavorable to carbon deposition. By combining both thermodynamic and kinetic conditions, it is not surprising that carbon deposition ranges from 400 - 760°C and the amount of carbon deposition has a maximum value at ~ 550°C.

Figure 4 shows the phase maps of the Fe-CO system at different pressures. As the pressure of carbon monoxide is increased, the Fe_3O_4 + C and FeO + C regions extend to higher temperature and the amount of carbon deposition increases (Table 5). These results are in agreement with Le Chatelier's principle.

Figure 5 shows the phase maps of system Fe-CO-H_2S at 1, 34 and 68 atm., respectively. By comparing the amount of carbon deposit in systems Fe-CO and Fe-CO-H_2S at 500°C (Table 6) the poisonous effect of sulfur on the catalyst is evident. The reason is that due to the strong affinity of Fe and S, FeS or FeS_2 first forms (from Figure 5, it can be seen that FeS and/or FeS_2 are always present in each phase region), then the excess Fe atoms catalyze carbon monoxide dissociation. However, at high temperature, the presence of a small amount of hydrogen in the system (1% H_2S in gas) results in the activated effect of hydrogen to exceed the poisonous effect of sulfur; consequently, the amount of carbon

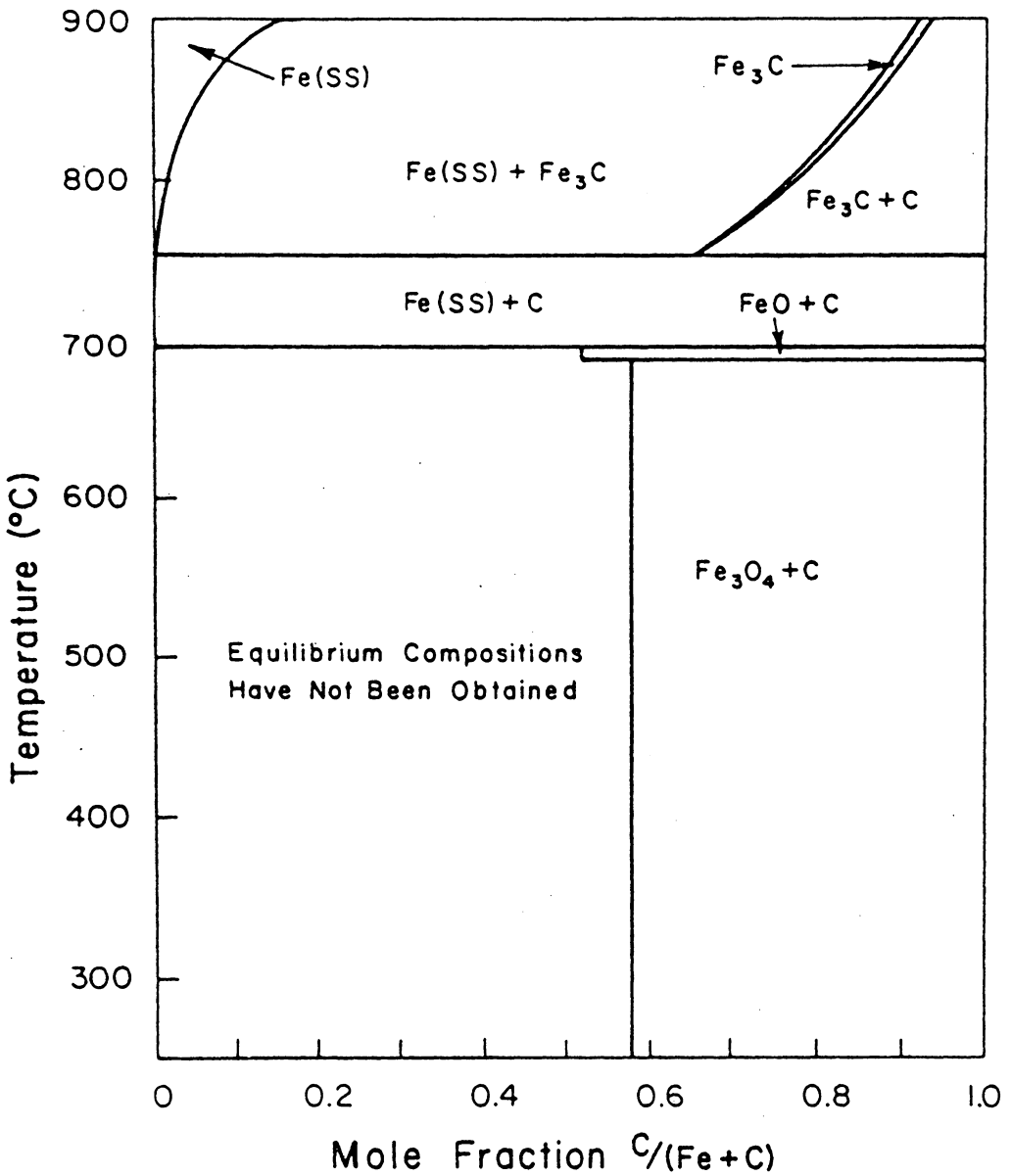

Fig. 4(a) Phase Map of System Fe - CO at 1 atm.

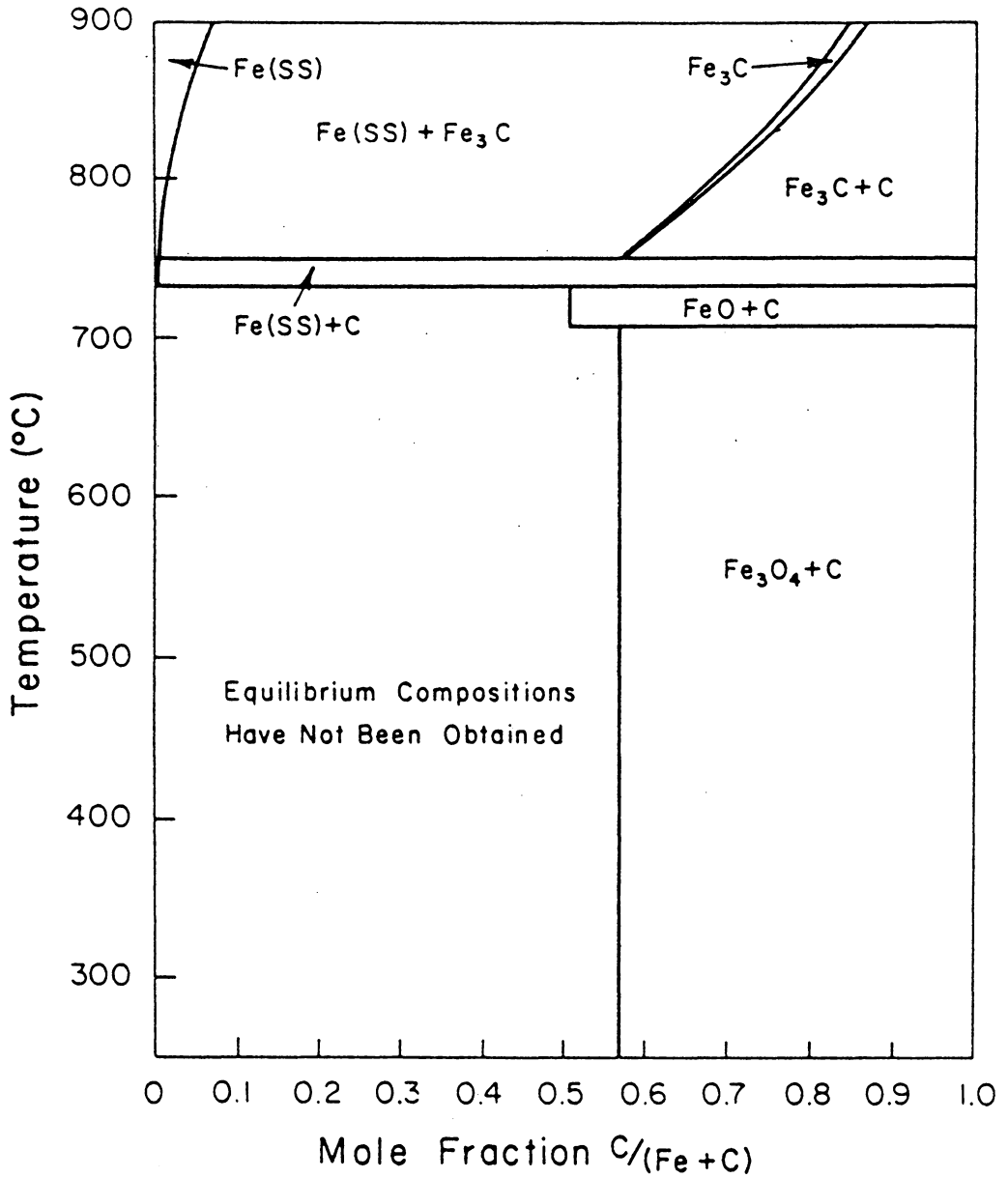

Fig. 4(b) Phase Map of System Fe - CO at 2 atm.

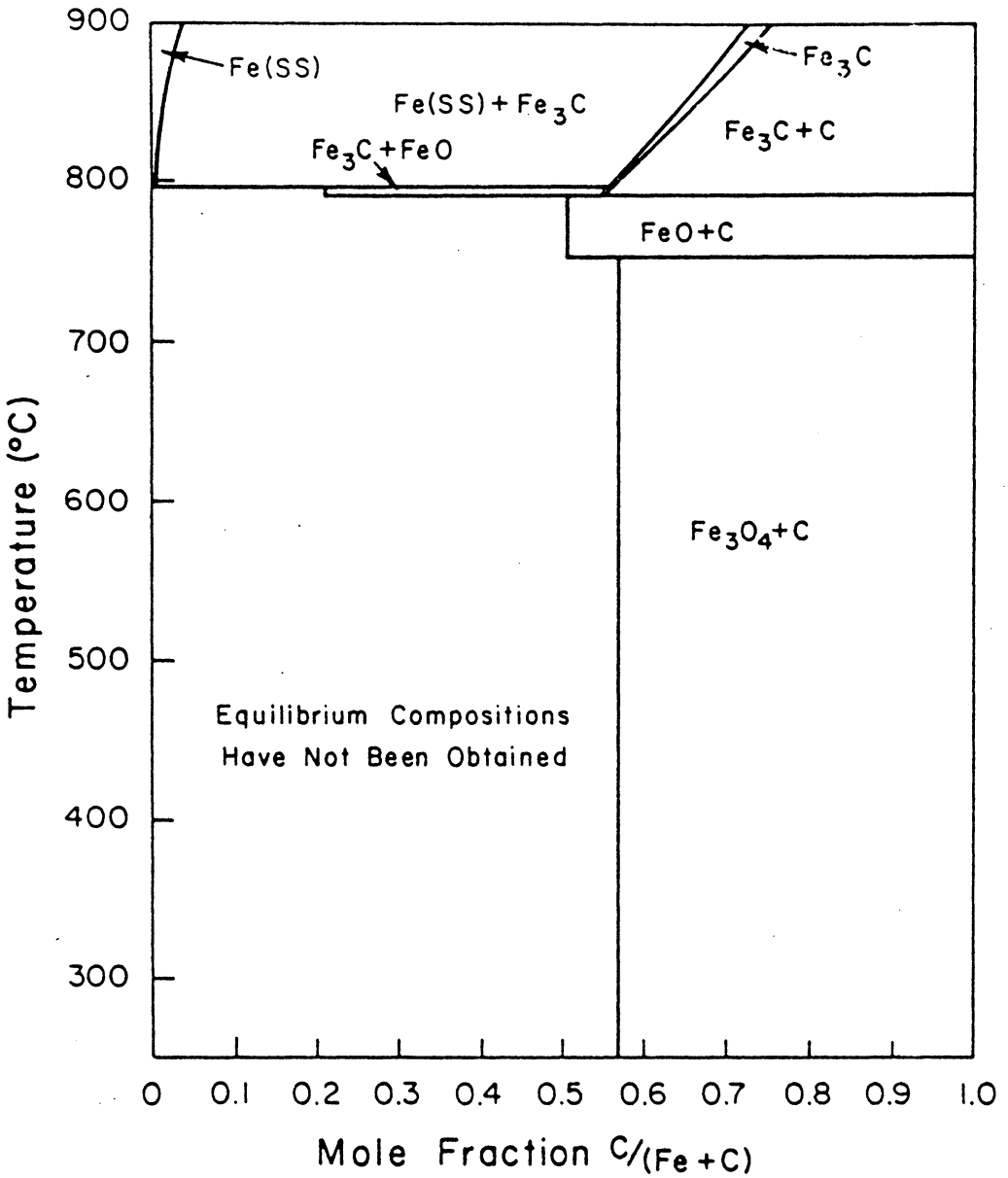

Fig. 4(c) Phase Map of System Fe - CO at 5 atm.

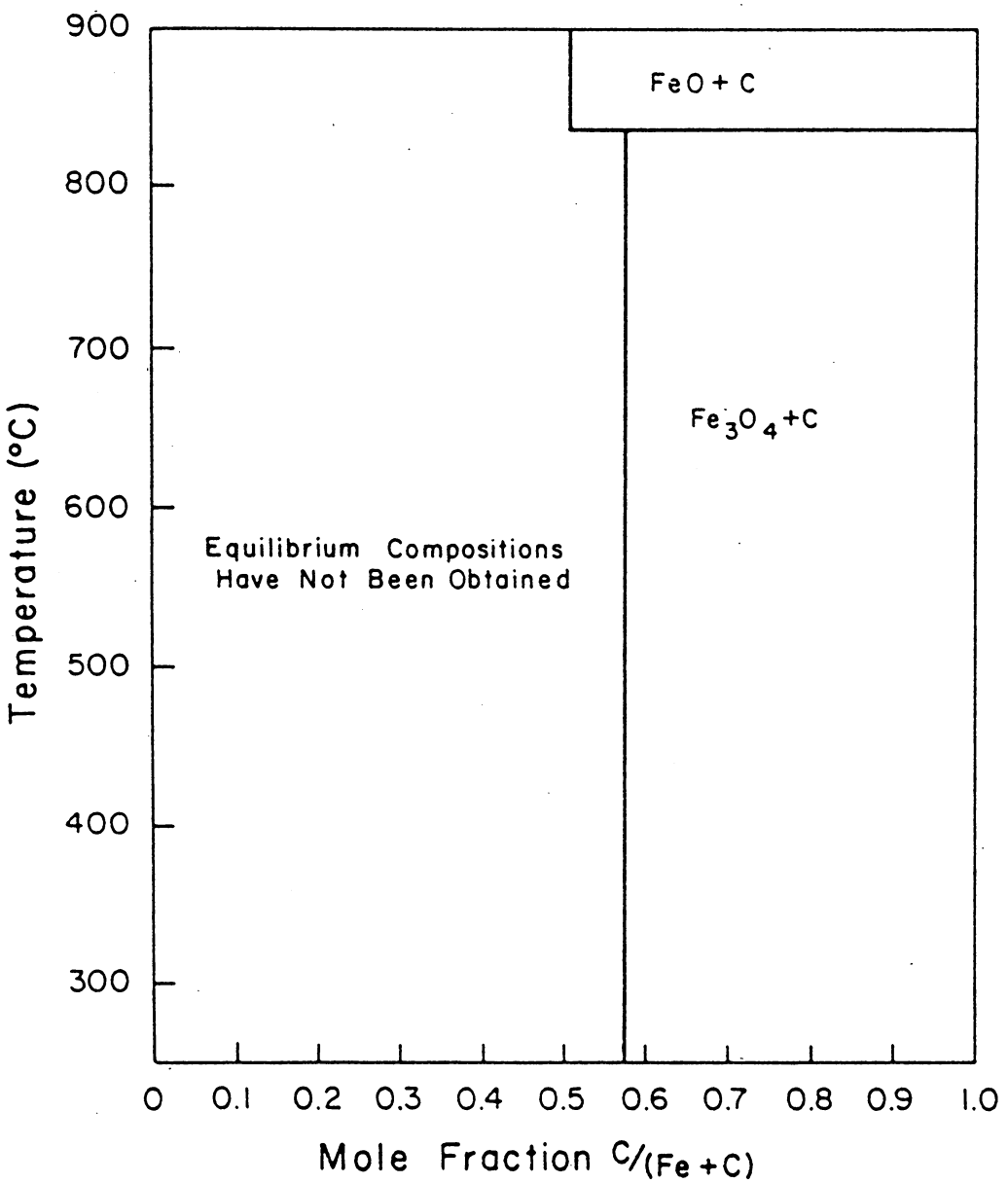

Fig. 4(d) Phase Map of System Fe - CO at 34 atm.

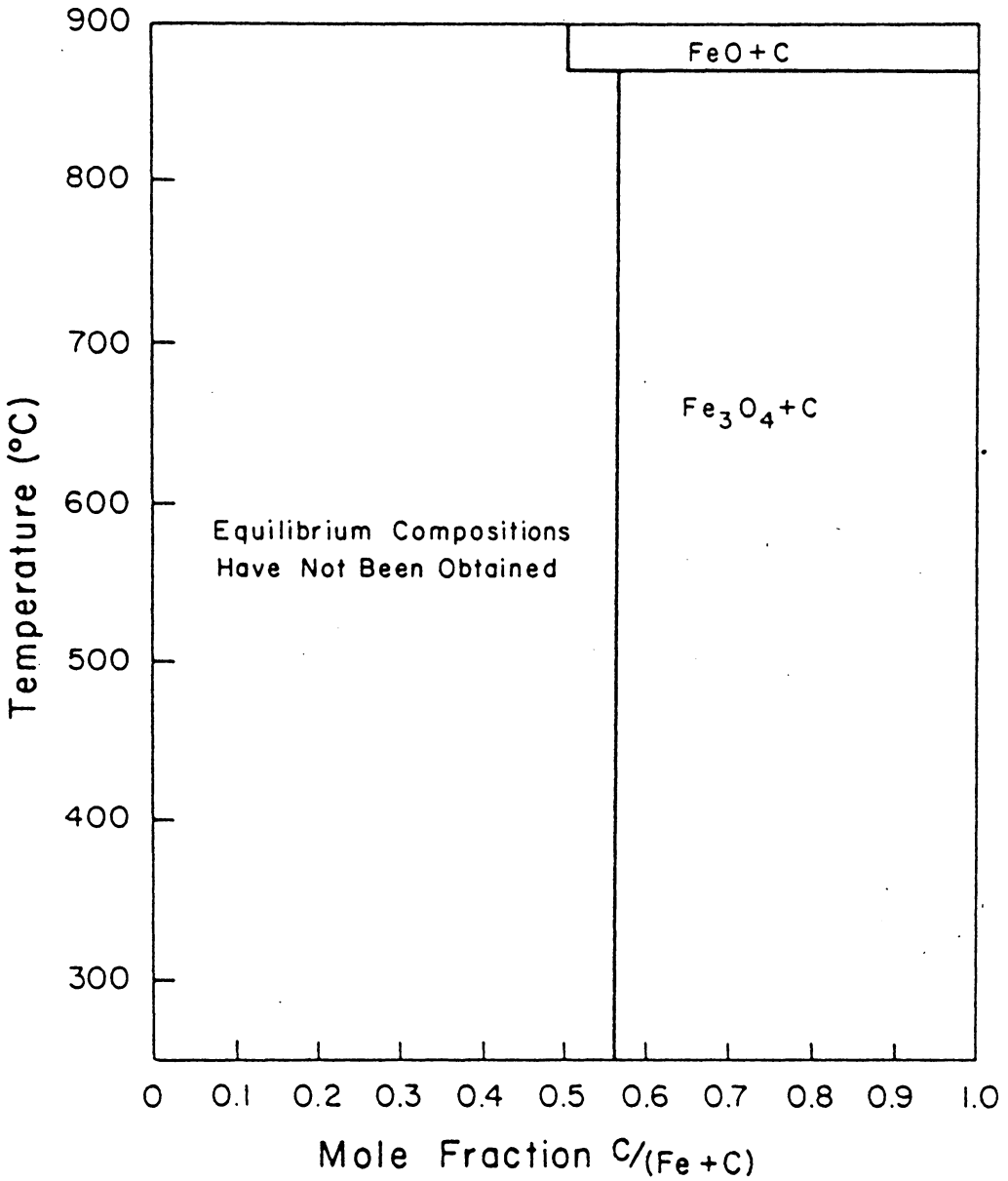

Fig. 4(e) Phase Map of System Fe - CO at 68 atm.

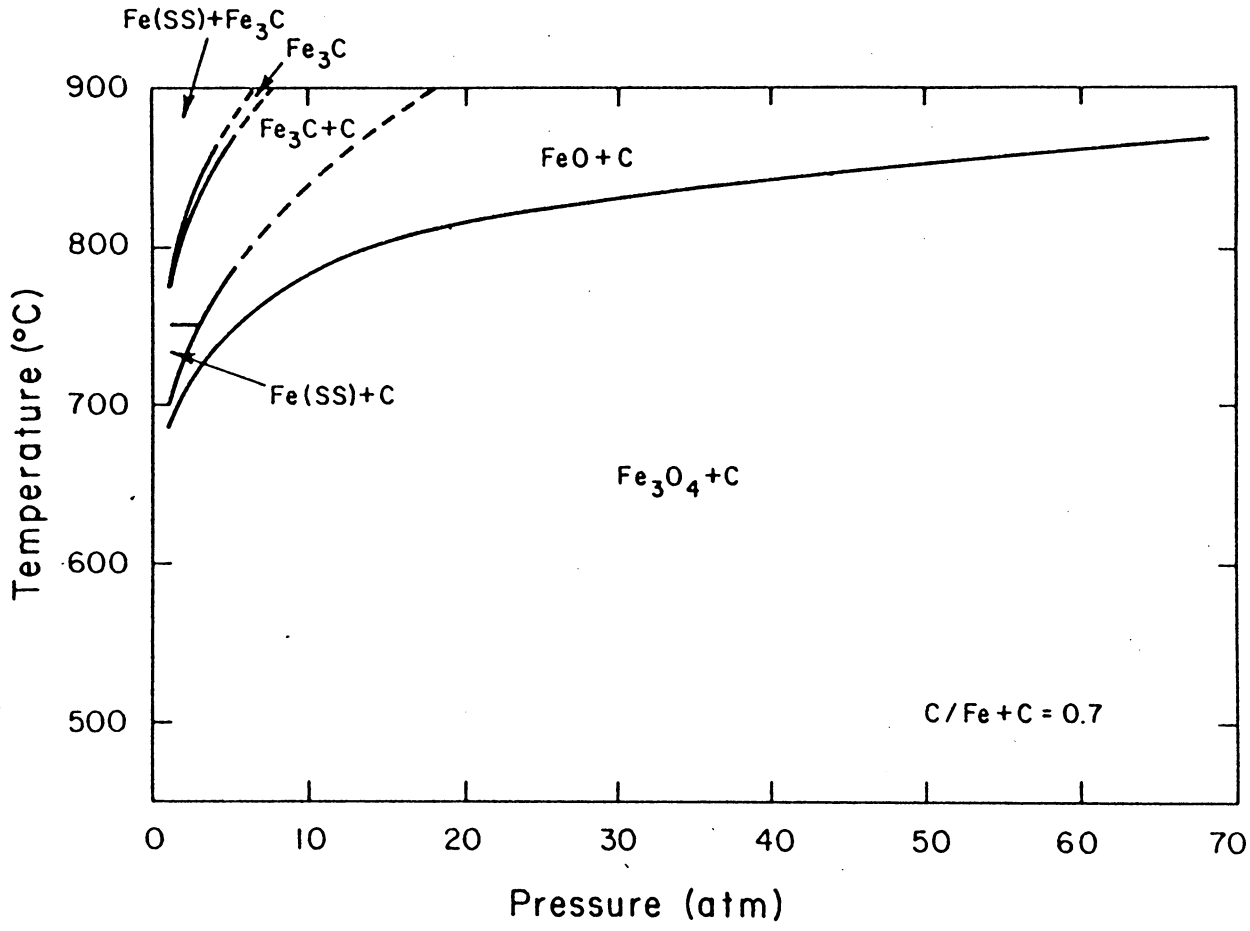

Fig. 4(f) Phase Map of System Fe - CO for the Composition of C/(Fe + C) = 0.7

Table 5. The Amount of Carbon Deposit (moles) of Fe-CO System at Different Pressures (500°C)

Pressure (atm)	Mole Fraction C/Fe + C						
	0.5	1.0	1.5	2.0	2.5	3.0	3.5
1	0.37932	0.62070	0.86209	1.1035	1.3449	1.5863	1.8277
34	0.38264	0.63117	0.87969	1.1282	1.3767	1.6253	1.8738
68	0.38285	0.63180	0.88076	1.1297	1.3787	1.6276	1.8766

Table 6. The Comparison of the Amount of Carbon Deposit (moles) of Systems Fe-CO and Fe-CO-H_2S at Different Temperatures (1 atm)

Temperature (^oC)	System	Mole Fraction C/Fe + C						
		0.5	1.0	1.5	2.0	2.5	3.0	3.5
500	Fe-CO	0.37932	0.62070	0.86209	1.1035	1.3449	1.5863	1.8277
	Fe-CO-H_2S	0.37757	0.61727	0.85695	1.0966	1.3363	1.5760	1.8157
700	Fe-CO	0.13905	0.27827	0.41746	0.55666	0.68585	0.83504	0.97424
	Fe-CO-H_2S	0.13937	0.27887	0.41837	0.55786	0.69736	0.83685	0.97635
800	Fe-CO	0	0.03810	0.09048	0.14286	0.19254	0.24762	0.30000
	Fe-CO-H_2S	0	0.04148	0.09556	0.14964	0.20371	0.25779	0.31186

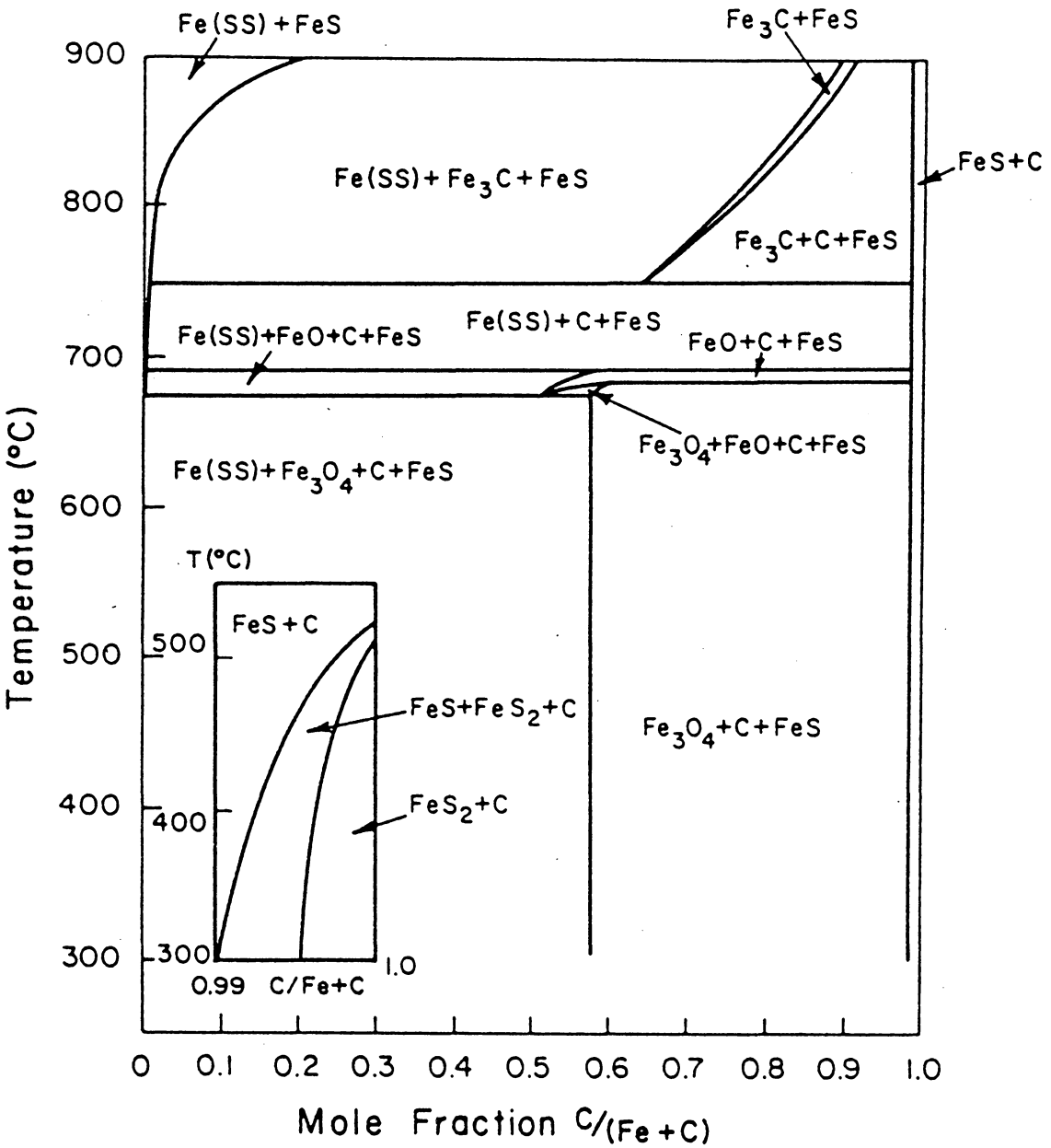

Fig. 5(a) Phase Map of System Fe - CO - H_2S at 1 atm. (Mole Fraction S/(C + S) = 0.01)

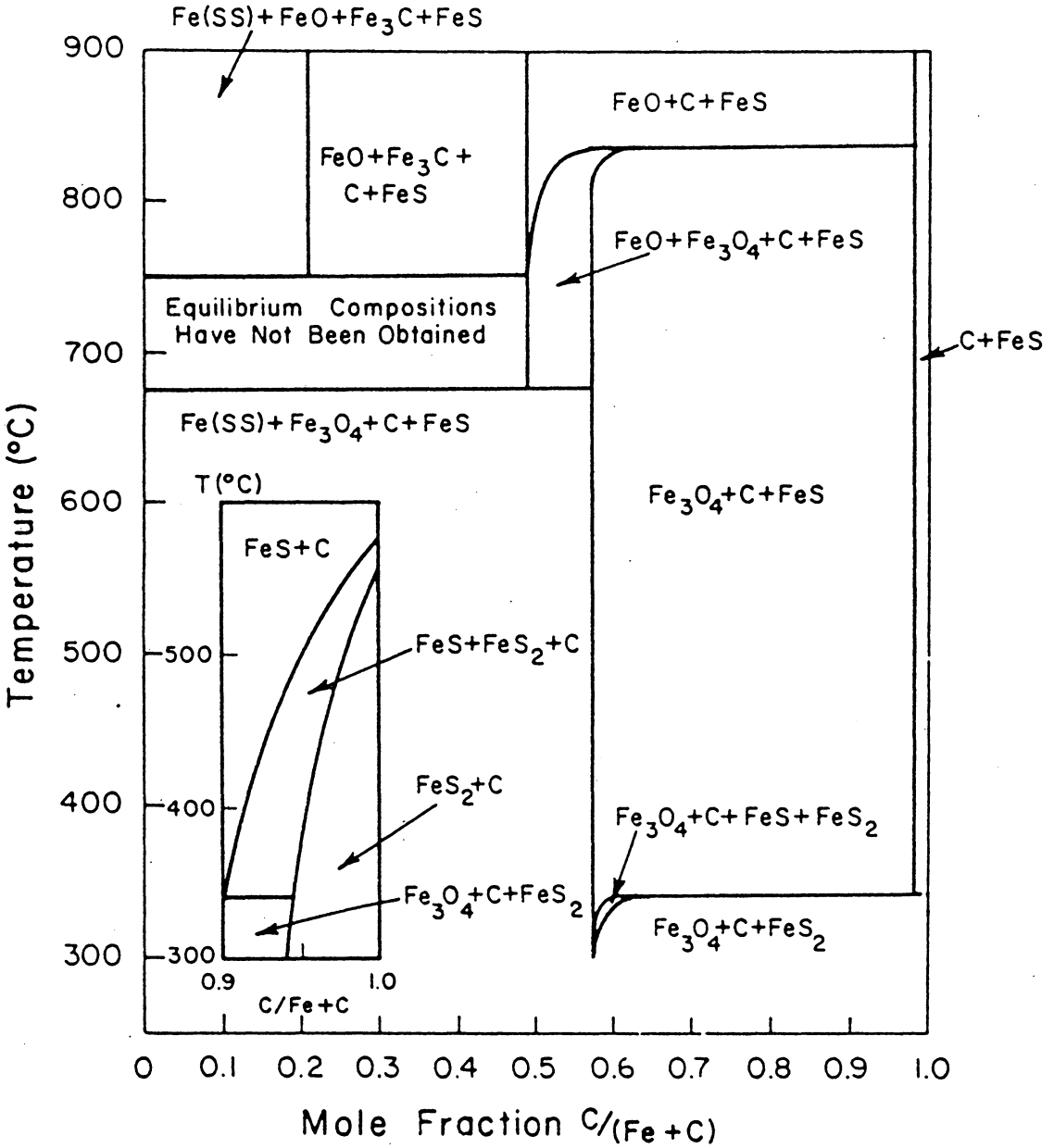

Fig. 5(b) Phase Map of System Fe - CO - H_2S at 34 atm. (Mole Fraction S/(C + S) = 0.01)

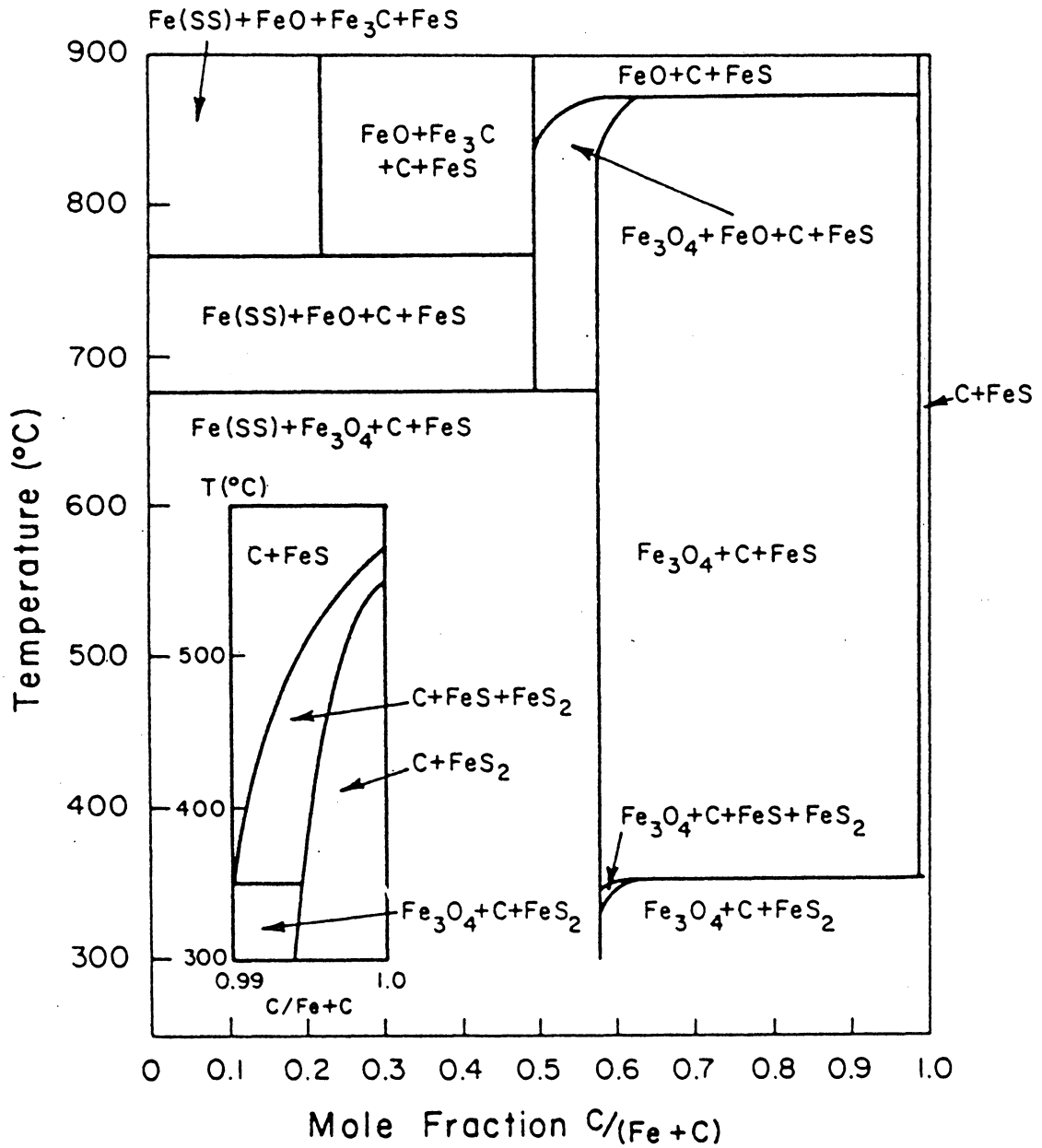

Fig. 5(c) Phase Map of System Fe - Co - H_2S at 68 atm. (Mole Fraction S/(C + S) = 0.01)

deposit in the Fe-CO-H_2S system is greater than that for the system Fe-CO. This is in agreement with Walker's conclusion.[8] In other words, at low temperature, the poisonous effect of sulfur surpasses the activated effect of hydrogen, whereas at higher temperatures, the markedly activated effect of hydrogen is predominant.

Figures 6-9 show the phase maps of Fe-CO-CO_2-H_2O-CH_4-NH_3-H_2S system* at 1 atm. for selected values of O/C+O = 0.5 - 0.8, H/C+H = 0.6 - 0.9, N/C+N = 0.03 and S/C+S = 0.015. The oxygen and hydrogen contents in this system are high (In Fe-CO-H_2S system discussed, the hydrogen content is assumed to be low). From Tables 7 and 8, it can be seen that for certain mole fraction of H/C+H, the amount of carbon deposit decreases with increasing oxygen content, and for certain mole fraction of O/C+O, the amount of carbon deposit decreases with increasing hydrogen content.

(3) Kinetic Data

In order to confirm reactions (2) - (8), some kinetic data and corresponding X-ray diffraction patterns of Fe_2O_3 pellet samples were determined.

---

*The gas composition used in this calculation is corresponding to the composition of gas generated by coal gasification.

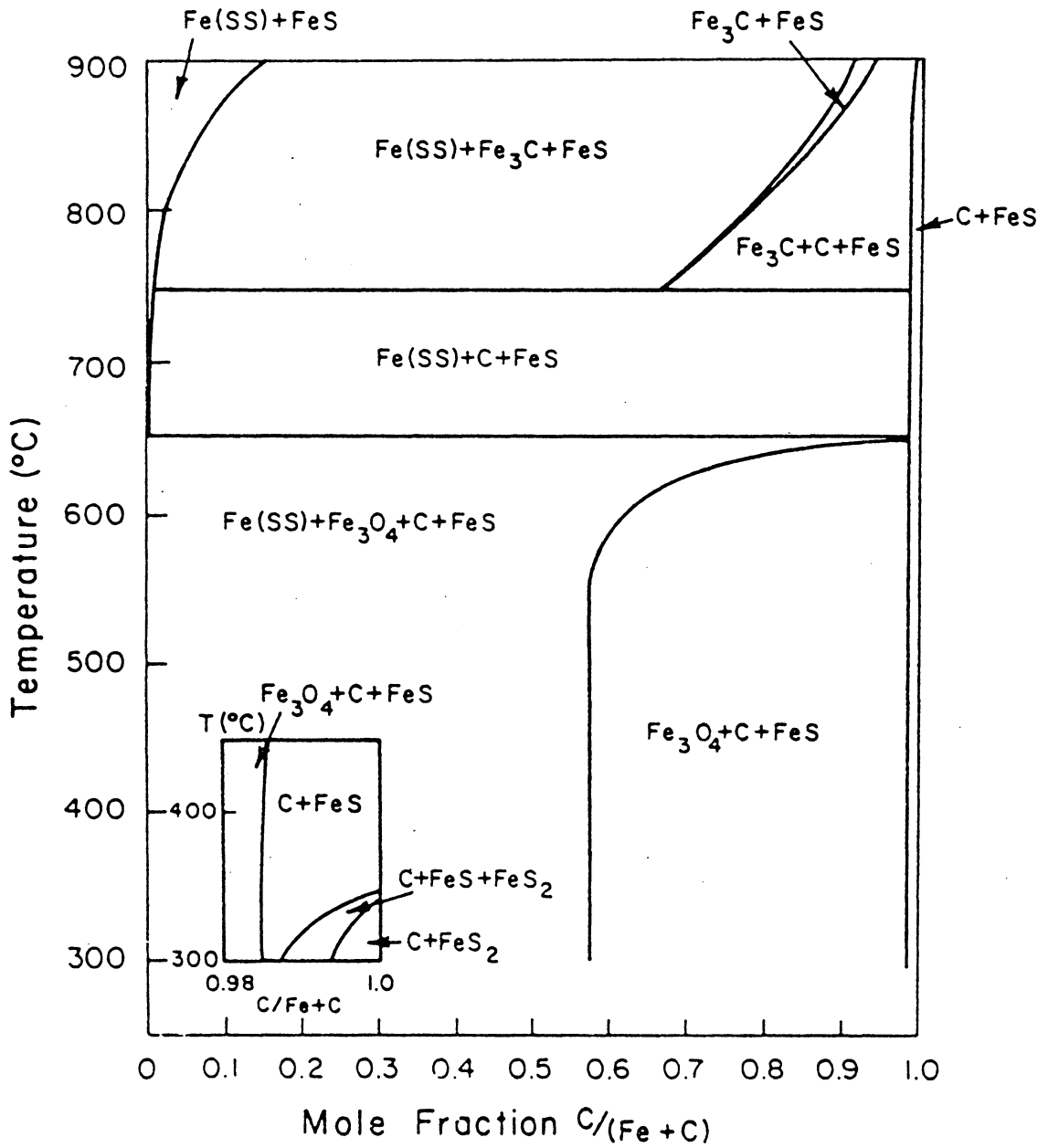

Fig. 6(a) Phase Map of System Fe - CO - CO_2 - H_2O - CH_4 - H_2S - NH_3 at 1 atm. (Mole Fraction O/(C + O) = 0.5, H/(C + H) = 0.6, N/(C + N) = 0.03, S/(C + S) = 0.015)

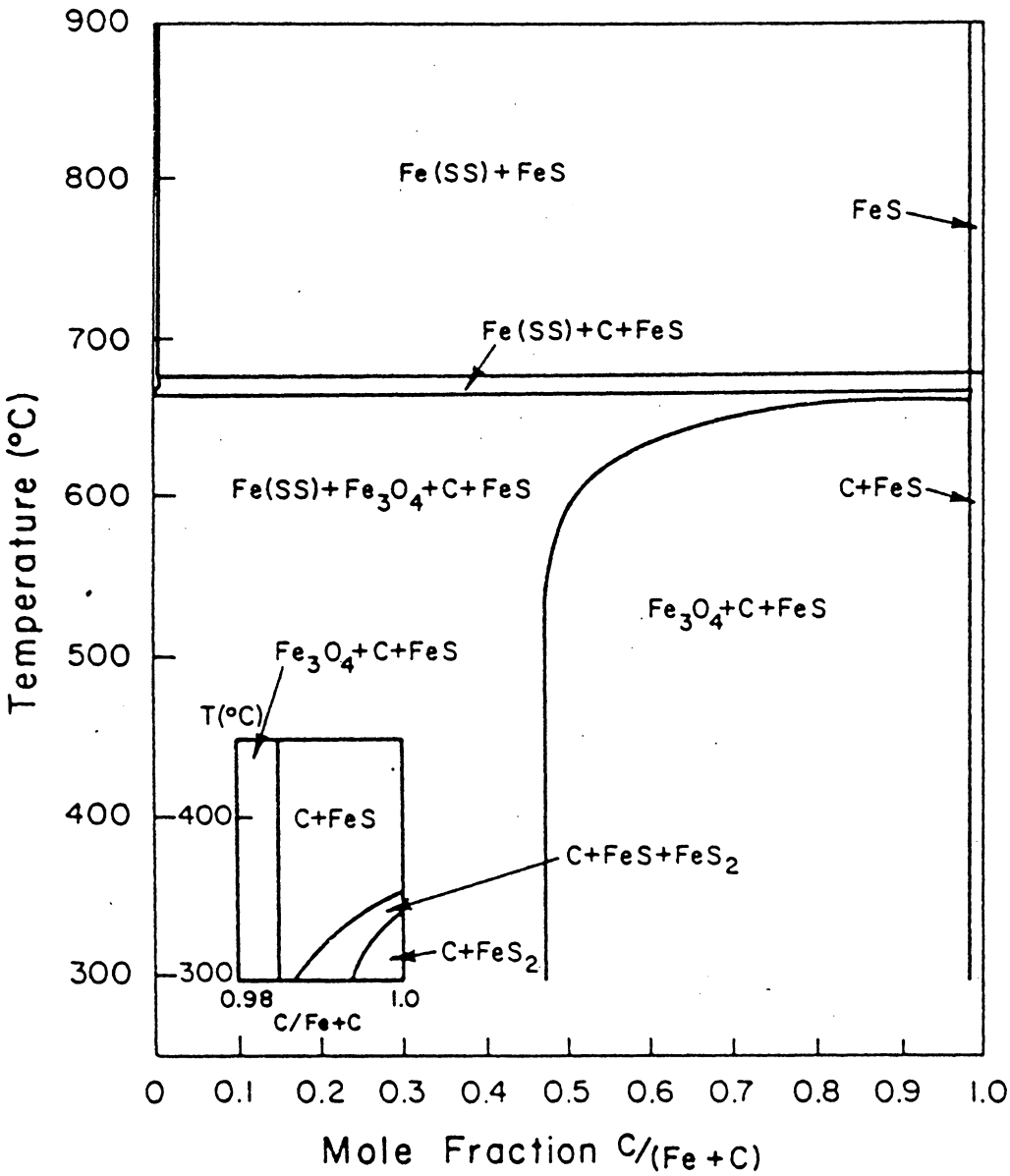

Fig. 6(b) (i) Phase Map of System Fe - CO - CO_2 - H_2O - CH_4 - H_2S - NH_3 at 1 atm. (Mole Fraction O/(C + O) = 0.6, H/(C + H) = 0.6, N/(C + N) = 0.03, S/(C + S) = 0.015)

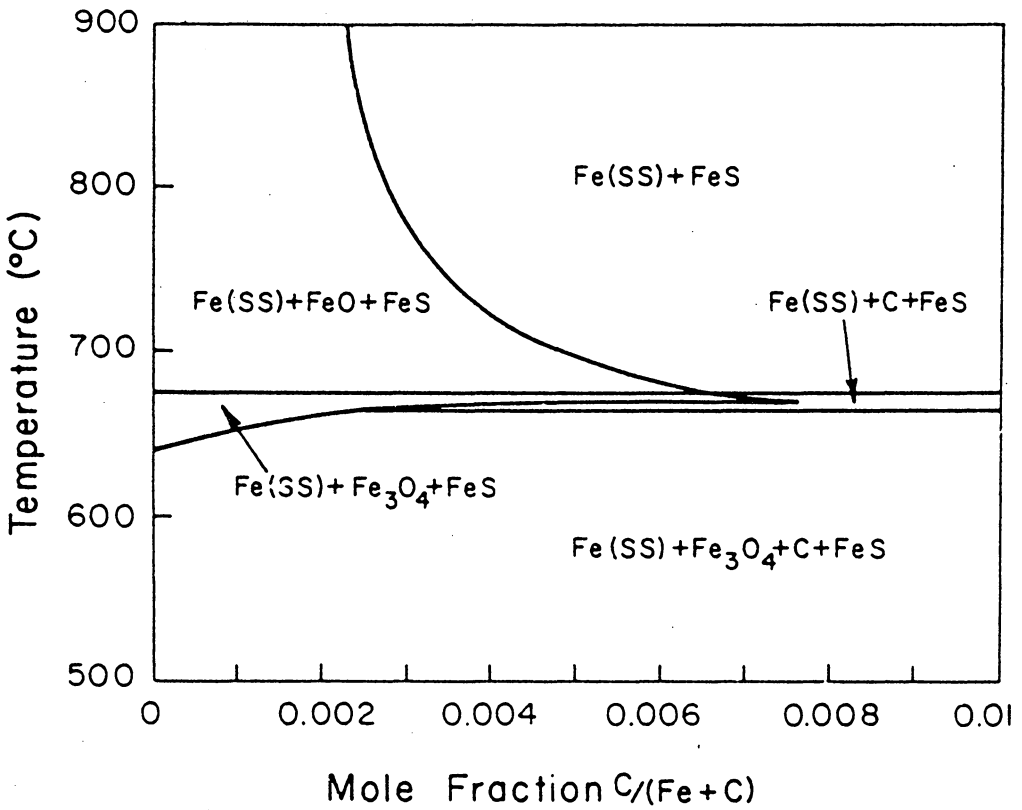

Fig. 6(b) (ii) The Upper Left Corner of Fig. 6(b) (i)

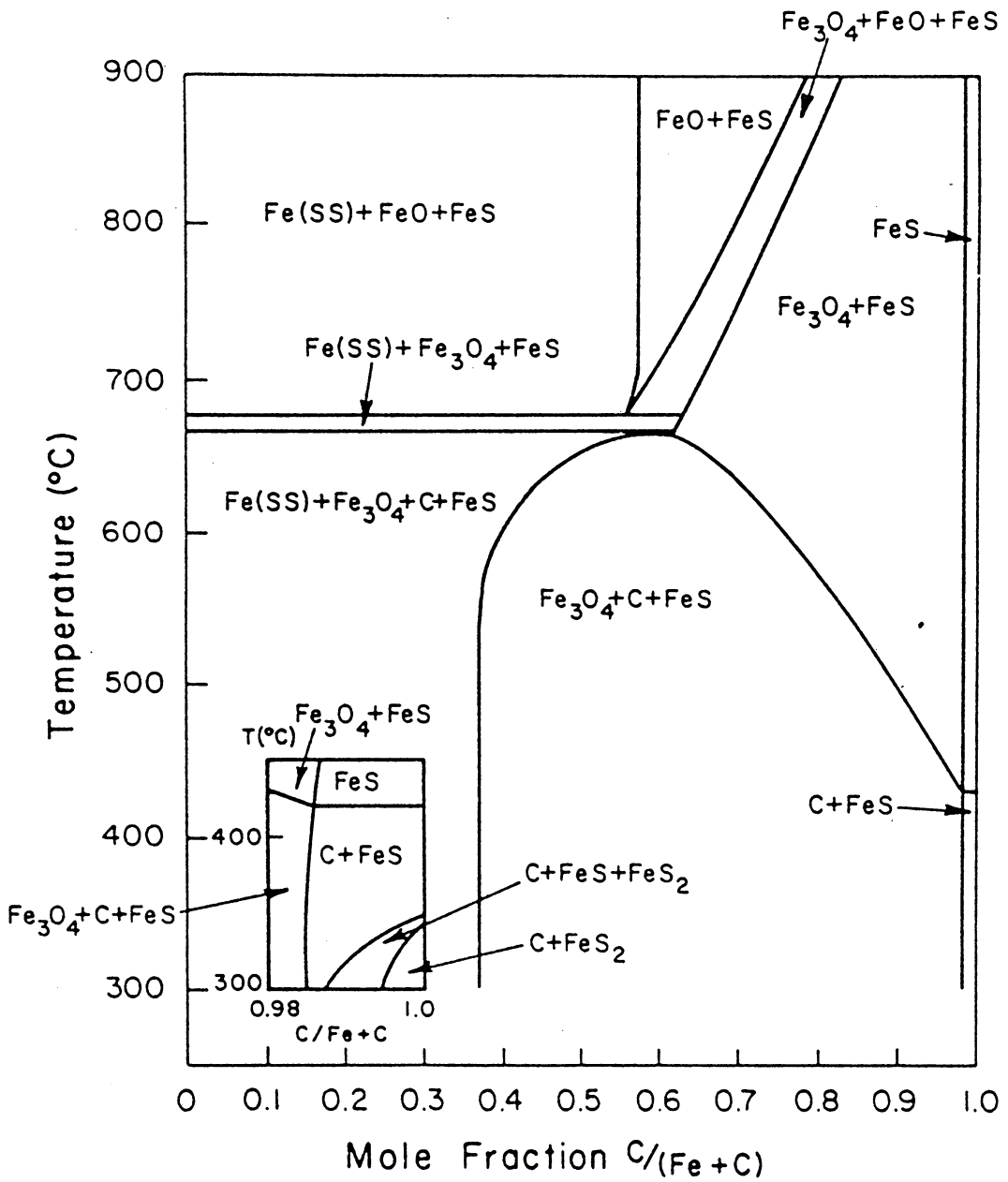

Fig. 6(c) Phase Map of System Fe - CO - CO_2 - H_2O - CH_4 - H_2S - NH_3 at 1 atm. (Mole Fraction O/(C + O) = 0.7, H/(C + H) = 0.6, N/(C + N) = 0.03, S/(C + S) = 0.015)

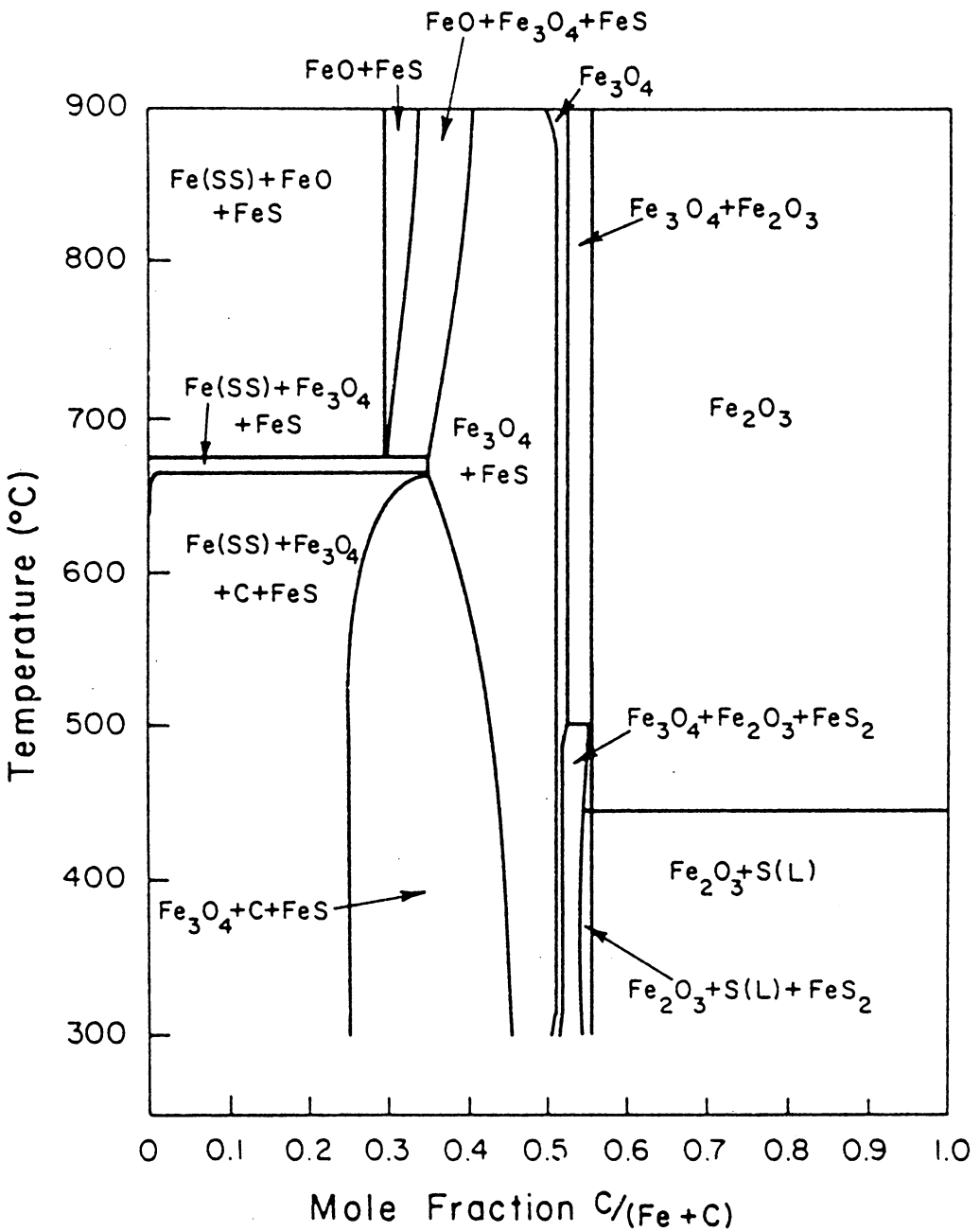

Fig. 6(d) (i) Phase Map of System Fe - CO - CO_2 - H_2O - CH_4 - H_2S - NH_3 at 1 atm. (Mole Fraction O/(C + O) = 0.8, H/(C + H) = 0.6, N/(C + N) = 0.03, S/(C + S) = 0.015)

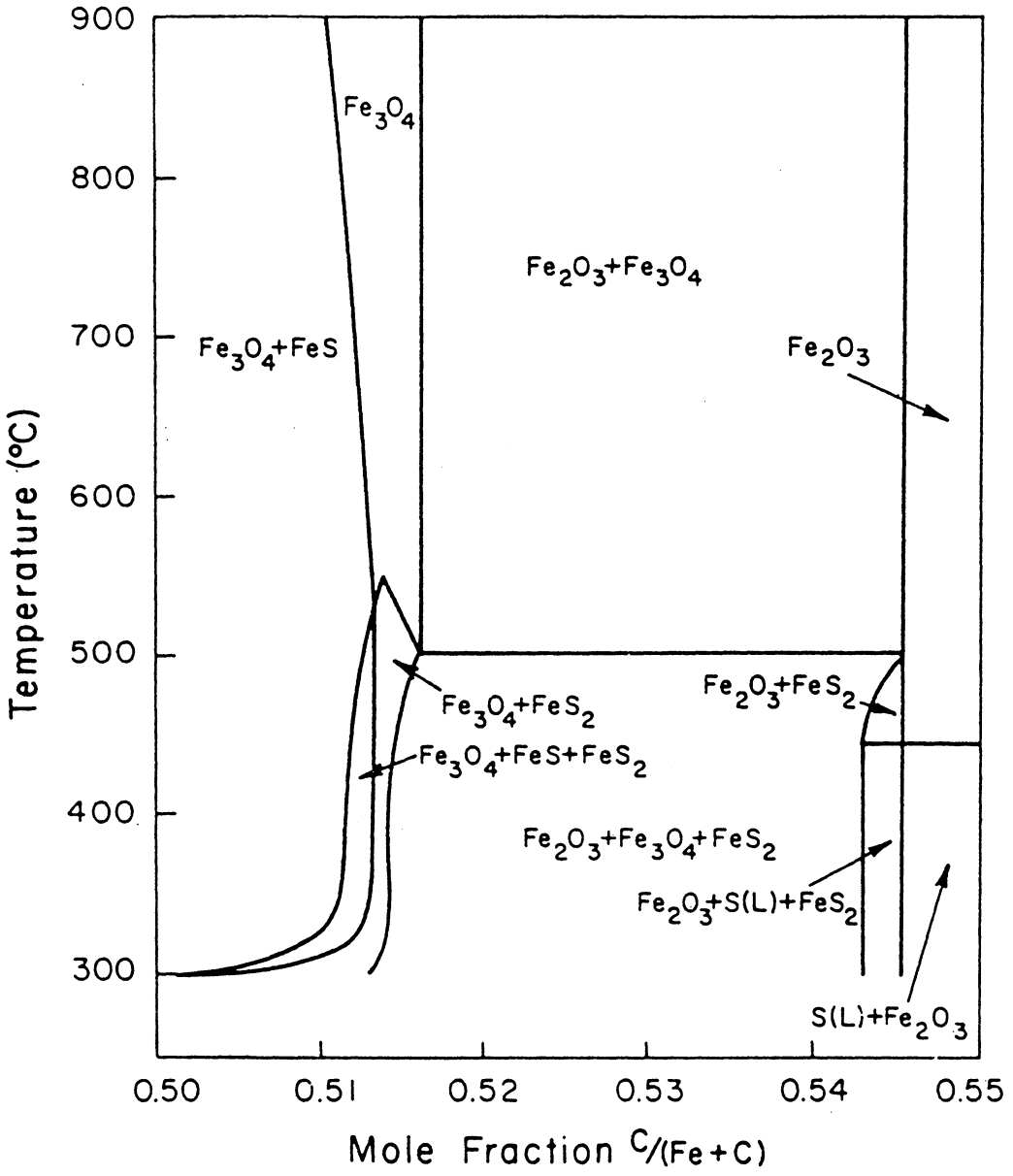

Fig. 6(d) (ii) The Magnified Graph of the Portion of C/(Fe + C) = 0.5 - 0.55 of Fig. 6(d) (i)

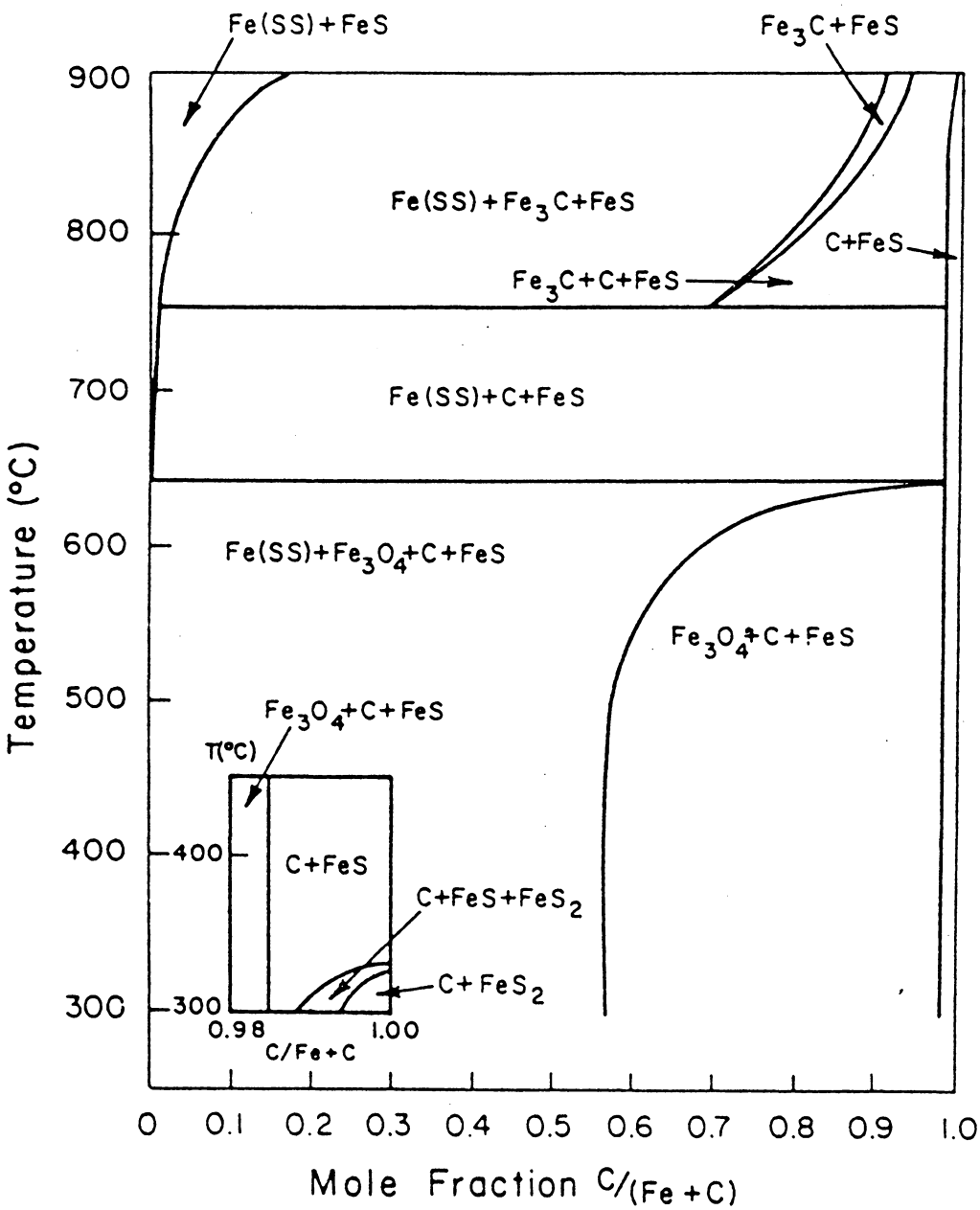

Fig. 7(a) Phase Map of System Fe - CO - CO_2 - H_2O - CH_4 - H_2S - NH_3 at 1 atm. (Mole Fraction O/(C + O) = 0.5, H/(C + H) = 0.7, N/(C + N) = 0.03, S/(C + S) = 0.015)

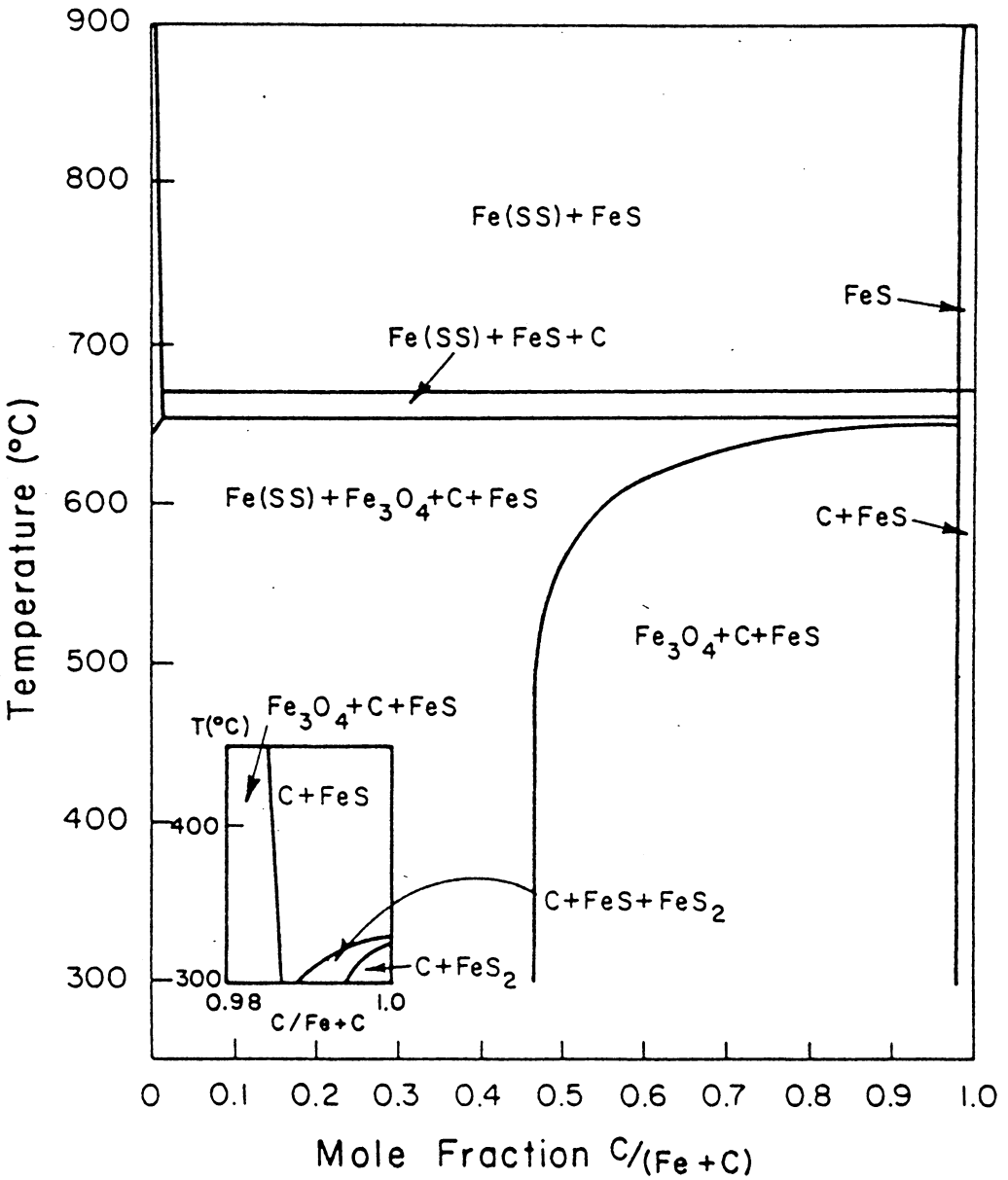

Fig. 7(b) (i) Phase Map of System Fe - CO - CO_2 - H_2O - CH_4 - H_2S - NH_3 at 1 atm. (Mole Fraction O/(C + O) = 0.6, H/(C + H) = 0.7, N/(C + N) = 0.03, S/(C + S) = 0.015)

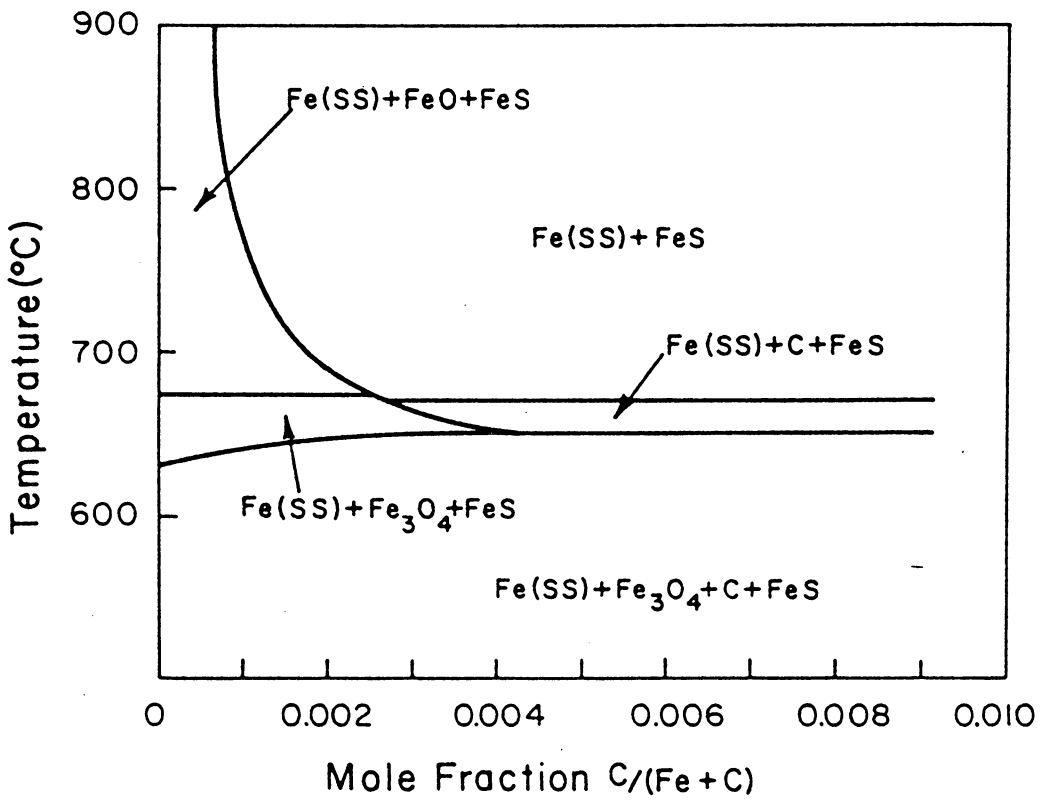

Fig. 7(b) (ii) The Upper Left Corner of Fig. 7(b) (i)

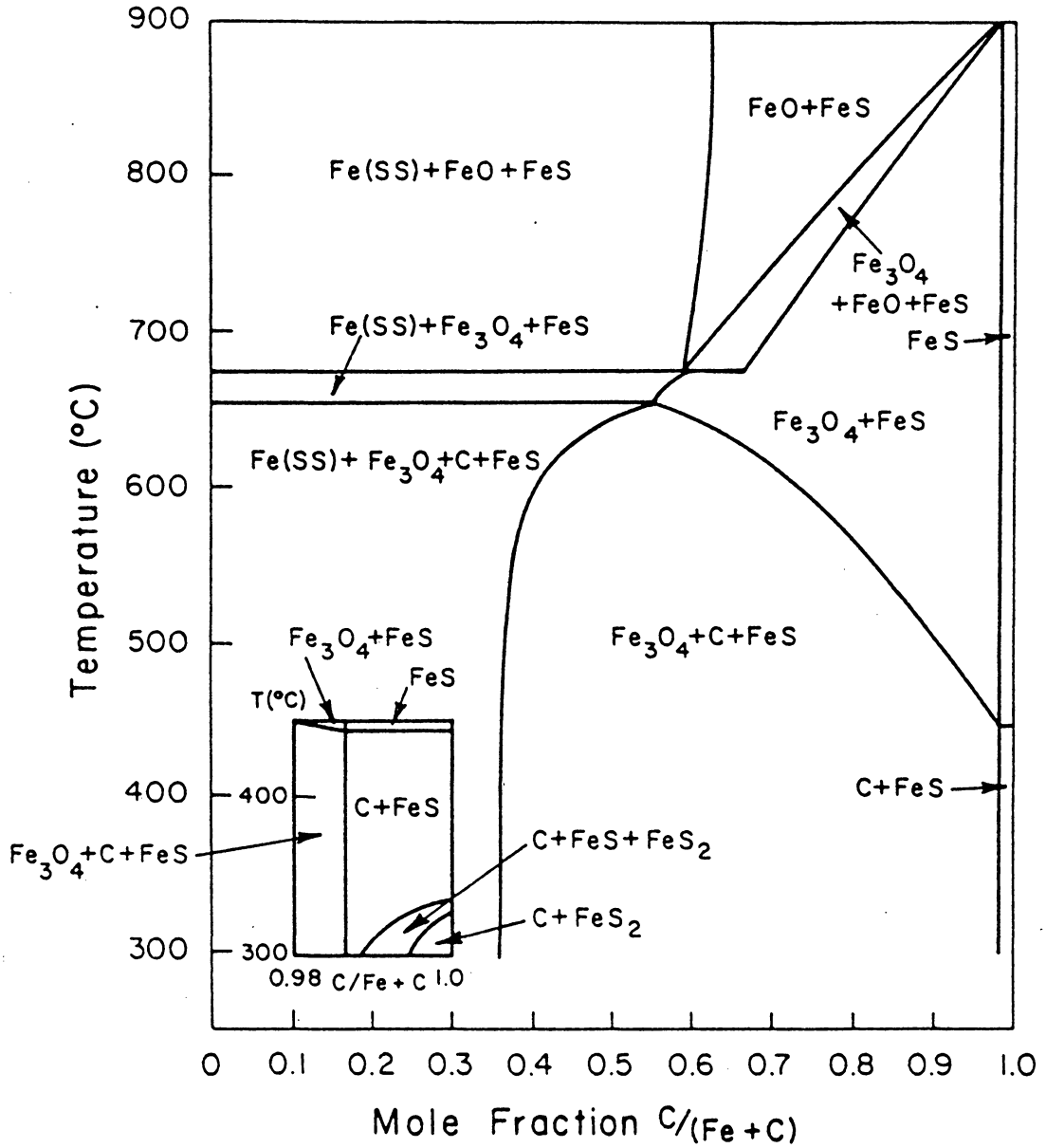

Fig. 7(c) Phase Map of System Fe - CO - CO_2 - H_2O - CH_4 - H_2S - NH_3 at 1 atm. (Mole Fraction O/(C + O) = 0.7, H/(C + H) = 0.7, N/(C + N) = 0.03, S/(C + S) = 0.015)

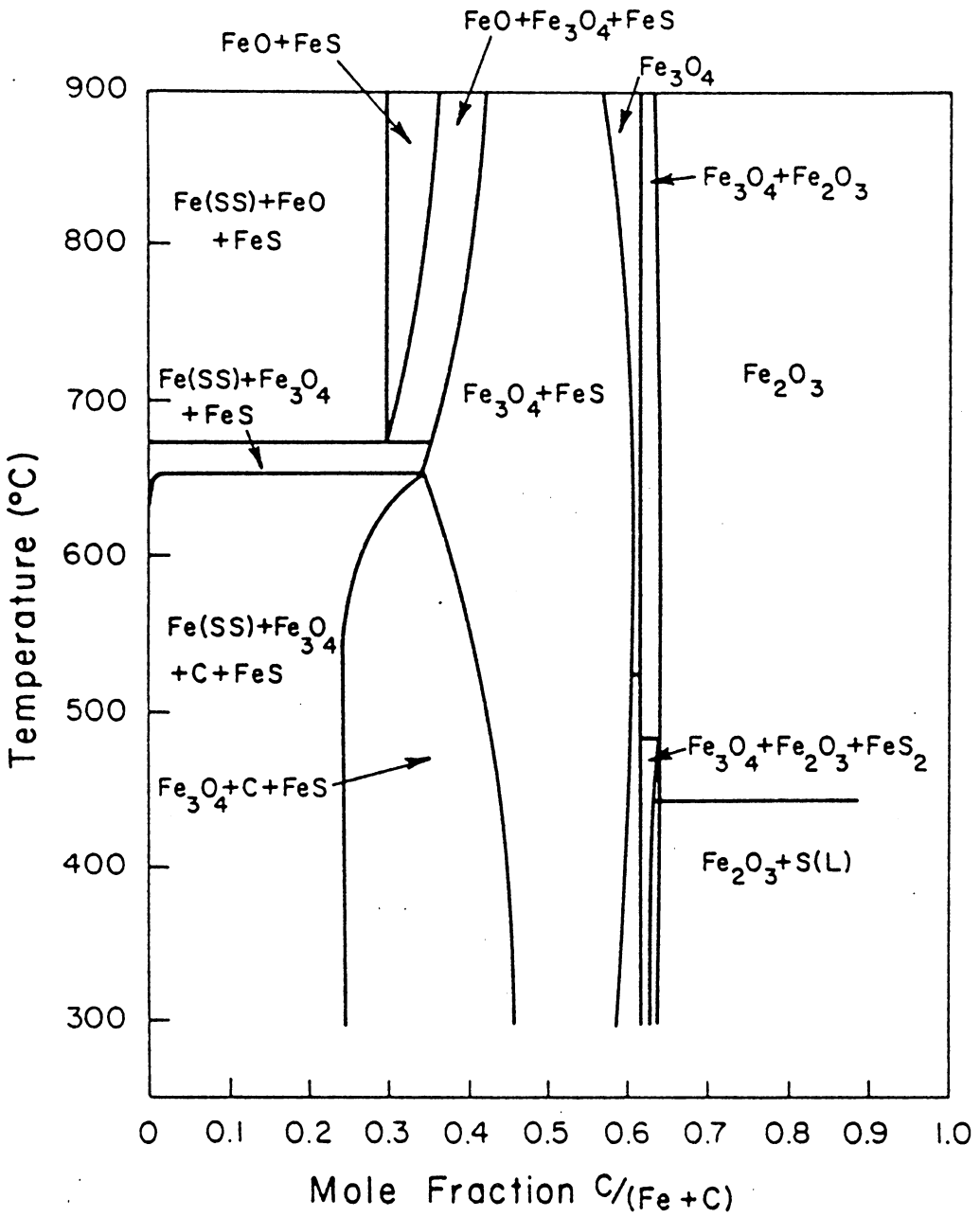

Fig. 7(d) (i) Phase Map of System Fe - CO - CO_2 - H_2O - CH_4 - H_2S - NH_3 at 1 atm. (Mole Fraction C/(C + O) = 0.8, H/(C + H) = 0.7, N/(C + N) = 0.03, S/(C + S) = 0.015)

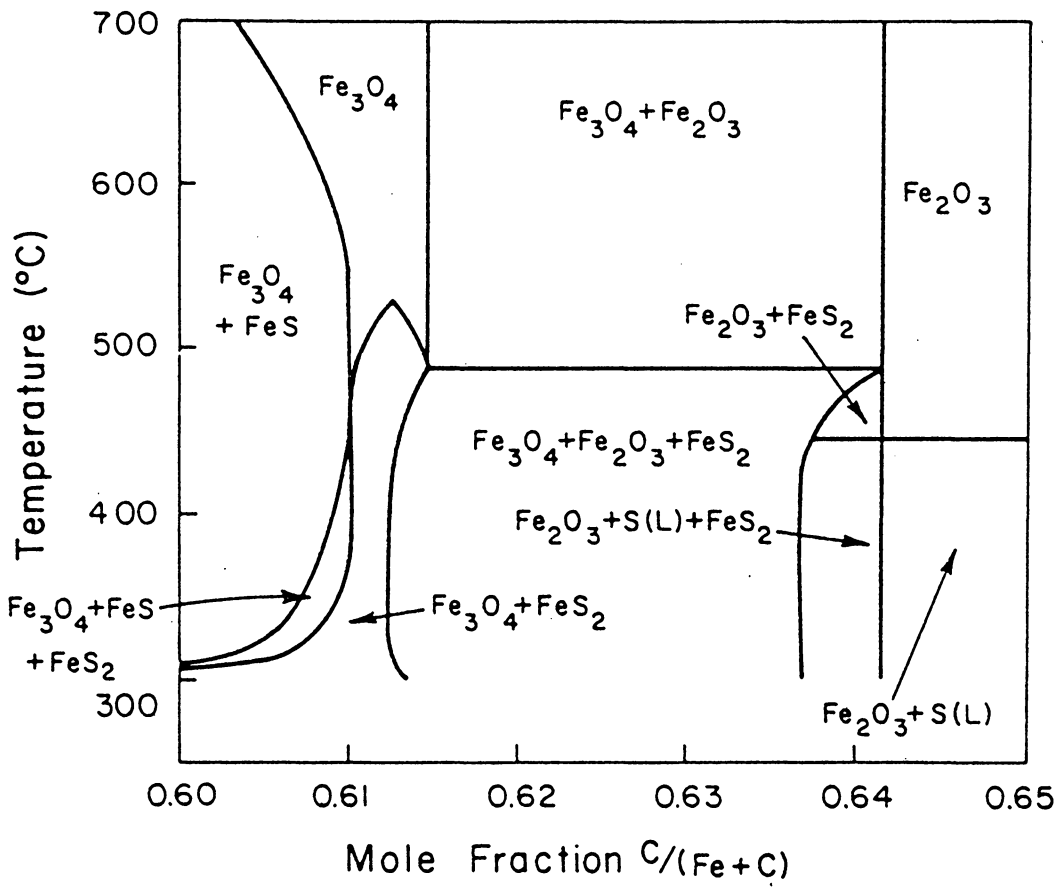

Fig. 7(d) (ii) The Magnified Graph of the Portion of C/(Fe + C) = 0.60 - 0.65 of Fig. 7(d) (i)

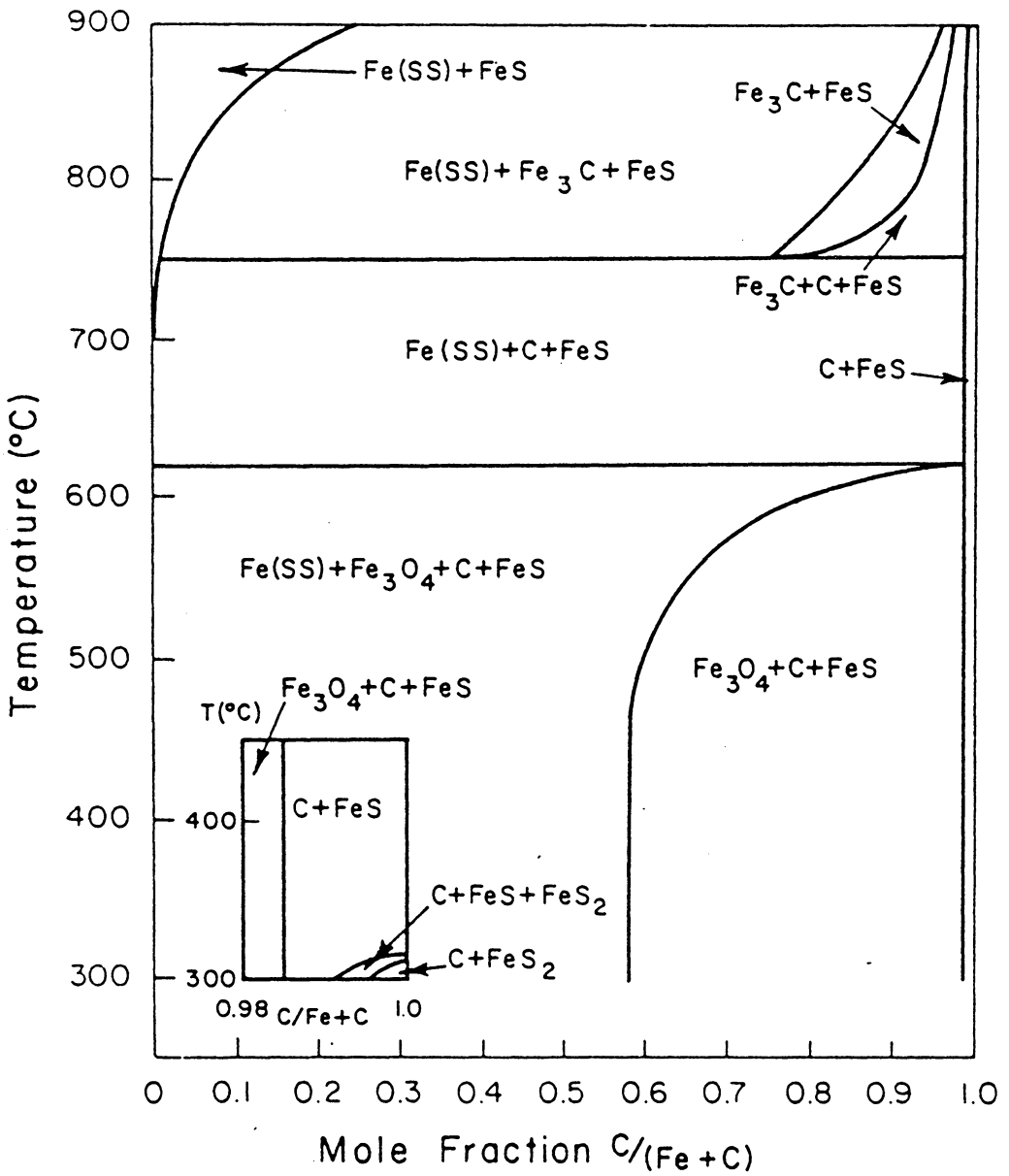

Fig. 8(a) Phase Map of Systems Fe - CO - CO_2 - H_2O - CH_4 - H_2S - NH_3 at 1 atm. (Mole Fraction O/(C + O) = 0.5, H/(C + H) = 0.8, N/(C + N) = 0.03, S/(C + S) = 0.015)

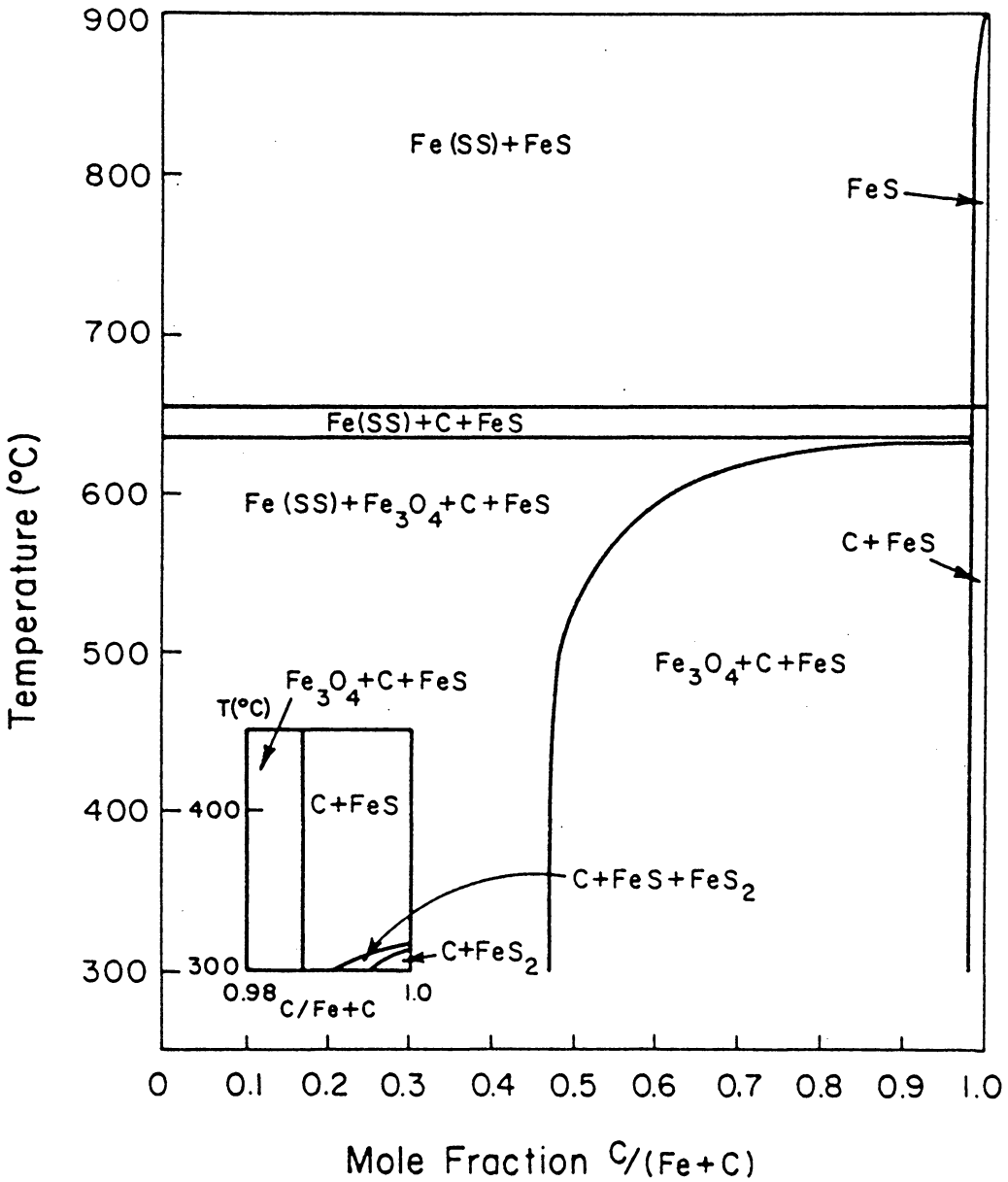

Fig. 8(b) Phase Map of Systems Fe - CO - CO_2 - H_2O - CH_4 - H_2S - NH_3 at 1 atm. (Mole Fraction O/(C + O) = 0.6, H/(C + H) = 0.8, N/(C + N) = 0.03, S/(C + S) = 0.015)

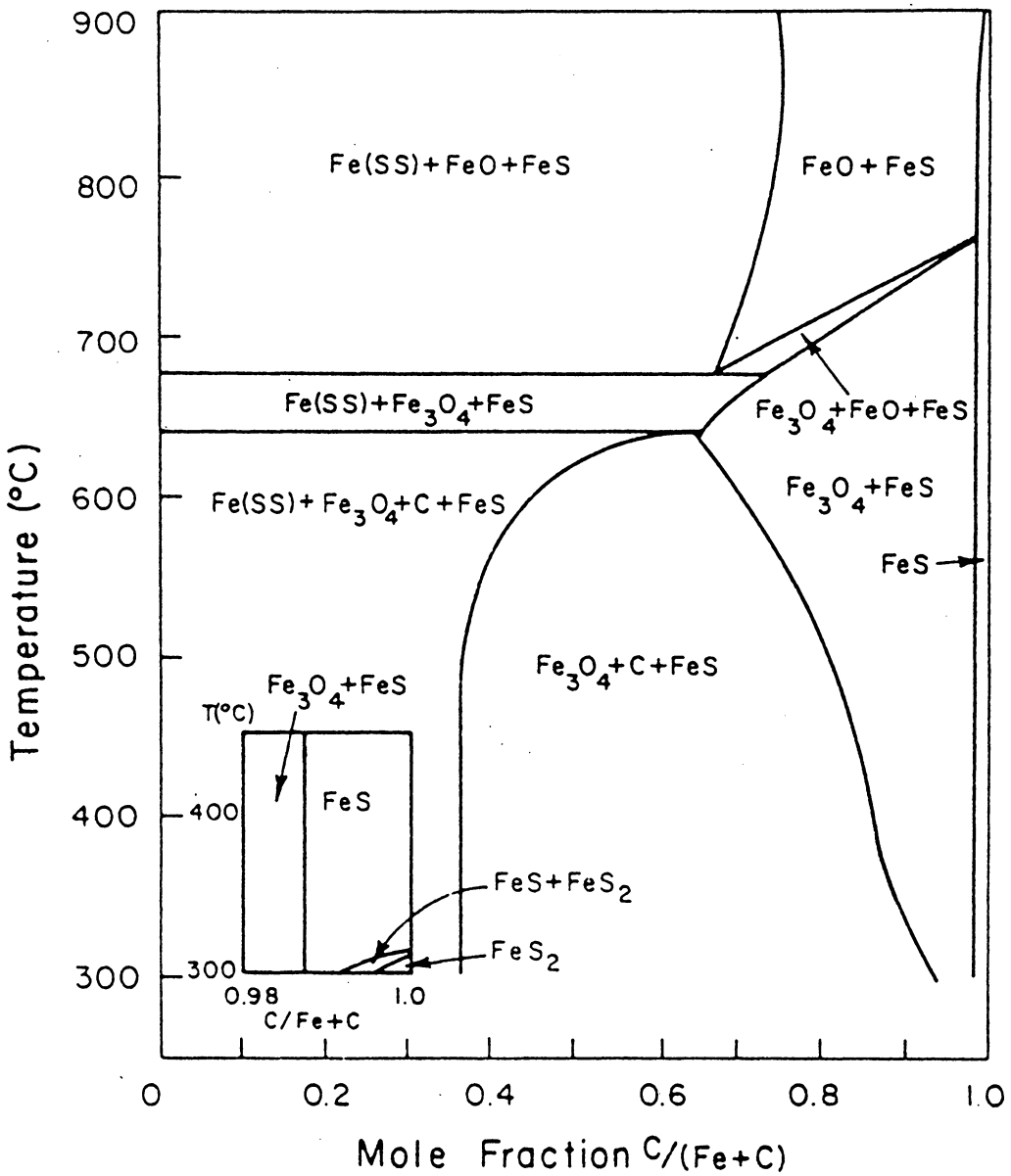

Fig. 8(c) Phase Map of System Fe - CO - CO_2 - H_2O - CH_4 - H_2S - NH_3 at 1 atm. (Mole Fraction O/(C + O) = 0.7, H/(C + H) = 0.8, N/(C + N) = 0.03, S/(C + S) = 0.015)

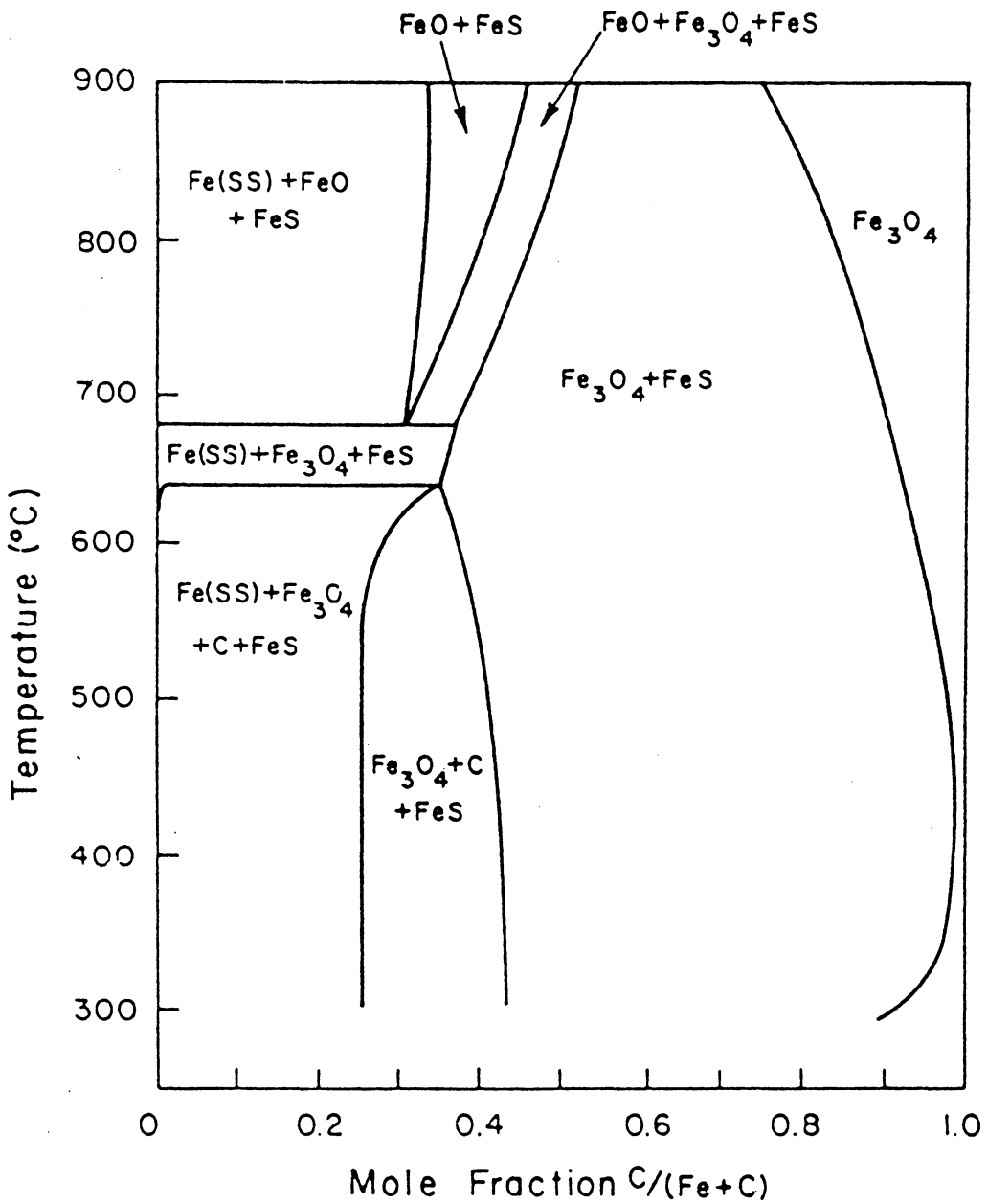

Fig. 8(d) (i) Phase Map of System Fe - CO - CO_2 - H_2O - CH_4 - H_2S - NH_3 at 1 atm. (Mole Fraction O/(C + O) = 0.8, H/(C + H) = 0.8, N/(C + N) = 0.03, S/(C + S) = 0.015)

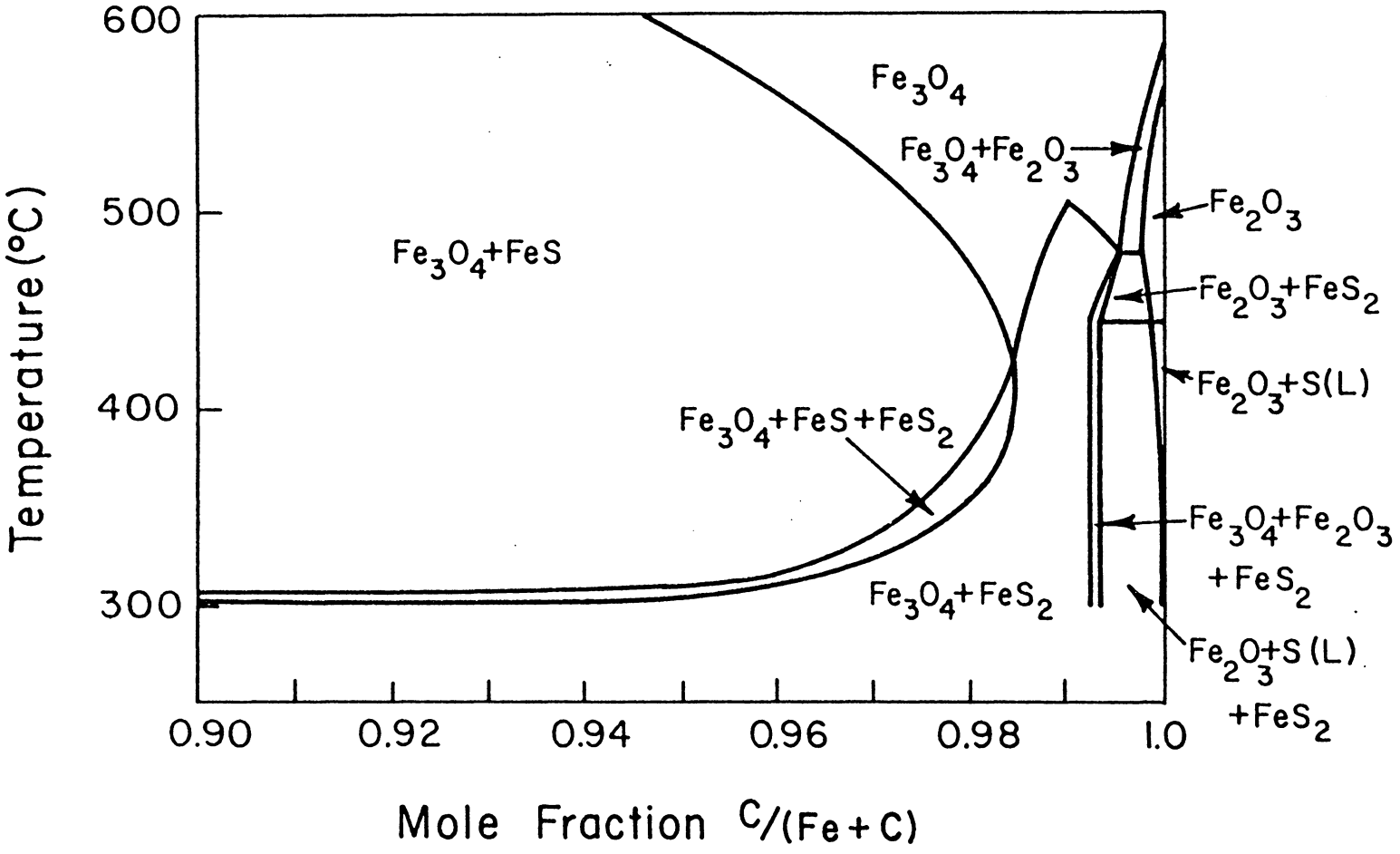

Fig. 8(d) (ii) The Lower Right Corner of Fig. 8(d) (i)

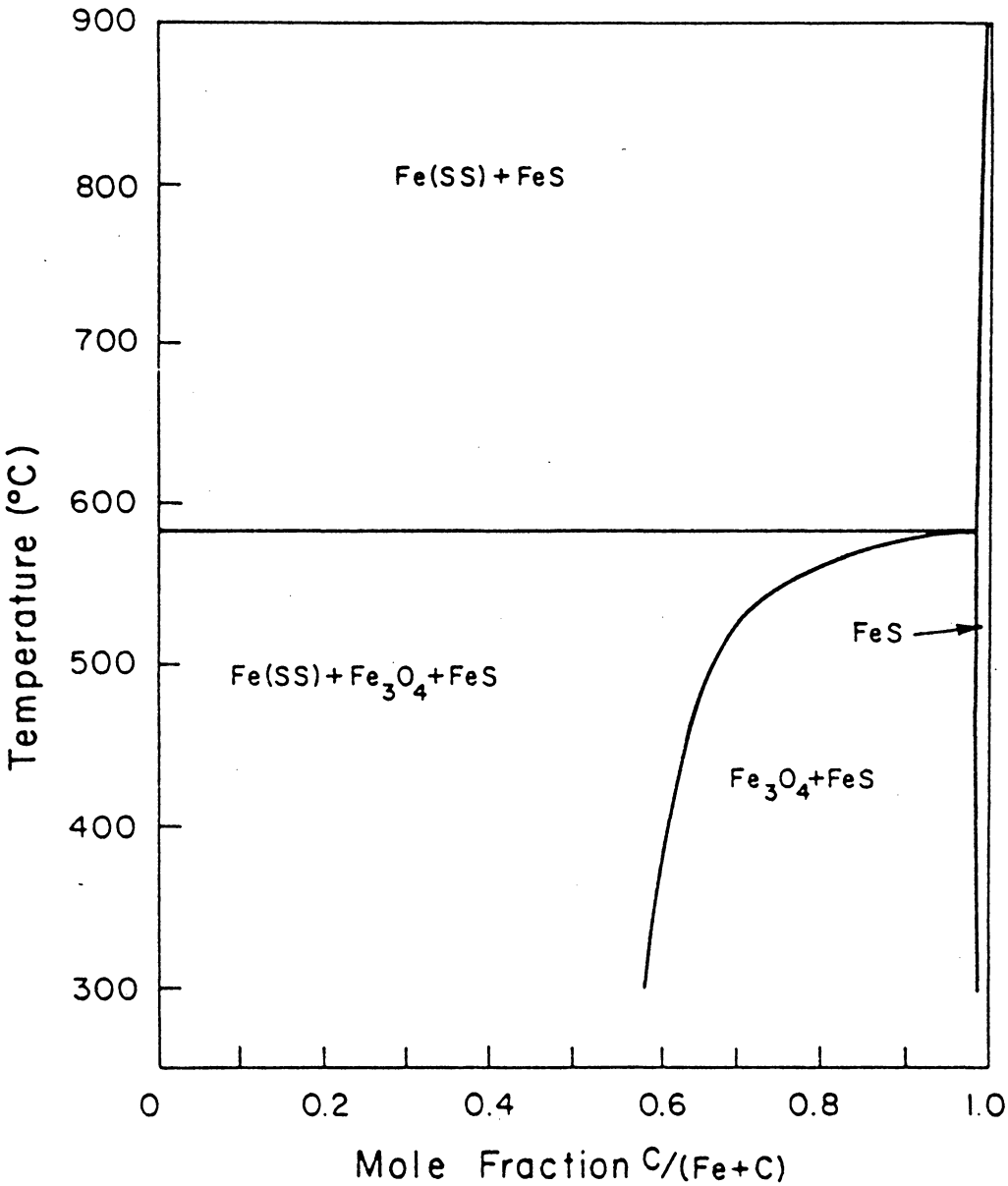

Fig. 9(a) Phase Map of System Fe - CO - CO_2 - H_2O - CH_4 - H_2S - NH_3 at 1 atm. (Mole Fraction O/(C + O) = 0.5, H/(C + H) = 0.9, N/(C + N) = 0.03, S/(C + S) = 0.015)

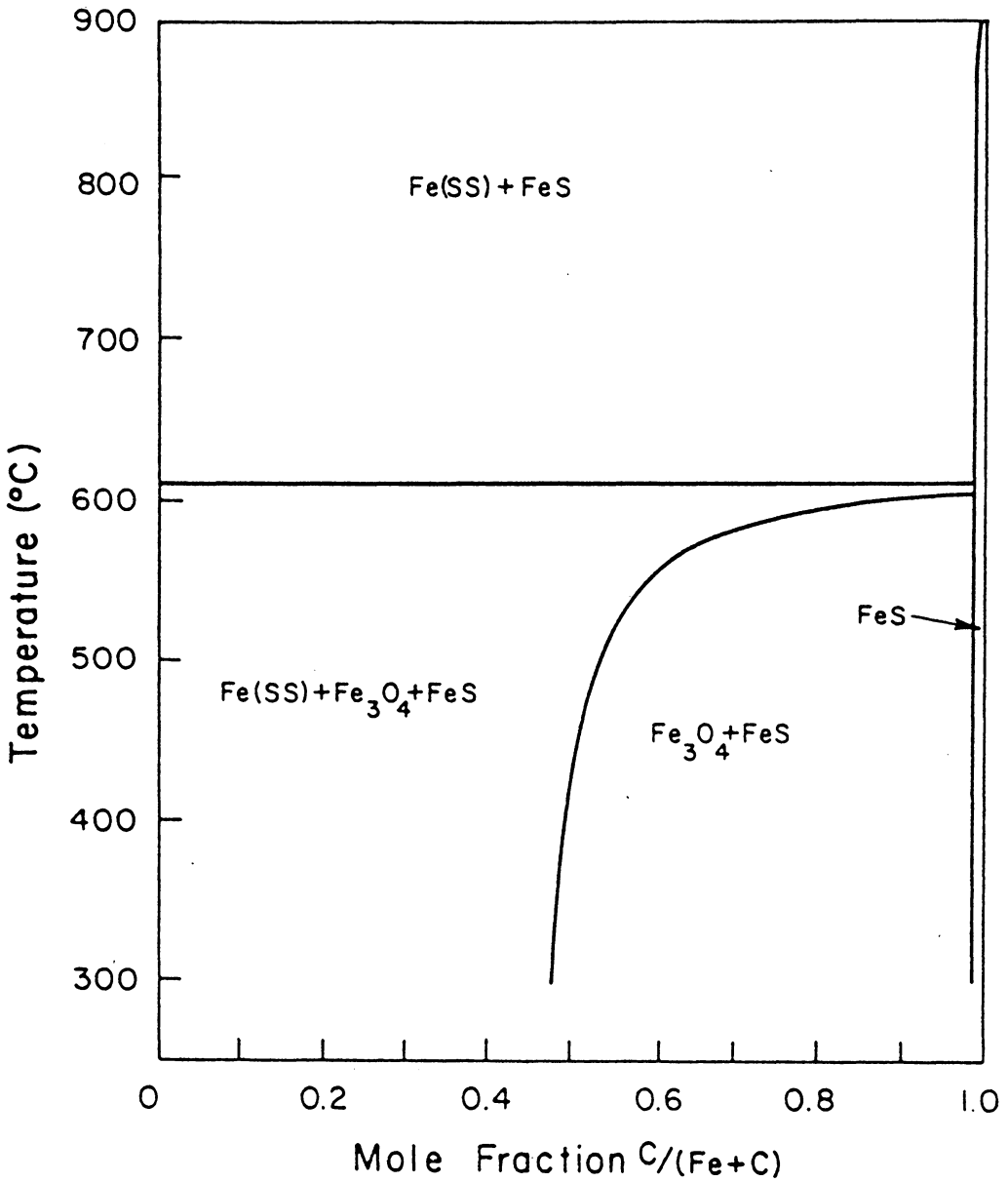

Fig. 9(b) Phase Map of System Fe - CO - CO_2 - H_2O - CH_4 - H_2S - NH_3 at 1 atm. (Mole Fraction O/(C + O) = 0.6, H/(C + H) = 0.9, N/(C + N) = 0.03, S/(C + S) = 0.015)

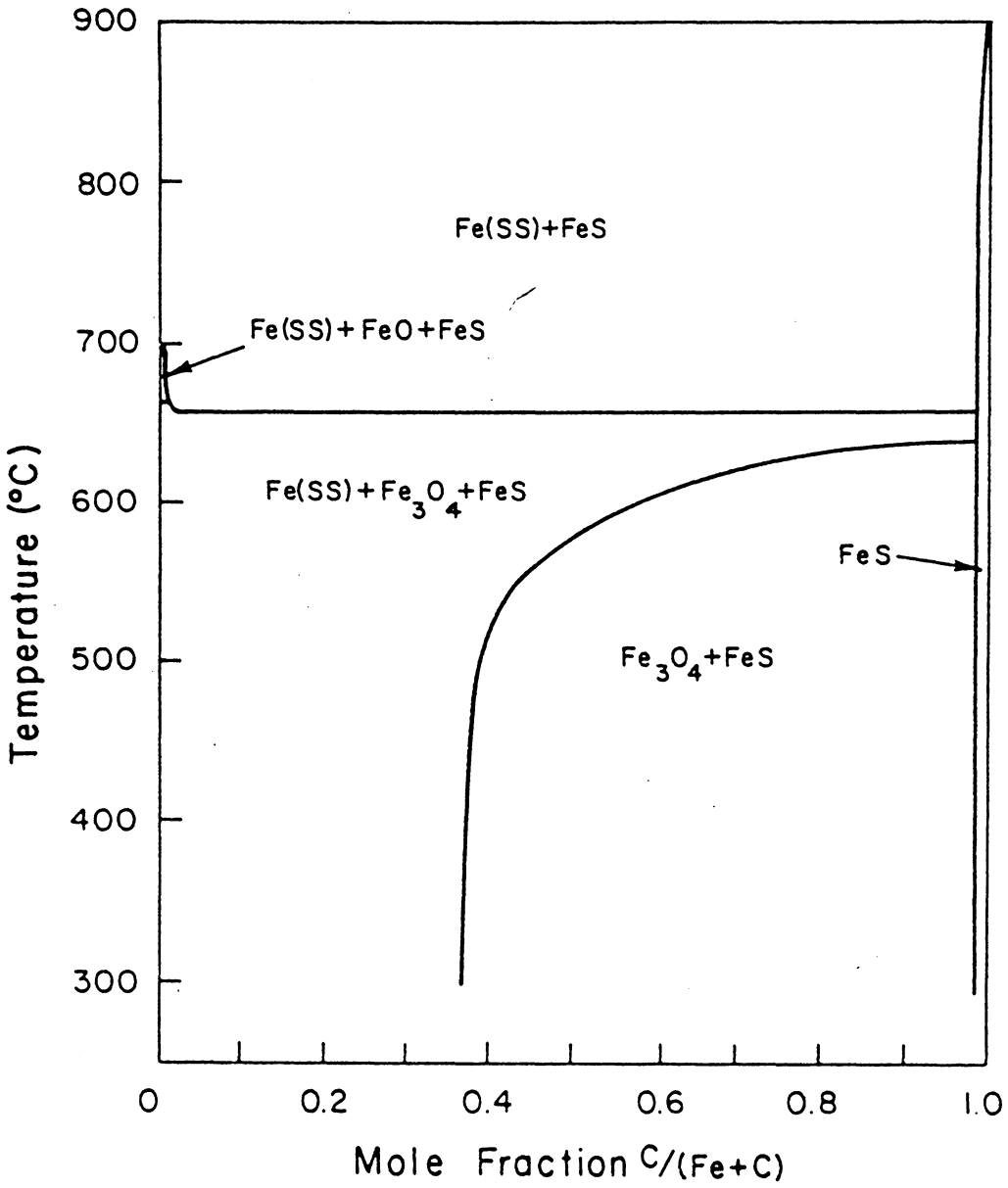

Fig. 9(c) (i) Phase Map of System Fe - CO - CO_2 - H_2O - CH_4 - H_2S - NH_3 at 1 atm. (Mole Fraction O/(C + O) = 0.7, H/(C + H) = 0.9, N/(C + N) = 0.03, S/(C + S) = 0.015)

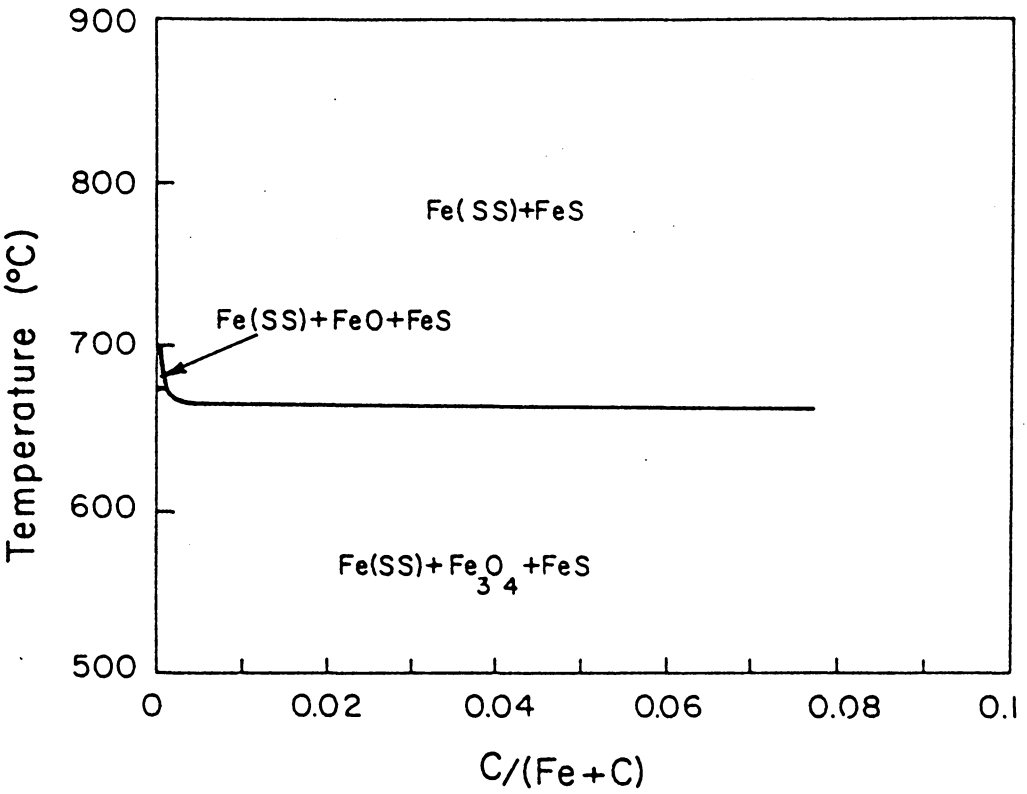

Fig. 9(c) (ii) The Upper Left Corner of Fig. 9(c) (i)

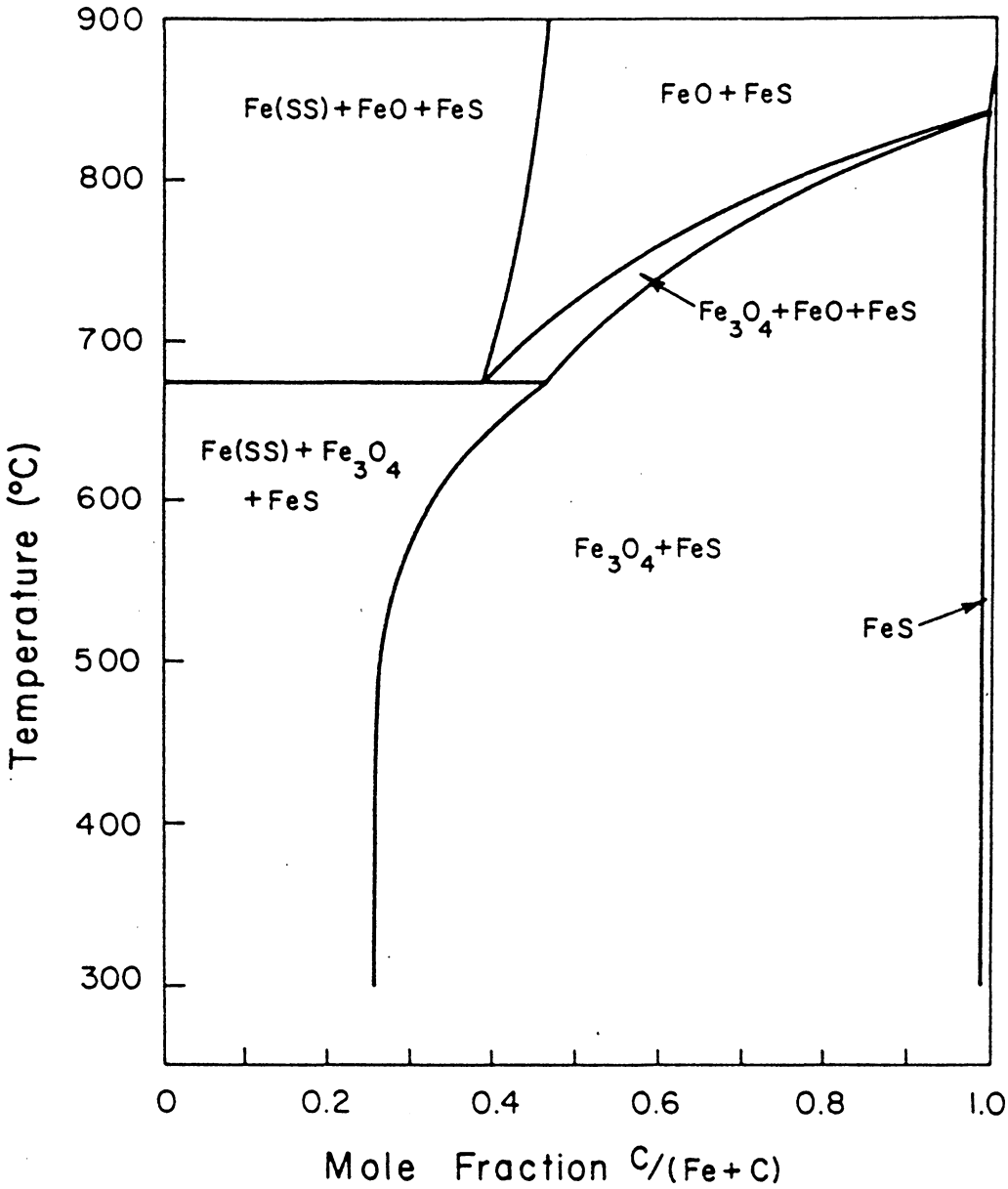

Fig. 9(d) Phase Map of System Fe - CO - CO_2 - H_2O - CH_4 - H_2S - NH_3 at 1 atm. (Mole Fraction O/(C + O) = 0.8, H/(C + H) = 0.9, N/(C + N) = 0.03, S/(C + S) = 0.015)

Table 7. The Effect of Oxygen on the Amount of Carbon Deposit (moles) of System $Fe-CO-CO_2-H_2O-CH_4-NH_3-H_2S$ (1 atm, 500°C, H/C+H = 0.7, N/C+N = 0.03, S/C+S = 0.015)

	Mole Fraction C/Fe + C			
O/C+O	0.5	1.5	2.5	3.5
0.5	0.30762	0.79742	1.276	1.7535
0.6	0.24366	0.54437	0.83999	1.135
0.7	0.08624	0.03139	0	0
0.8	0	0	0	0

Table 8. The Effect of Hydrogen on the Amount of Carbon Deposit (moles) of System Fe-CO-CO_2-H_2O-CH_4-NH_3-H_2S (1 atm, 500°C O/C+O = 0.6, N/C+N = 0.03, S/C+S = 0.015)

	Mole Fraction C/Fe + C			
H/C+H	0.5	1.5	2.5	3.5
0.6	0.27137	0.59231	0.90969	1.2267
0.7	0.24366	0.54437	0.83999	1.135
0.8	0.03935	0	0	0

Figures 10 and 11 are the kinetic curves (weight increment vs time) of Fe_2O_3 pellets for testing carbon monoxide dissociation. Table 9 shows the corresponding results of X-ray diffraction examinations of these samples, in which semi-quantitative analysis (the analysis of the relative amount of iron oxides, Fe and Fe_3C) is calculated according to the following formulas:

$$I = \frac{K_2 R}{2\mu} \tag{10}$$

$$R = \frac{1}{V^2}\left[|F|^2 \, p\left(\frac{1+\cos^2 2\theta}{\sin^2\theta\cos\theta}\right)\right] \tag{11}$$

$$K_2 = \left(\frac{I_o e^4}{m^2 c^4}\right)\left(\frac{\lambda^3 A}{32\pi r}\right) \tag{12}$$

where I —— integrated intensity per unit length of diffraction line

I_o —— intensity of incident beam

e, m —— charge and mass of the electron, respectively

c —— velocity of light

λ —— wavelength of incident radiation

r —— radius of diffractometer circle

A —— cross-sectional area of incident beam

V —— volume of unit cell

F —— structural factor (a function of θ)

μ —— linear absorption coefficient

p —— multiplicity factor

θ —— angle of x-ray incidence at which the strongest diffraction line occurs

$$F_{HKL} = \sum_{1}^{n} fn\, e^{2\pi i(HU_n+KV_n+LW_n)} \qquad (13)$$

where fn —— atomic scattering factor of each atom in unit cell

(H K L) —— Bragg diffraction indices of the crystal plane at which the strongest diffraction line is reflected

U_n, V_n, W_n —— functional coordinates of each atom in unit cell

$$I_\alpha : I_\beta : I_\lambda : \ldots = (R_\alpha C_\alpha) : (R_\beta C_\beta) : (R_\lambda C_\lambda) : \cdots \qquad (14)$$

$$C_\alpha + C_\beta + C_\lambda + \ldots = 1 \qquad (15)$$

where α, β, λ —— phases present in the sample volume

$C_\alpha, C_\beta, C_\lambda$ —— fractions of α, β, λ phases, respectively.

The whole process may be divided into several stages. In order to verify the reactions (2) - (8), the first three stages will be discussed here.

(A) Reduced stage. The first stage is the process of the reduction of Fe_2O_3. This can be verified by weight loss ($\Delta W<0$), X-ray diffraction data and the calculation of activation energy.

According to X-ray diffraction data (Table 9), the first stage can further be divided into two substages.

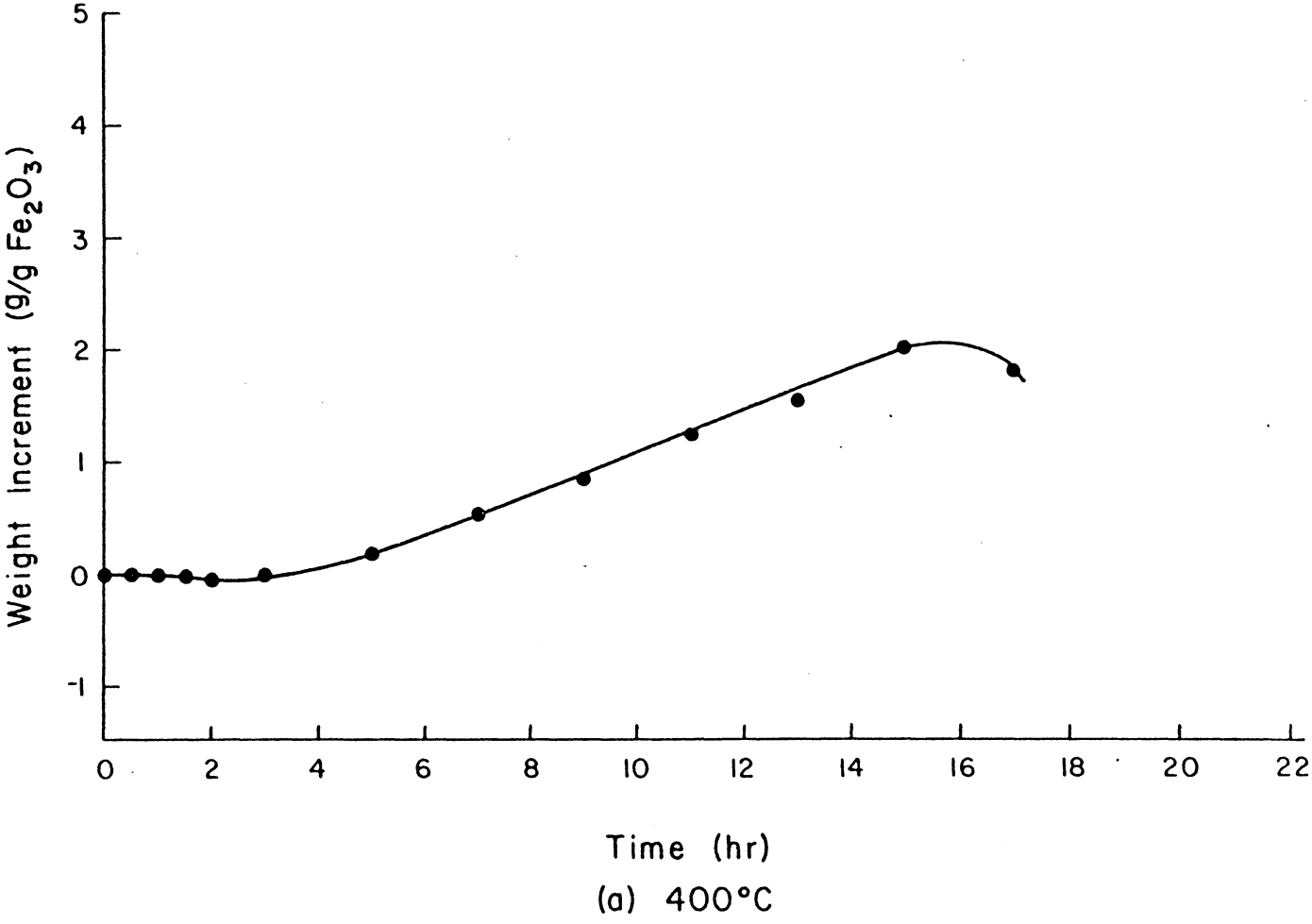

Fig. 10(a) Kinetic Curves for Carbon Monoxide Disintegration on Fe_2O_3 at Different Temperatures (1 atm., The Flow Rate of CO is 35 ml/min)

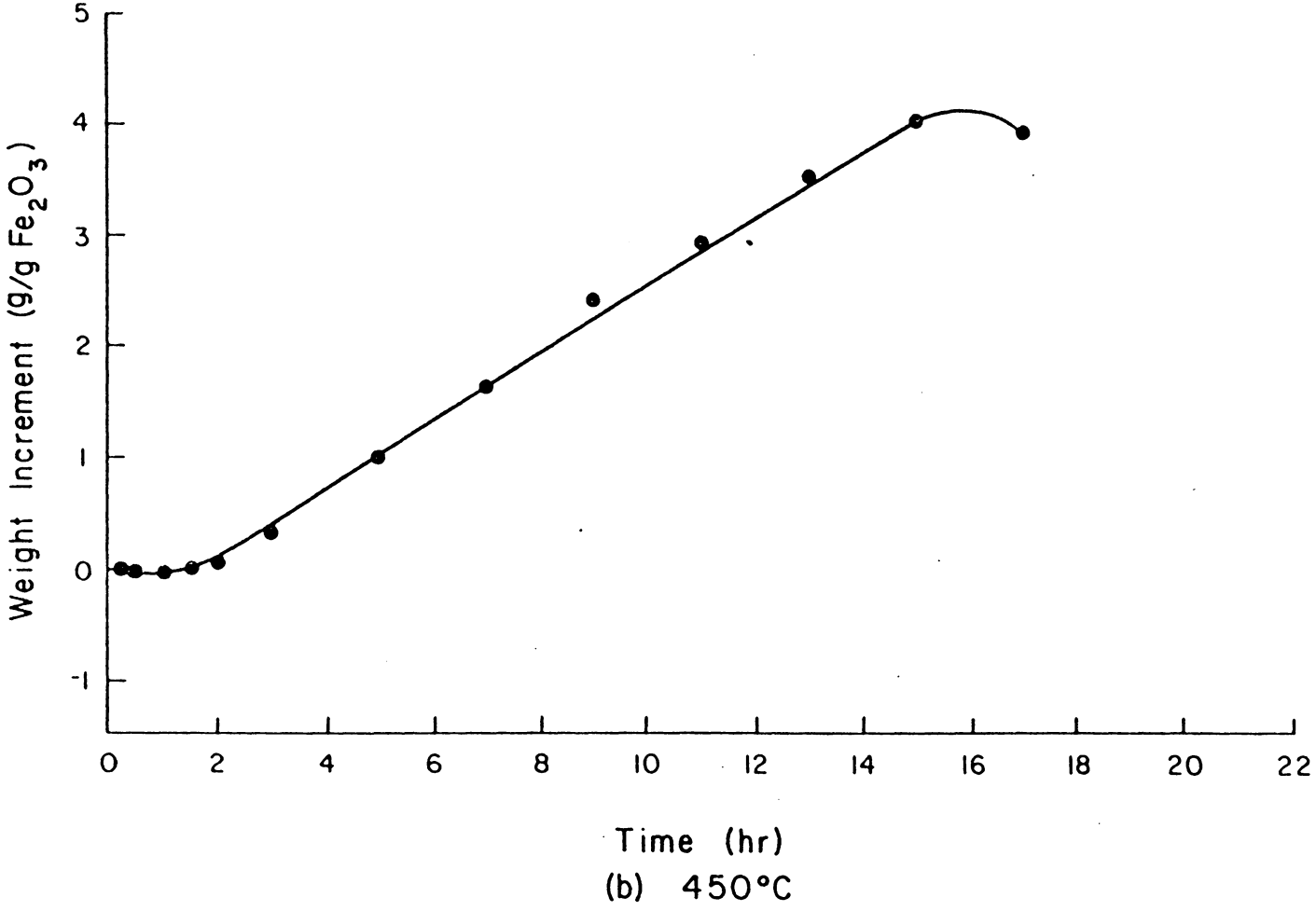

Fig. 10(b) Kinetic Curves for Carbon Monoxide Disintegration on Fe_2O_3 at Different Temperatures (1 atm., The Flow Rate of CO is 35 ml/min)

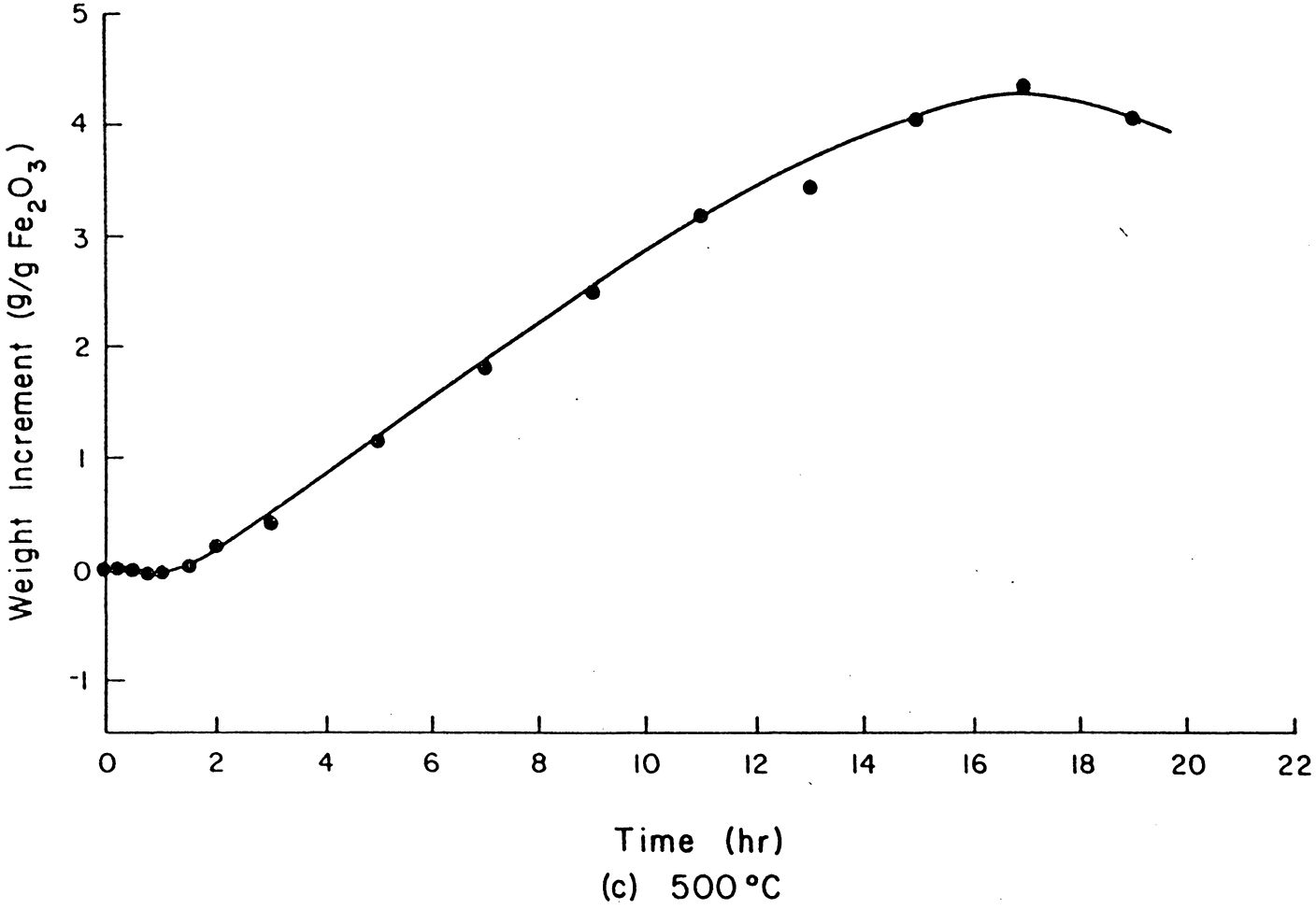

Fig. 10(c) Kinetic Curves for Carbon Monoxide Disintegration on Fe_2O_3 at Different Temperatures (1 atm., The Flow Rate of CO is 35 ml/min)

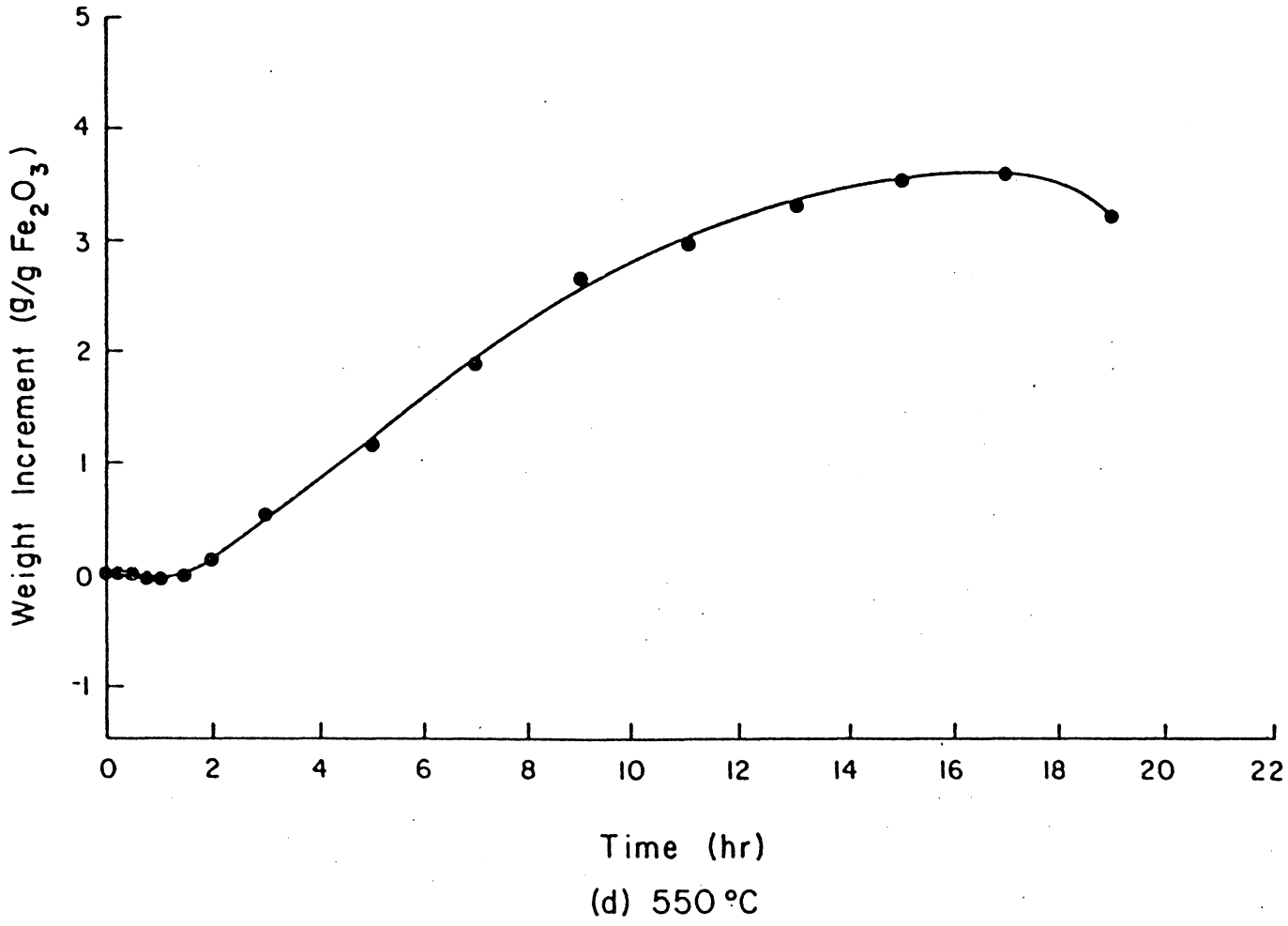

Fig. 10(d) Kinetic Curves for Carbon Monoxide Disintegration on Fe_2O_3 at Different Temperatures (1 atm., The Flow Rate of CO is 35 ml/min)

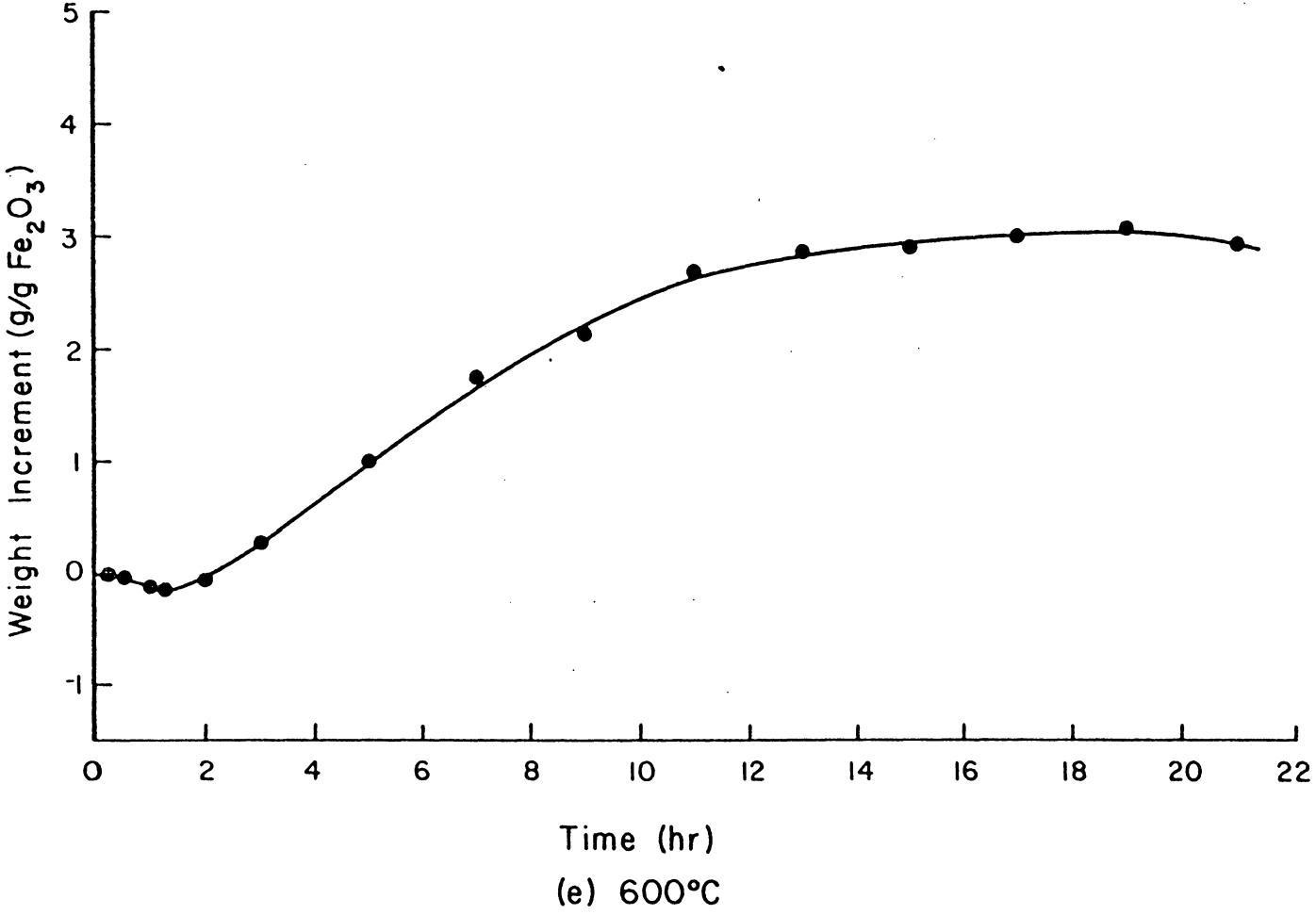

Fig. 10(e) Kinetic Curves for Carbon Monoxide Disintegration on Fe_2O_3 at Different Temperatures (1 atm., The Flow Rate of CO is 35 ml/min)

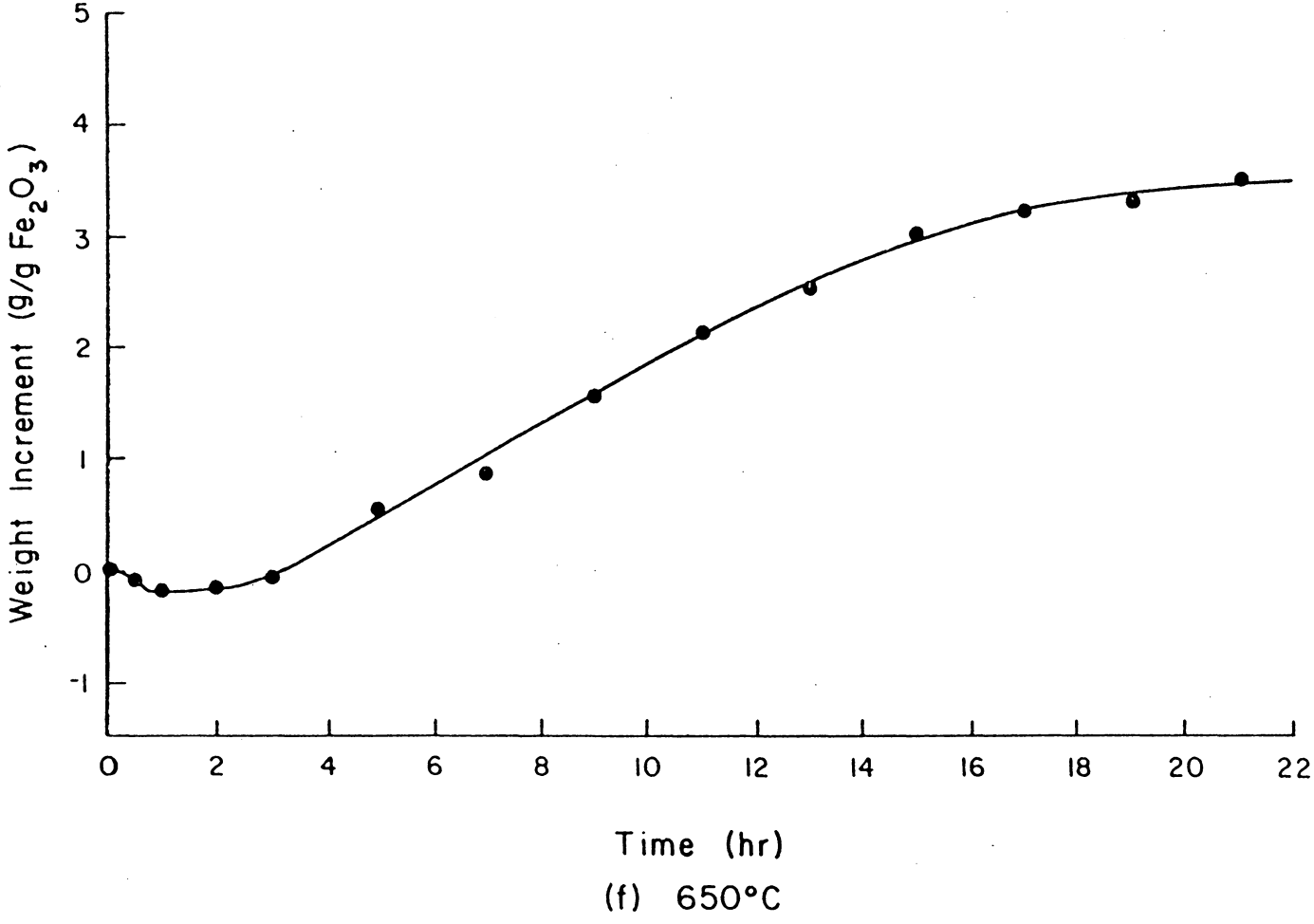

Fig. 10(f) Kinetic Curves for Carbon Monoxide Disintegration on Fe_2O_3 at Different Temperatures (1 atm., The Flow Rate of CO is 35 ml/min)

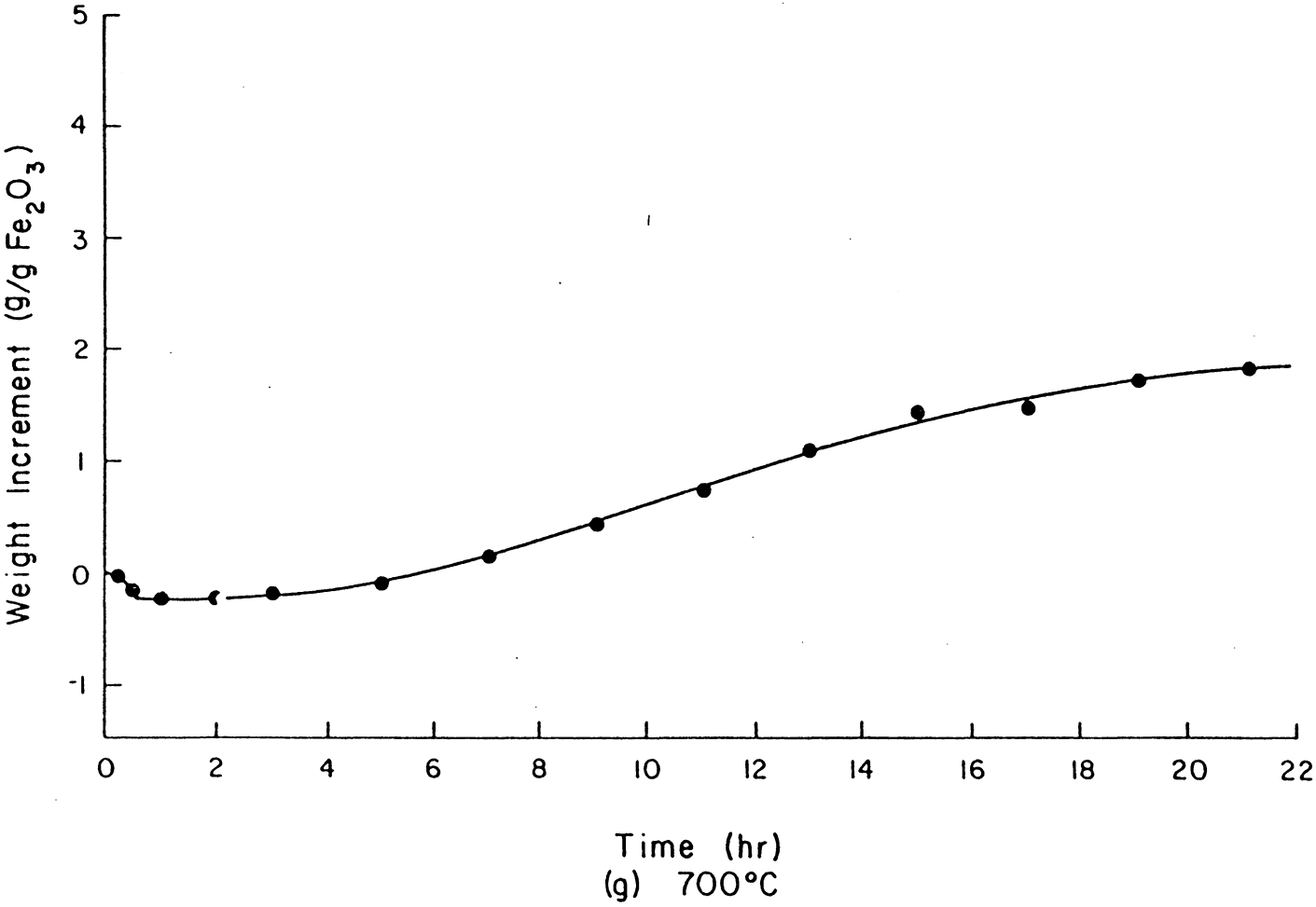

Fig. 10(g) Kinetic Curves for Carbon Monoxide Disintegration on Fe_2O_3 at Different Temperatures (1 atm., The Flow Rate of CO is 35 ml/min)

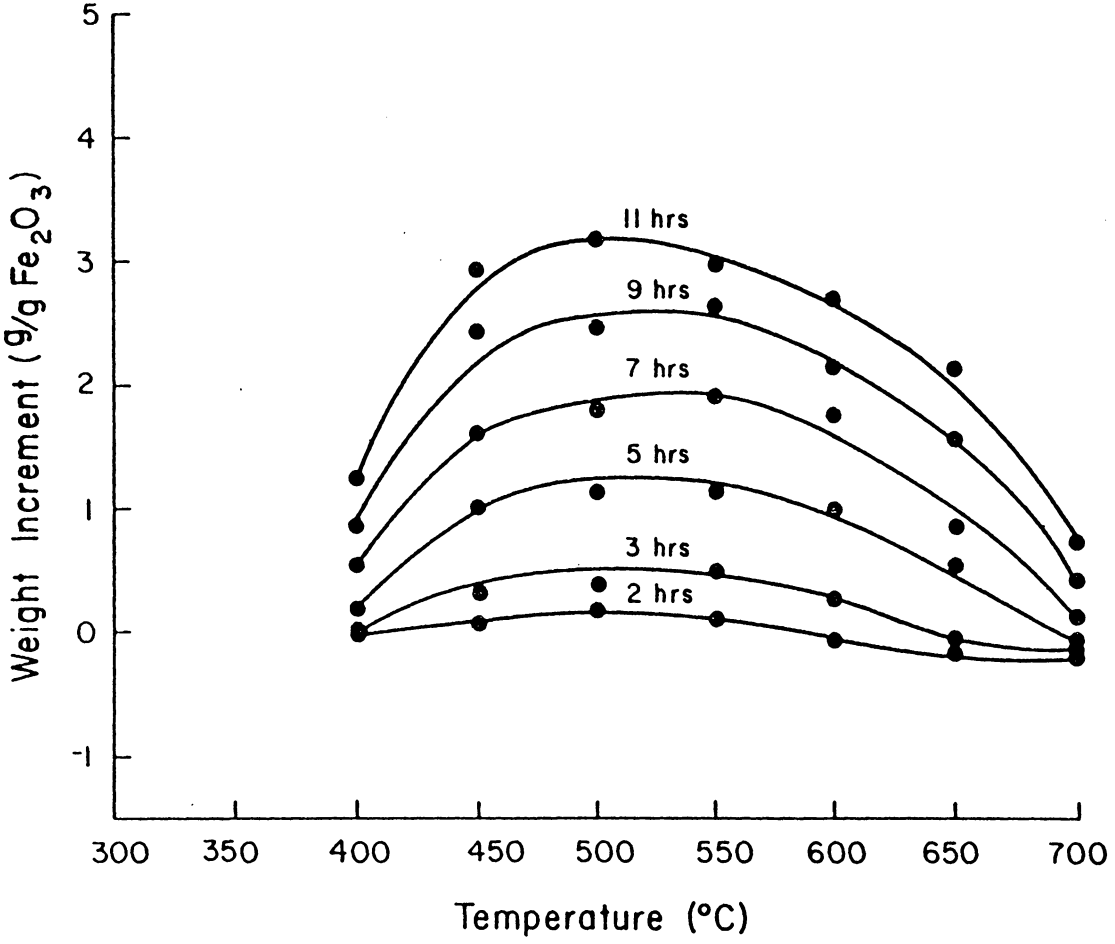

Fig. 10(h) Kinetic Curves for Carbon Monoxide Disintegration on Fe_2O_3 at Different Temperatures (1 atm., The Flow Rate of CO is 35 ml/min)

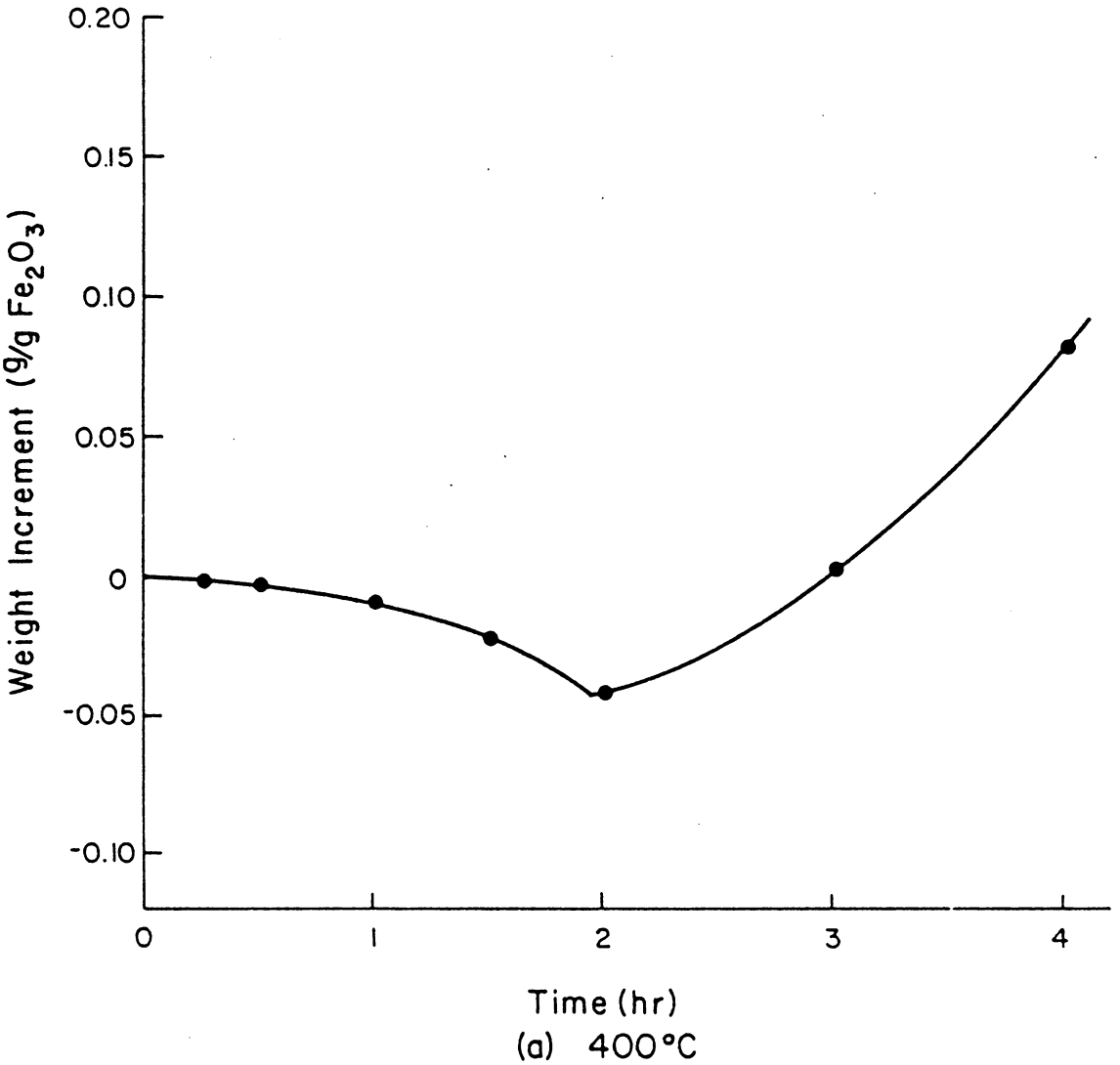

Fig. 11(a) Kinetic Curves of Carbon Monoxide Disintegration on Fe_2O_3 at First Few Hours (1 atm., The Flow Rate of CO is 35 ml/min)

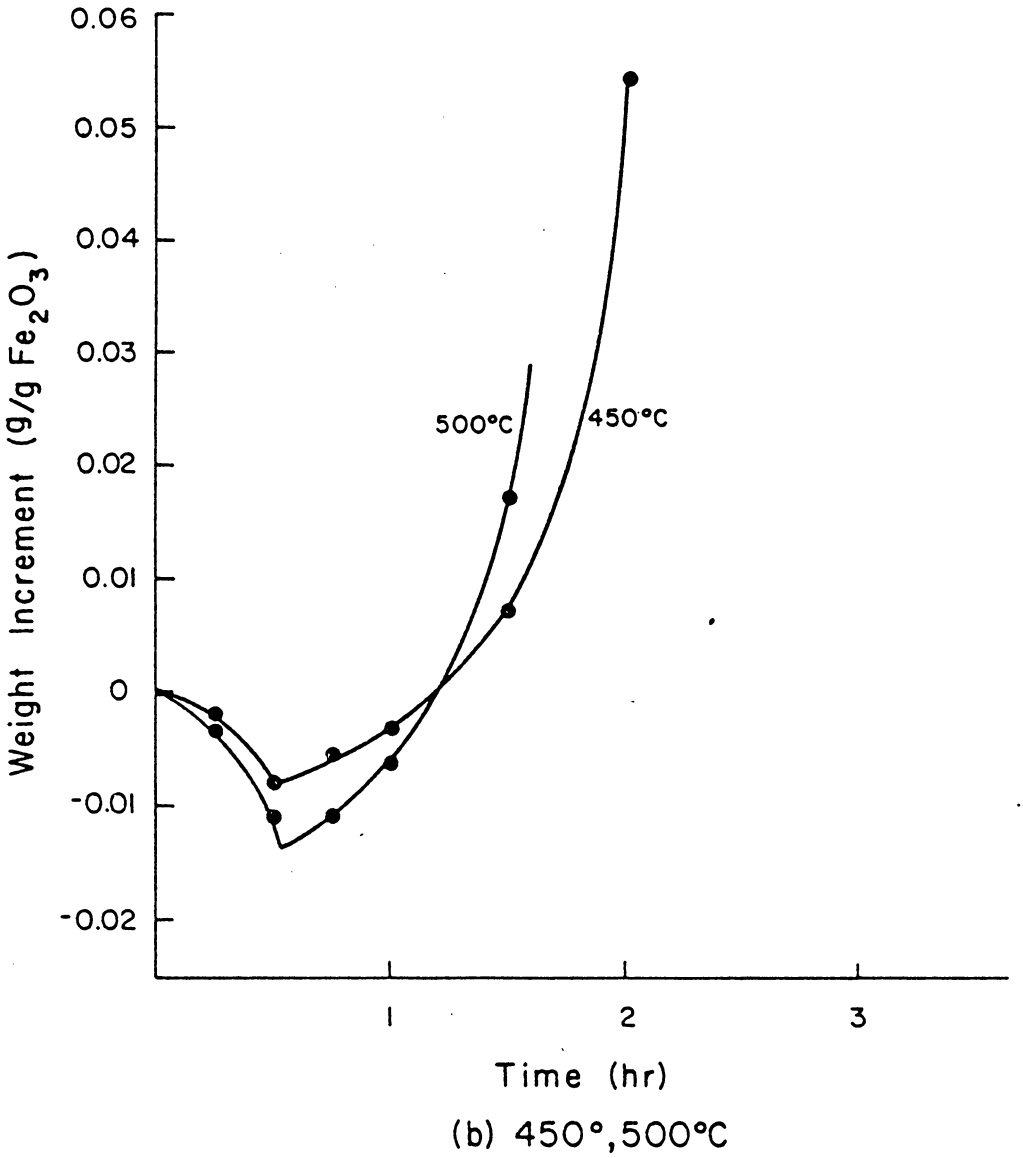

Fig. 11(b) Kinetic Curves of Carbon Monoxide Disintegration on Fe_2O_3 at First Few Hours (1 atm., The Flow Rate of CO is 35 ml/min)

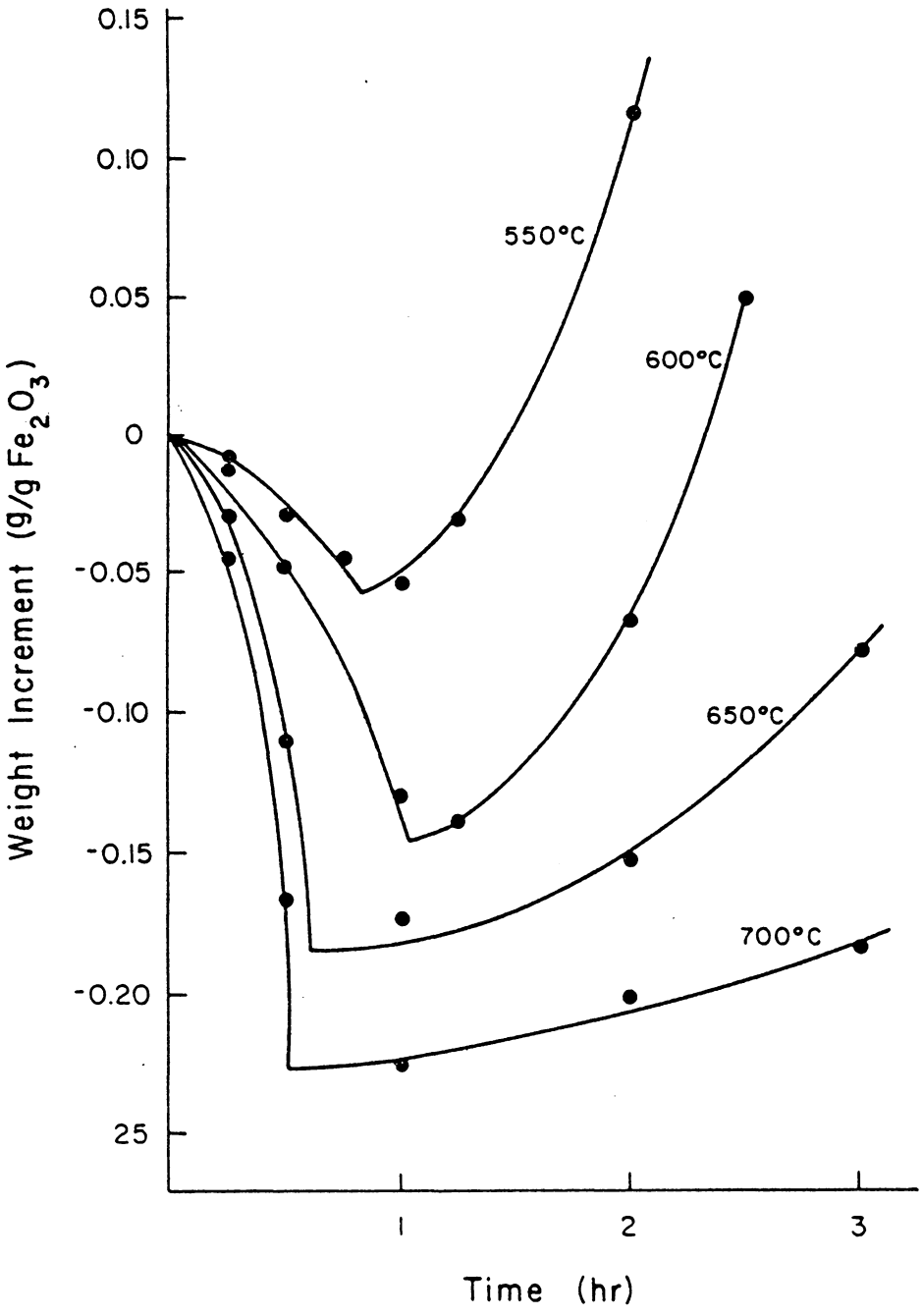

(c) 550°, 600°, 650° and 700°C

Fig. 11(c) Kinetic Curves of Carbon Monoxide Disintegration on Fe_2O_3 at First Few Hours (1 atm., The Flow Rate of CO is 35 ml/min)

Table 9. The Results of X-Ray Diffraction Patterns of Samples Corresponding to the Kinetic Curves in Figure 10

(a) 450°C

Test Time (hr)	Volume %							
	Fe_2O_3	Fe_3O_4	FeO	Fe	Fe_3C	Fe_2C	FeC	G
$\frac{1}{4}$	>99	Tr.	-	-	-	-	-	-
$\frac{1}{2}$	-	Tr.	-	Tr.	Bal	-	-	-
1	-	Tr.	-	Tr.	Bal	W	W	W
3	-	Tr.	-	Tr.	Bal	W	W	S
5	-	Tr.	-	Tr.	Bal	W	M	VS
7	-	Tr.	-	Tr.	Bal	M	M	VS
9	-	Tr.	-	Tr.	Bal	M	M	VS
13	-	Tr.	-	Tr.	Bal	M	M	VS
17	-	-	-	Tr.	Bal	M	M	VS

W - weak diffraction lines

M - medium diffraction lines

S - strong

VS - very strong

Tr. - Trace (< 1%)

(b) 500°C

Test Time (hr)	Volume %							
	Fe_2O_3	Fe_3O_4	FeO	Fe	Fe_3C	Fe_2C	FeC	G
$\frac{1}{4}$	97	3	-	-	-	-	-	-
$\frac{1}{2}$	10	2.5-3	-	Tr.	Bal	W	W	S
1	-	1-2	-	Tr.	Bal	W	W	S
3	-	Tr.	-	Tr.	Bal	W	M	VS
5	-	Tr.	-	Tr.	Bal	M	M	VS
9	-	-	-	Tr.	Bal	M	M	VS
13	-	-	-	Tr.	Bal	M	M	VS
17	-	-	-	Tr.	Bal	M	M	VS

(c) 550°C

Test Time (hr)	Volume %							
	Fe_2O_3	Fe_3O_4	FeO	Fe	Fe_3C	Fe_2C	FeC	G
$\frac{1}{4}$	-	2.5	1.5-2	Tr.	Bal	-	-	-
$\frac{1}{2}$	-	Tr.	Tr.	Tr.	Bal	-	-	-
1	-	Tr.	Tr.	Tr.	Bal	W	W	W
3	-	Tr.	Tr.	Tr.	Bal	W	M	S
5	-	Tr.	Tr.	Tr.	Bal	M	M	VS
9	-	Tr.	-	Tr.	Bal	M	M	VS
13	-	Tr.	-	Tr.	Bal	M	M	VS

(d) 650°C

Test Time (hr)	Volume %							
	Fe_2O_3	Fe_3O_4	FeO	Fe	Fe_3C	Fe_2C	FeC	G
$\frac{1}{4}$	-	4-4.5	93-94	2-2.5	-	-	-	-
1	-	-	1.5-2	Tr.	Bal	-	W	W
3	-	-	-	Tr.	Bal	W	W	W
5	-	-	-	Tr.	Bal	W	W	S
7	-	-	-	Tr.	Bal	W	M	VS
9	-	-	-	Tr.	Bal	M	M	VS
13	-	-	-	Tr.	Bal	M	M	VS
17	-	-	-	Tr.	Bal	M	M	VS

(e) 700°C

Test Time (hr)	Volume %							
	Fe_2O_3	Fe_3O_4	FeO	Fe	Fe_3C	Fe_2C	FeC	G
$\frac{1}{4}$	7.0	Tr.	4-5	Tr.	Bal	-	-	-
$\frac{1}{2}$	-	Tr.	4	Tr.	Bal	-	W	W
1	-	Tr.	Tr.	Tr.	Bal	-	W	W
3	-	Tr.	Tr.	Tr.	Bal	W	M	W
5	-	Tr.	Tr.	Tr.	Bal	W	M	S
7	-	-	-	Tr.	Bal	W	M	S
9	-	-	-	Tr.	Bal	M	M	S
13	-	-	-	Tr.	Bal	M	M	VS
17	-	-	-	Tr.	Bal	M	M	VS

(a) Early first stage. Table 9 illustrates that at the beginning of these experiments, Fe_2O_3 is dramatically reduced to Fe_3O_4 and/or FeO. This process can also be substantiated by the calculation of activation energies. Kinetic curves (Figure 11) show that the plots of weight loss vs. time for the early first stage are parabolic curves, so that

$$\Delta W = at^2$$

The rate of this process is expressed as

$$R_1 = - \frac{d(\Delta W)}{dt} = -2at \qquad (16)$$

The calculated R_1 values are listed in Table 10. Correspondingly, Arrhenius plot ($\ln R_1$ vs. 1/T) is shown in Figure 12 *, in which all measured data are fitted by a straight line. The activation energy calculated by using the Arrhenius equation is 17,000 cal/mole, which is the same order of magnitude of the activation energy of chemical reaction (10,000 - 100,000 cal/mole). Therefore, at the early first stage, the process is a chemical reaction.

Referring to the X-ray data (Table 9), it is evident that this chemical reaction is the reduction of α-Fe_2O_3 because, at the early first stage, the occurrence and increas-

*In view of errors in measurement, error bars are introduced in all Arrhenius plots.

Table 10. The Rates of Reaction at Early First Stage.

Temperature ^{o}C	400	450	500	550	600	650	700
a	-0.0117	-0.0352	-0.0538	-0.1472	0.1904	-0.4392	-0.7104
R_1 0.01 hr * ($g/gFe_2O_3 \cdot hr$)	2.34×10^{-4}	7.04×10^{-4}	1.076×10^{-3}	2.944×10^{-3}	3.808×10^{-3}	8.784×10^{-3}	1.4208×10^{-2}
$\ln R_1$ 0.01	-8.3602	-7.2587	-6.8345	-5.8280	-5.5706	-4.7348	-4.2540

* Because the purpose of this calculation is to obtain the activation energy of this reaction by Arrhenius equation, $\ln \frac{R_1}{R_2} = \frac{Q}{R} (\frac{1}{T2} - \frac{1}{T1})$, the time adopted for calculating R_I does not change the value of activation energy.

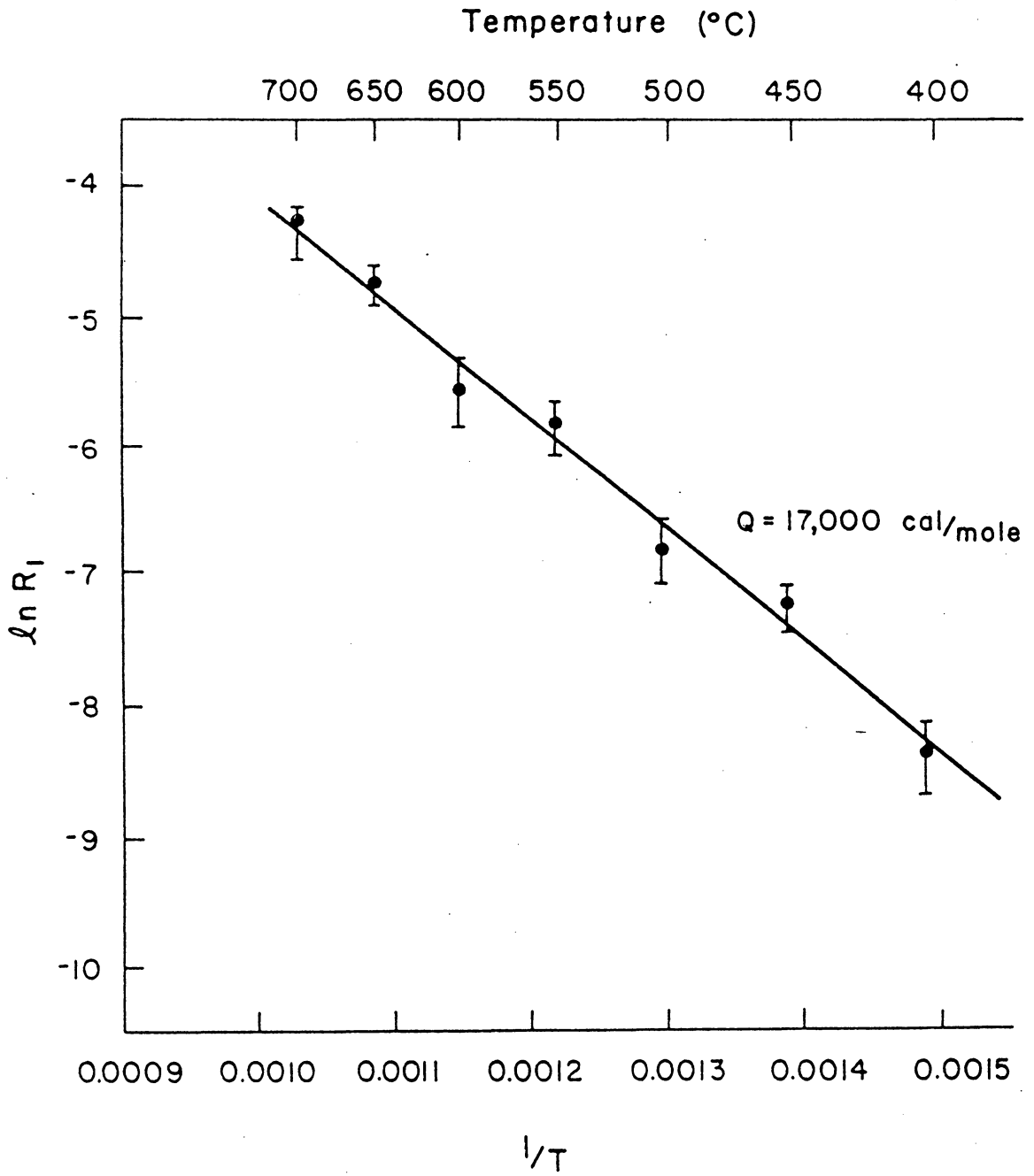

Fig. 12 Plot of $\ln R_1$ vs. 1/T at Early First Stage

ing intensities of Fe_3O_4 and FeO diffraction peaks are related to the weakening of the intensities of α-Fe_2O_3 diffraction peaks. It is also evident that, at temperature below 500°C, the chemical reaction involves the formation of Fe_3O_4, i.e. Fe_2O_3 is reduced to Fe_3O_4; at high temperatures (500°C - 700°C) the chemical reaction involves the formations of both Fe_3O_4 and FeO. The following reactions are consistent with the experimental observations:

$$3Fe_2O_3 + CO = 2Fe_3O_4 + CO_2 \qquad (2)$$

$$Fe_2O_3 + CO = 2FeO + CO_2 \qquad (7)$$

(>500°C)

(b) Late first stage. Fe_3O_4 or FeO generated from the reduction of Fe_2O_3 can further be reduced to Fe, according to the following reactions:

$$Fe_3O_4 + 4CO = 3Fe + 4CO_2 \qquad (3)$$

$$FeO + CO = Fe + CO_2 \qquad (18)$$

The disappearance of the peaks of Fe_3O_4 and/or FeO and the development of the peaks of α-Fe in the X-ray diffraction patterns (Table 9) support the above reactions (3) and (18). However, X-ray diffraction data also show that at late first stage there exist Fe_3C peaks in the samples in addition to the occurrence of α-Fe peaks. In other words, Fe_3C may be formed by the reaction between reduced Fe atoms and CO according to the following reaction[24]

$$3Fe + 2CO = Fe_3C\ ^* + CO_2 \qquad (19)$$

(B) Accelerated stage. The second stage is the process of carbon deposition, with a rate that increases with increasing test time.

(a) To determine whether Fe or Fe_3C catalyzes carbon deposition, an additional experiment was done. Two Fe_3C samples were tested for 1/2 hr at 500°C and 700°C. The results are listed in Table 11. If Fe_3C were the catalyst, both samples should have carbon deposition. Nevertheless, the results did not show this. Instead, the experimental results can explain why active Fe atom is a catalyst. It is well known that Fe_3C is a metastable carbide and its free energy of formation is

$$\Delta_f G \text{ (cal/mole)} = 6940 - 6.70T$$

The lower the temperature, the less the stability of Fe_3C and the easier the decomposition of Fe_3C. Consequently, at 500°C (lower temperature) the Fe atoms generated from the decomposition of Fe_3C catalyzed carbon deposition after 1/2 hr, while at 700°C (higher temperature), the relative stability of Fe_3C, i.e. the absence of decomposed Fe, is res-

---

*Although Fe_3C is a metastable carbide, thermodynamic calculation shows that for reaction (19), G (cal/mole) = -42,495 + 38.24T, i.e. the formation of Fe_3C is favorable in the temperature range used in this work.

Table 11. The Results for Testing Carbon Deposition on Fe_3C at Different Temperatures.

Sample	Test Temperature °C	Test Time (hr)	Flow Rate of CO (ml/min)	Weight Increment (g/g Fe_3C)	Carbon Deposition
Fe_3C (granule)	500°	$\frac{1}{2}$	35	0.0102	Yes
Fe_3C (granule)	700	$\frac{1}{2}$	35	-0.0049	No

ponsible for obtaining a carbon-free sample after 1/2 hr.

(b) Because the development of carbon deposition is always behind the generation of reduced Fe atom, there is an incubation period for carbon deposition, which is mentioned in the literature.[1]

(c) X-ray diffraction data (Figure 13) show that graphite always exists along with FeC and Fe_2C in the samples. The discovery of these intermediates testifies to the existence of predicted reactions (2) - (8).

(d) Activation energy. The rates of carbon deposition at the beginning of the second stage R_2 * listed in Table 12 were calculated from the slopes of the tangent lines of the kinetic curves (Figure 11). A plot of R_2 vs T shown in Figure 14 is a typical rate temperature dependence curve of adsorption.[25] The Arrhenius plot (Figure 15) shows a linear relationship between $\ln R_2$ and 1/T. This

---

*From X-ray diffraction data (Table 9), the amounts of iron oxides in all samples slightly change with increasing time after the second stage; therefore, the weight losses due to the reduction of iron oxides are extremely low. For this reason, the weight increment W can be considered as the increment of carbon deposition so that the slopes of these curves can express the rates of carbon deposition.

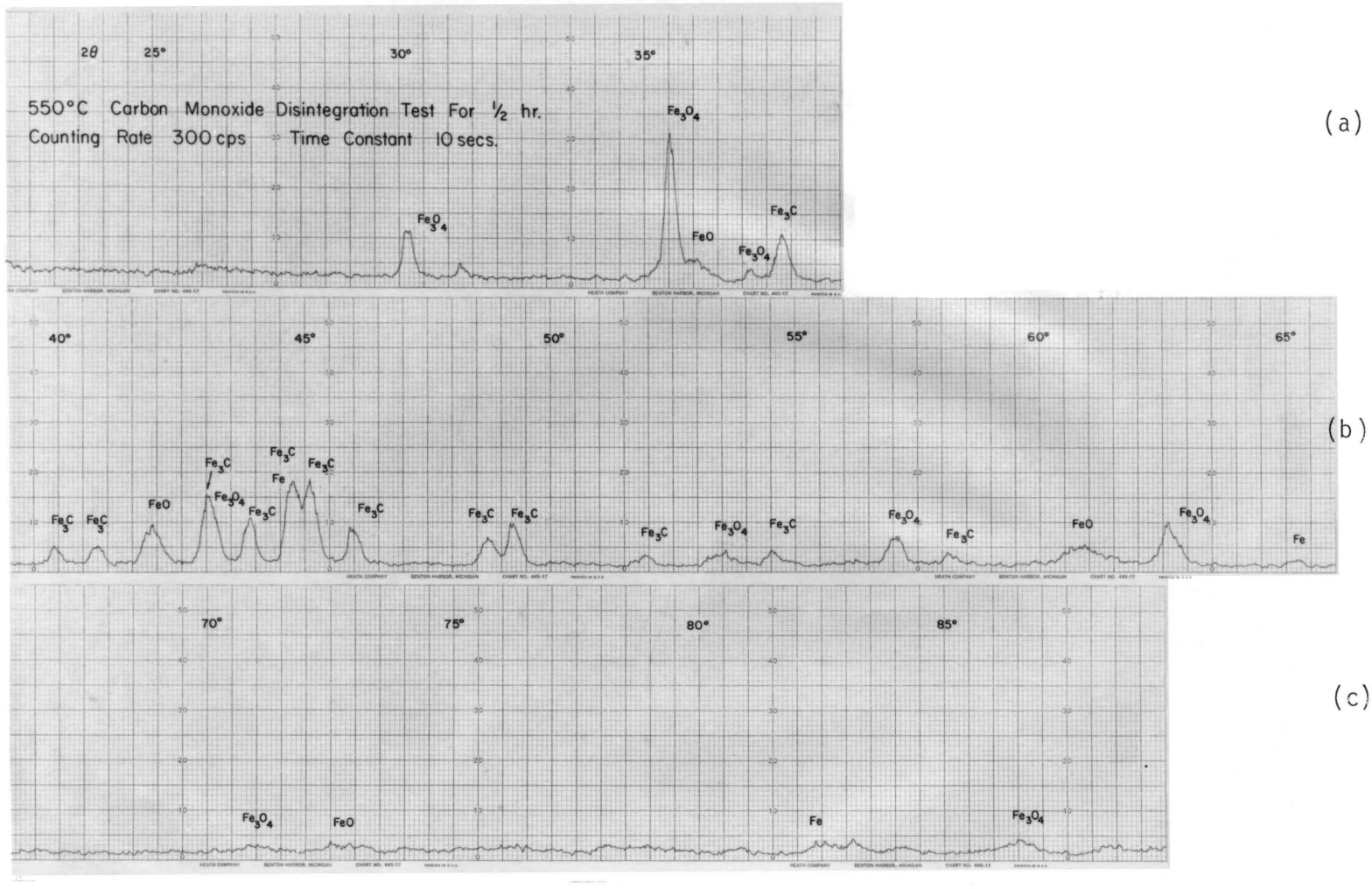

Fig. 13(a) X-ray Diffraction Pattern of Sample Without Carbon Deposit

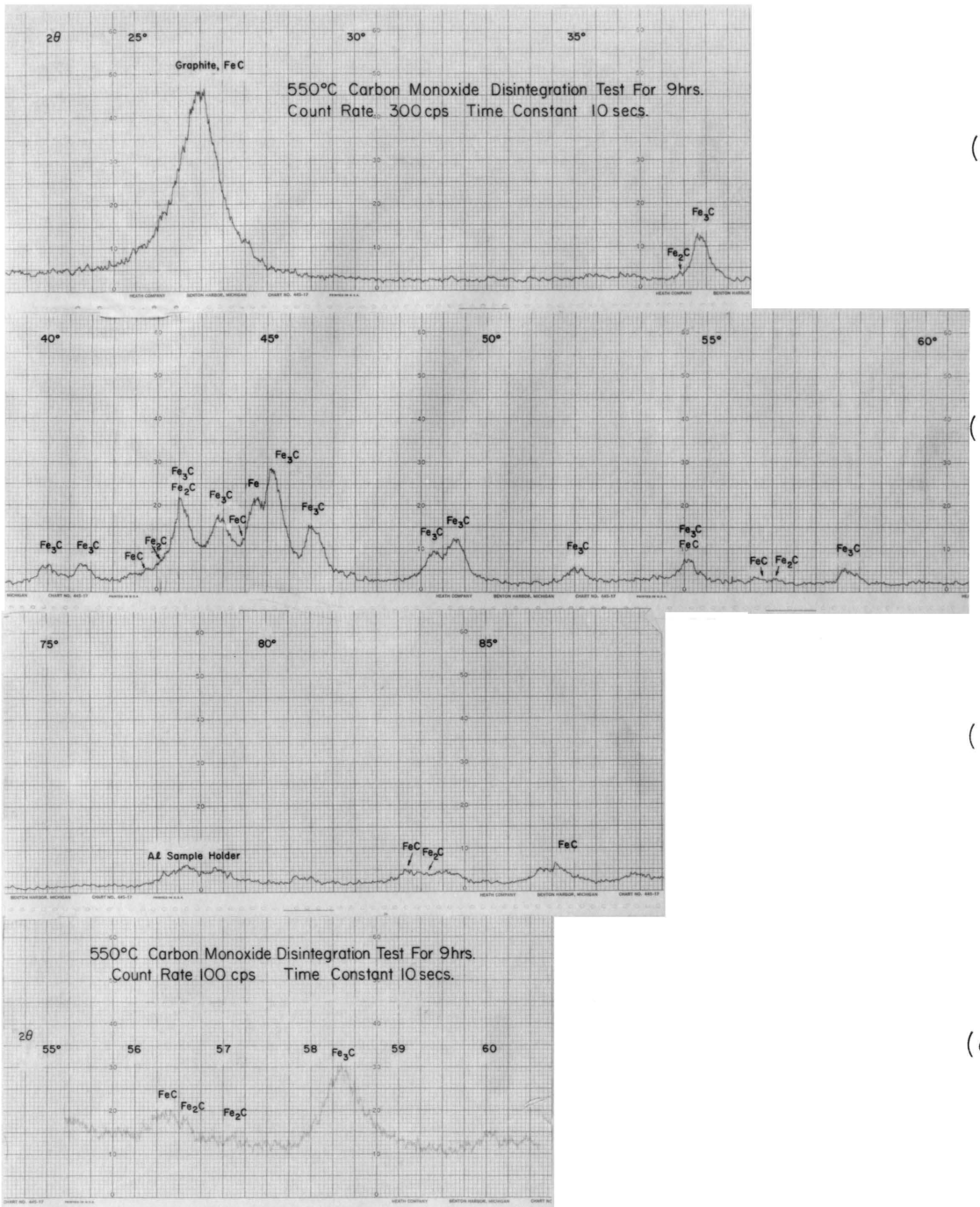

Fig. 13(b) X-ray Diffraction Pattern of Sample with Carbon Deposit (Notice the peaks of FeC and Fe_2C)

(a),(b),(c) ---Count Rate 300 cps, Scanning Rate 1/min.

(d) ----------Count Rate 100 cps, Scanning Rate 0.1/min.

Table 12. The Rates of Carbon Deposition at the Beginning of Second Stage.

Temperature ^{o}C	400	450	500	550	600	650	700
R_2 (g/gFe_2O_3 hr)	0.006	0.009	0.0125	0.017	0.015	0.007	0.004
ln R_2	-5.116	-4.711	-4.382	-4.075	-4.200	-4.962	-5.521

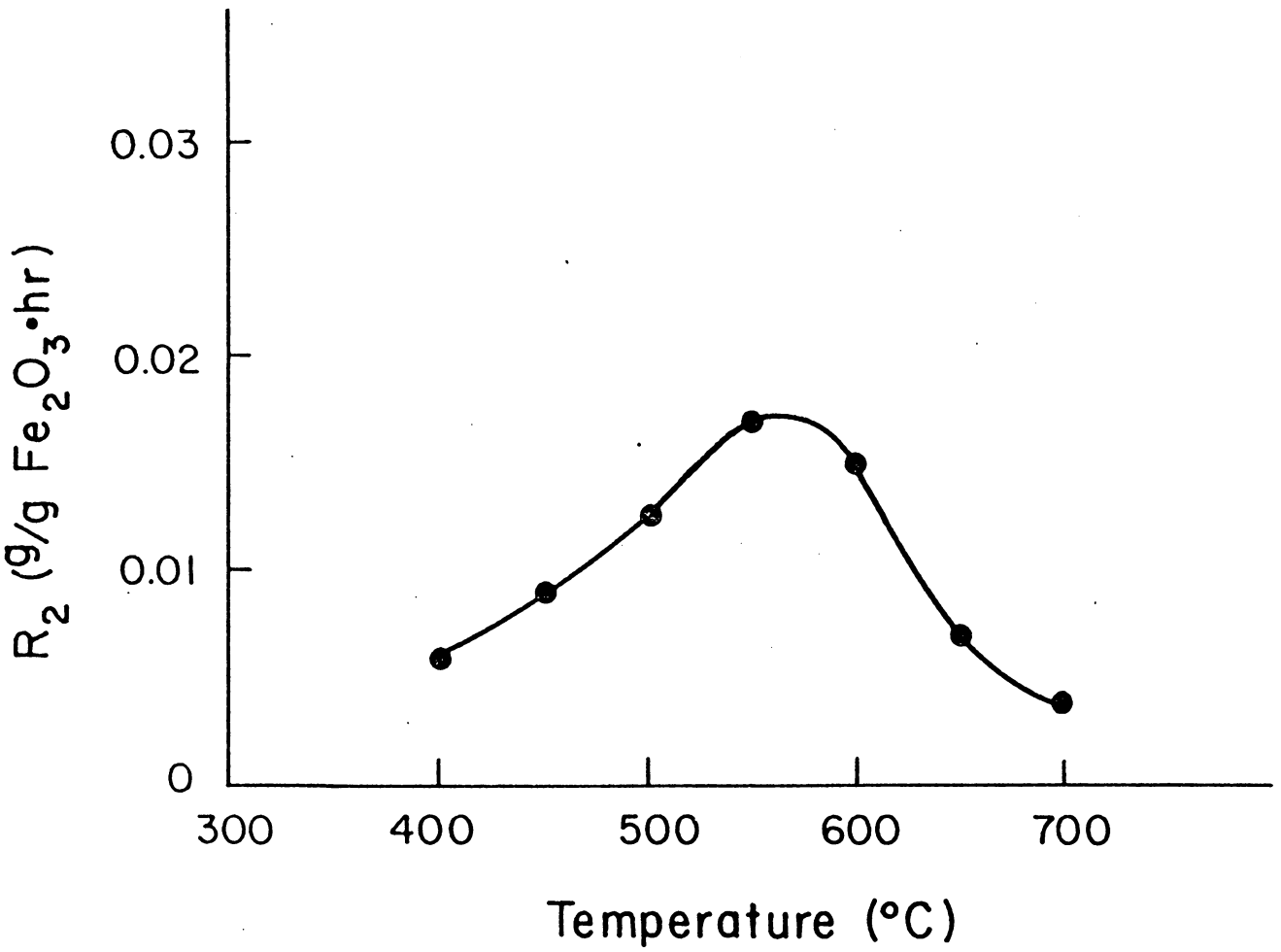

Fig. 14 Rates of Carbon Monoxide Disintegration at the Beginning of Second Stage

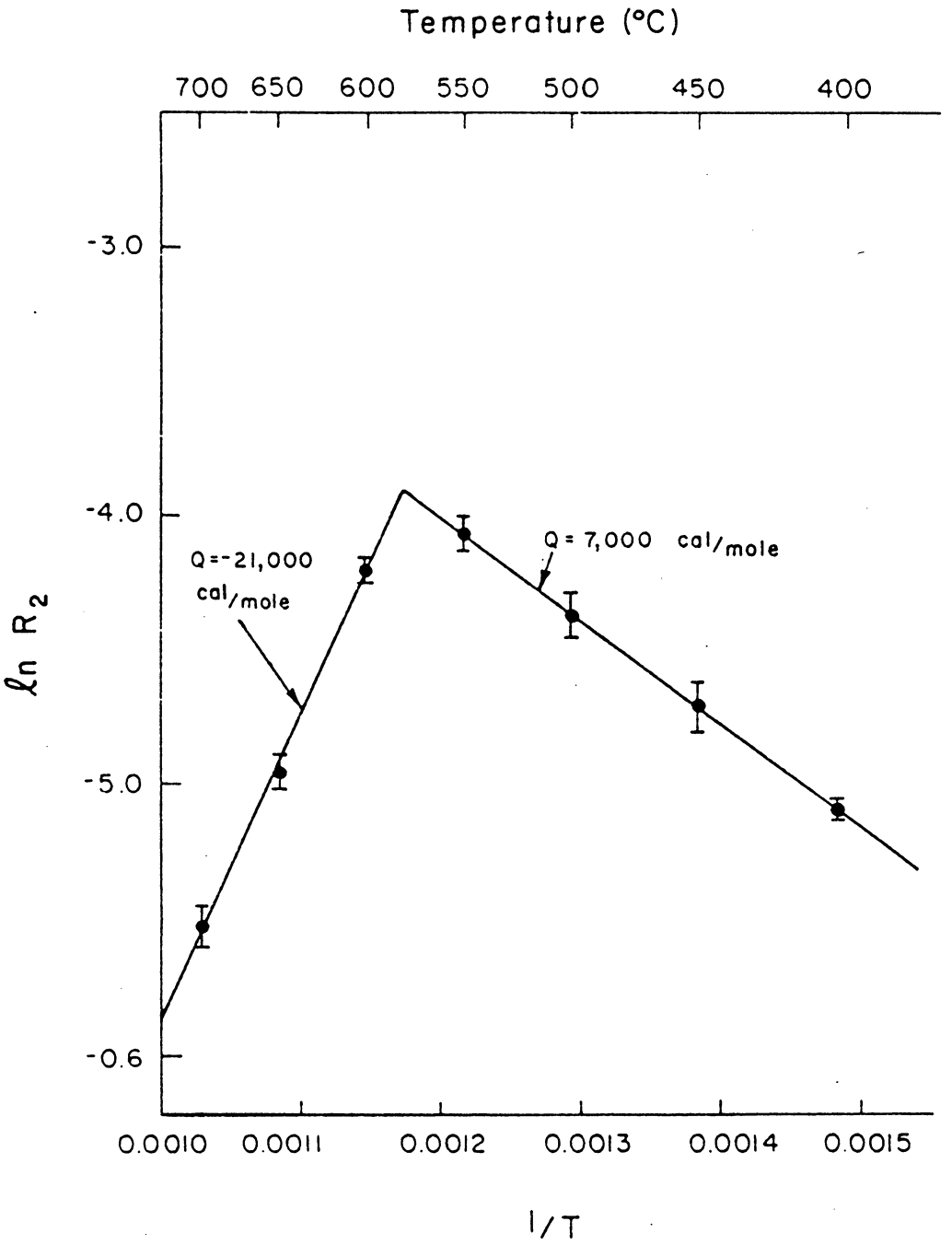

Fig. 15 $\ln R_2$ vs. 1/T at the Beginning of Second Stage

implies that the rate-controlling process may be a single step, e.g. at low temperature (higher 1/T) the activation energy calculated from the Arrhenius plot is 7,000 cal/mole, which is the same order of magnitude of the activation energy of chemisorption (1,000 - 10,000 cal/mole); therefore, the rate-controlling step may be chemisorption of carbon monoxide on reduced Fe atoms. A sudden drop in the Arrhenius curve at high temperatures means a negative activation energy is involved (Q = -21,000 cal/mole), which can be explained by (1) the degradation of the catalytic behavior * or (2) the reaction has a negative activation enthalpy $\Delta H^{\ddagger}$ (i.e. exothermic process) for the formation of activated complex $(Fe...CO)^{\ddagger}$.

By using the kinetic and X-ray diffraction data of the first and second stages (the reduction of α-Fe_2O_3 and the adsorption of carbon monoxide on reduced Fe atoms), reactions (2) - (4) have been substantiated. In order to express the possibility of reactions (5) - (8), i.e. the generation and decomposition of iron carbides, the discussion of the third stage is necessary.

---

*The degradation of the catalytic behavior is the result of decreasing the number of molecules striking the surface of the catalyst and shortening the residence time of molecules on the surface at elevated temperatures.

(C) Steady state stage. The characteristics of this stage are the following:

(a) There exists a linear relationship between weight increment ΔW and time, so that the rates of carbon deposition are constants. If the mechanism, reactions (2) - (8), is correct:

$$3Fe_2O_3 + CO = 2Fe_3O_4 + CO_2 \quad (2)$$

$$Fe_3O_4 + 4CO = 3Fe + 4CO_2 \quad (3)$$

$$Fe + CO \rightarrow (Fe...CO)^{\ddagger} \quad (4)$$

$$(Fe...CO)^{\ddagger} \rightarrow FeC + O \quad (5)$$

$$O \xrightarrow{CO} CO_2$$

$$2FeC \rightarrow Fe_2C + \text{Graphite} \quad (6)$$

$$3Fe_2C \rightarrow 2Fe_3C + \text{Graphite} \quad (7)$$

$$Fe_3C \rightarrow 3Fe + \text{Graphite} \quad (8)$$

then, the constant rate of carbon deposition means that during the third stage, the amounts of Fe, FeC, Fe_2C and Fe_3C phases are constant; i.e., at constant temperature the rate of generation and the rate of decomposition of these phases should be equal. This is confirmed by the X-ray diffraction data.

(b) The graph of $\ln R_3$ vs. 1/T, plotted by Table 13 and Figure 16, is a curve rather than a straight line (Figure 17); therefore, the mechanism for this stage must involve several complex steps, rather than a single reaction.

(c) Furthermore, the plot of $\ln R_3$ vs 1/T is convex. This implies that the rate of reaction is controlled by serial steps, as proposed in reactions (2) - (8). Some of the serial steps control the rate of reaction at low temperature, while others control the rate at high temperature. For example, at low temperature, the plot of $\ln R_3$ vs 1/T is nearly a straight line, so that activation energy can be calculated, which is about 7,000 cal/mole, the same value as the activation energy at the beginning of the second stage. This implies that chemisorption may be the predominant rate controlling process. At intermediate temperatures, the rate controlling steps may include the generation and decomposition of iron carbides FeC, Fe_2C and Fe_3C, in addition to the chemisorption of carbon monoxide. At high temperature, the decrease of the Arrhenius plot can be explained as the degradation of the catalytic behavior and negative activation enthalpy $\Delta H^{\ddagger}$ of the formation of the activated complex $(Fe...CO)^{\ddagger}$.

These kinetic characteristics confirm the serial reactions (5) - (8).

Table 13. The Rate of Carbon Deposition at Steady State Stage.

Temperature (^{o}C)	400	450	500	550	600	650	700
R_3 ($g/gFe_2O_3 \cdot hr$)	0.2	0.29	0.35	0.375	0.34	0.275	0.15
$\ln R_3$	-1.6094	-1.2379	-1.0498	-0.9808	-1.0788	-1.2910	-1.8971

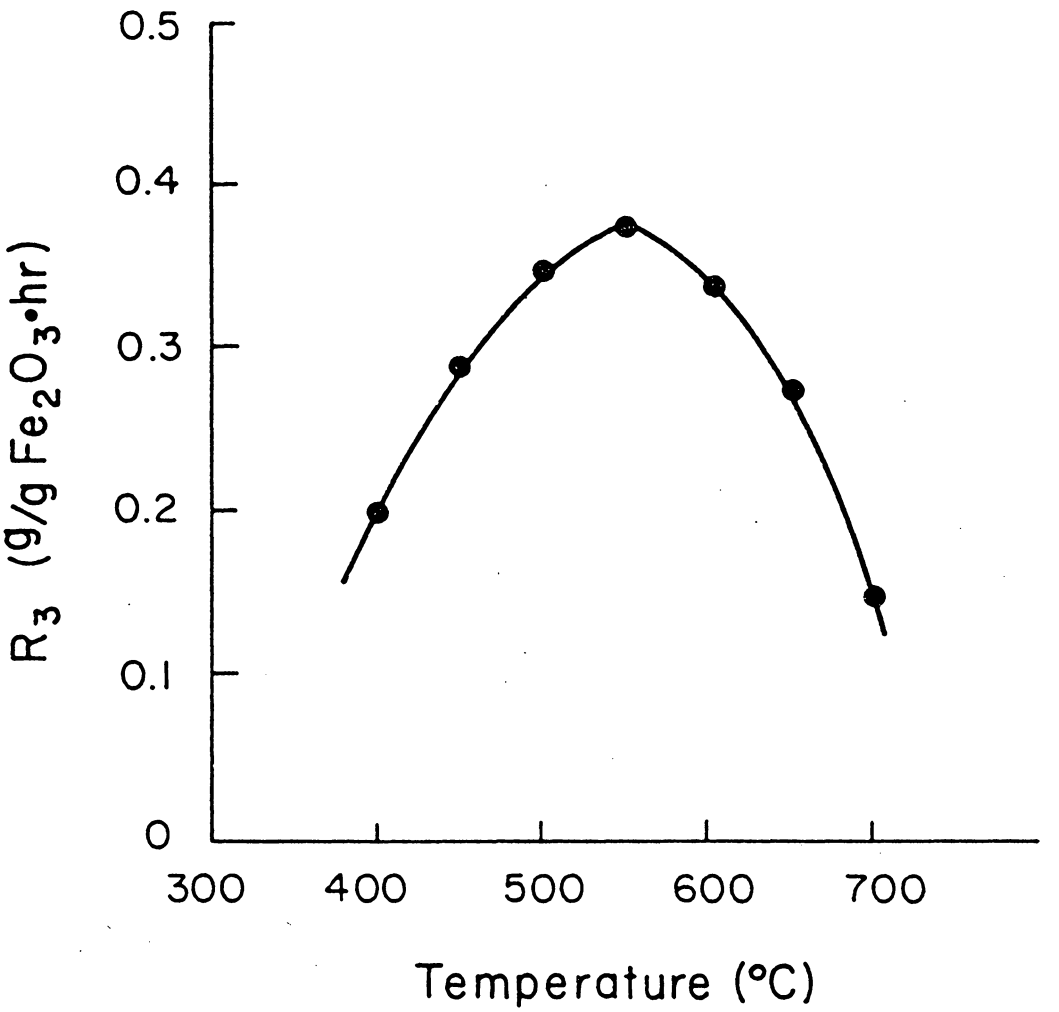

Fig. 16 Rates of Carbon Deposition vs. Temperature at Steady State Stage

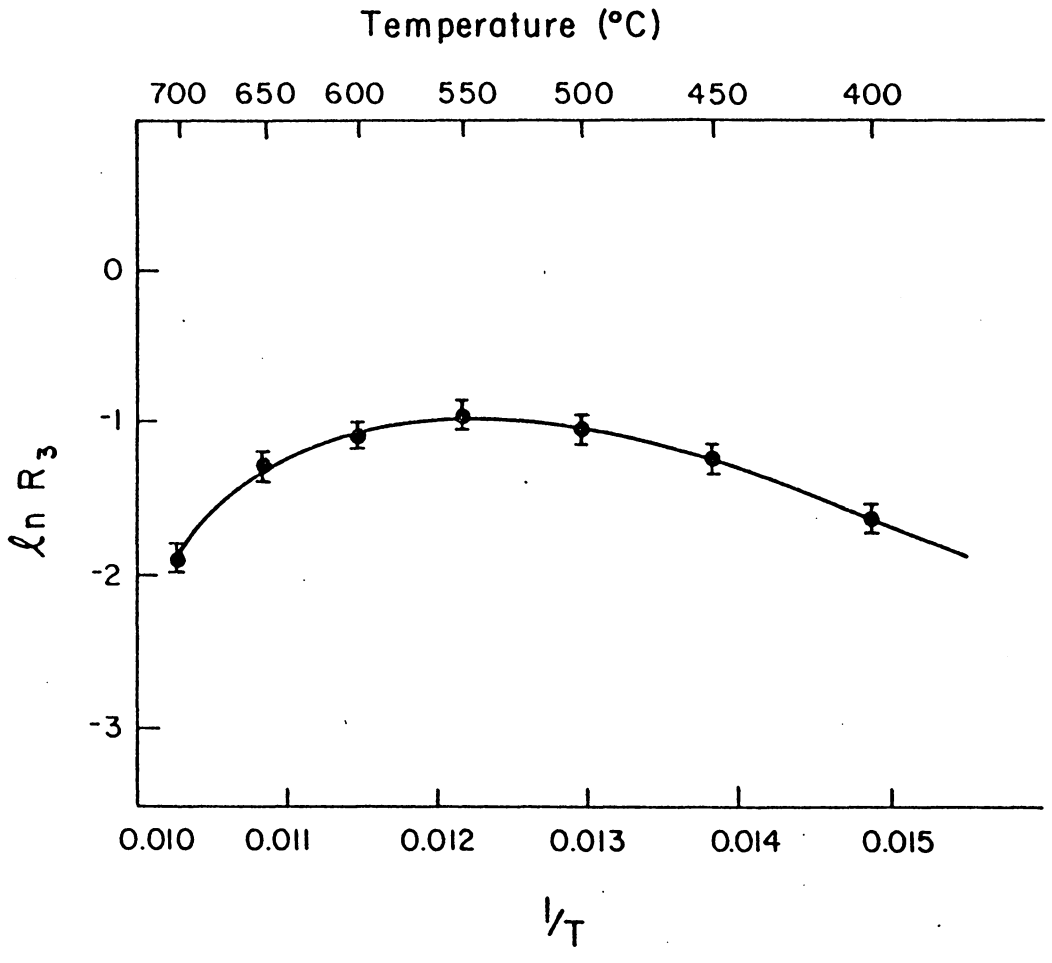

Fig. 17 Plot of $\ln R_3$ vs. 1/T at Steady State Stage

IV. CONCLUSION

(1) Among the iron phases tested, α-Fe_2O_3 has the most catalytic effect on carbon monoxide dissociation, while α-Fe crystal, iron sulfides and carbon do not have such effect.

(2) Active Fe atom generated from the reduction of iron oxides is the actual catalyst for the Boudouard reaction. The catalytic process which is confirmed by thermodynamical calculations, kinetic data and x-ray diffraction data can be written as the following:

$$3\ Fe_2O_3 + CO = 2\ Fe_3O_4 + CO_2$$

$$Fe_3O_4 + 4\ CO = 3\ Fe + 4\ CO_2$$

and $T > 500°C$

$$Fe_2O_3 + CO = 2\ FeO + CO_2$$

$$FeO + CO = Fe + CO_2$$

due to the strong covalent bonds between the active Fe atom and carbon and the larger surface area of porous structure obtained from the reduction of oxides, carbon monoxide is adsorbed and disintegrated.

$$6\ Fe + 12\ CO = 6\ FeC + 6\ CO_2$$

$$6\ FeC \rightarrow 3\ Fe_2C + 3\ C$$

$$3\ Fe_2C \rightarrow 2\ Fe_3C + C$$

$$2\ Fe_3C \rightarrow 6\ Fe + 2\ C$$

(3) From the calculations of activation energy, it is known that due to the formation of porous structure during the reduction of iron oxides, chemisorption and the decomposition of iron carbides rather than diffusion are the rate controlling processes for carbon deposition, if the sample is α- Fe_2O_3.

REFERENCES

(1) T. K. Baker and P. S. Harris, Chemistry and Physics of Carbon, V. 14, edited by P. L. Walker, Jr. and P. A. Thrower, p. 83-165.

(2) P. L. Walker, Jr. and J. M. Thomas, Carbon 8, 103 (1970).

(3) G. C. Bond, Catalysis by metals, Chapter 3, Academic Press, 1962.

(4) M. Niwa and J. H. Lunsford, J. Catal., 75, 302-313 (1982).

(5) V. J. Kehrer and H. Leidheiser, J. Phys. Chem. 58, 550 (1954).

(6) T. F. Berry, R. N. Ames and R. B. Snow, J. Amer. Cer. Soc., 39, 308-318 (1956).

(7) L. A. Haas, S. E. Khalafalla and P. L. Weston, Jr., U.S. Bureau of Mines, Rep. Invest. 7064 (1968).

(8) P. L. Walker, Jr., J. F. Rakszawski and G. R. Imperial, J. Phys. Chem., 63, 140 (1959).

(9) A. Sacco, Jr. and J. C. Caulmare, Coke Formation on Metal Surfaces, p. 177-192, edited by L. F. Albright and R. T. K. Baker, American Chemical Society, 1982.

(10) H. H. Podgurski, J. T. Kummer, T. W. Dewitt and P. H. Emmett, J. Am. Ceram. Soc., 72, 5382 (1950).

(11) G. D. Renshaw, C. Roscoe and P. L. Walker, Jr., J. Catal., 18, 164-183 (1970).

(12) C. Martin, Thesis, Virginia Polytechnic Institute and State University, 1982.

(13) A. Clark, The Theory of Adsorption and Catalysis, Chapters 7 and 15, Academic Press, 1970.

(14) G. M. Schwab, Semiconductor Surface Physics, p. 283, U. Penn Press, Philadelphia (1957).

(15) E. T. Turkdogan and J. V. Vinters, Metall. Trans. 2, 3175 (1971).

(16) R. L. Dekock and H. B. Gray, Chemical Structure and Bonding, Chapters 2 and 4, The Benjamin/Cummings Publishing Co., 1980.

(17) G. Eriksson. Acta Chemica Scandinavica, 25, 2651-2658 (1971).

(18) G. Eriksson. Chemica Scripta, 8, 100-103 (1975).

(19) T. M. Besmann. Oak Ridge Laboratory, April 1977.

(20) E. T. Turkdogan, Physical Chemistry of High Temperature Technology, Academic Press, 1980.

(21) J. Chipman, Metall. Trans., 3, 55-64 (1972).

(22) B. D. Cullity, Elements of X-ray diffraction, Addison-Wesley Publishing Company, Inc., Chapter 14, 1967.

(23) W. B. Pearson, Handbook of Lattice spacings and Structures of Metals, V. 2, Pergamon Press Ltd., 1967.

(24) L. J. E. Hofer, Catalysis, IV, p. 411-416, Edited by P. H. Emmett, Reinhold Publishing Corporation, 1956.

(25) J. W. Moore and R. G. Pearson, Kinetics and Mechanism, Chapter 2, John Wiley and Sons, Inc., 1981.

APPENDIX 1

SOLGASMIX Computer Program

In order to calculate the mole fraction of each species present in a equilibrium system, the key point of SOLGASMIX program is minimizing the Gibbs free energy of a system.

There are three basic equations for SOLGASMIX program.

(1) The total Gibbs free energy of the system

$$G = \sum_i x_i g_i \qquad \text{(A1-1)}$$

$$g_i = g_i^{\circ} + RT \ln a_i \qquad \text{(A1-2)}$$

where x_i —— mole number of a speicies

g_i —— chemical potential of a species

g_i° —— chemical potential of a species at 1 atm

a_i —— activity of a species

For gaseous species

$$a_i = p_i = \frac{x_i}{X} P \qquad \text{(A1-3)}$$

where p_i —— partial pressure of i^{th} species in gas

P —— total pressure of the gaseous phase

X —— total mole number of gaseous phase

For condensed species

$$a_i = 1 \tag{A1-4}$$

(2) Mass balance constraints, which can be written as

$$\sum_{i=1}^{m} (A_{ij})_g (\chi_i)_g + \sum_{i=1}^{s} (A_{ij})_c (\chi_i)_c = b_j \tag{A1-5}$$

$$(j = 1, 2, \ldots l)$$

where b_j —— total moles of j^{th} element

l —— total number of elements in the system

$(A_{ij})g$, $(A_{ij})_c$ —— numbers of the atoms of j^{th} element in a molecule of i^{th} species of gaseous and condensed phase, respectively.

(3) A search for a minimum value of Gibbs free energy G, subject to the mass balance relation (A1-5). By using Lagrange's method of indetermined multipliers, the following equations are obtained

$$(g_i^o/RT)_g + \ln p + \ln(\chi_{ig}/X) - \sum_{j=1}^{l} \pi_j (A_{ij})_g = 0 \tag{A1-6}$$

(For gaseous phase), $(i = 1, 2, \ldots m)$

$$(g_i^o/RT)_c - \sum_{j=1}^{l} \pi_j (A_{ij})_c = 0 \tag{A1-7}$$

(For condensed phase) $(i = 1, 2, \ldots s)$

where π_j - Lagrangian multipliers

Equations (A1-5) and (A1-6) are expanded in a Taylor series about an arbitrary point (y_{1g}, y_{2g}, ... y_{mg}, y_{1c}, y_{2c} ... y_{sc}), neglecting terms involving derivatives of second and higher orders. After rearranging, the following equations are obtained

$$\sum_{j=1}^{l} \pi_j \sum_{i=1}^{m} y_{ig}(A_{ij})_g = \sum_{i=1}^{m} \left\{ y_{ig} \left[(g_i^o/RT)_g + \ln p + \ln(y_{ig}/Y) \right] \right\} \qquad \text{(A1-8)}$$

where $$Y = \sum_{i=1}^{m} y_{ip}$$

$$\sum_{k=1}^{l} \pi_k \left[\sum_{i=1}^{m} (A_{ij})_g (A_{ik})_g y_{ig} \right] + \left[\left(\frac{x}{y} - 1\right) \right] \sum_{i=1}^{m} (A_{ij})_g (y_{ig})$$

$$+ \sum_{i=1}^{s} (A_{ij})_c \chi_{ic} = \sum_{i=1}^{m} (A_{ij})_g \left[y_{ig} (g_i^o/RT)_g + \ln p + \ln(y_{ig}/Y) \right] - C_j$$

$$(j, k = 1, 2, 3, \ldots l) \qquad \text{(A1-9)}$$

where C_j - a correction term in case where the initial guess of mole numbers does not satisfy the mass balance relations (A1-5), $C = \sum_{i=1}^{m} (A_{ij})_g y_{ig}$.

Now, the (l + s + 1) equations (A1-7), (A1-8) and (A1-9) can solve l + s + 1 unknowns $\pi_j (j = 1, 2 \ldots l)$, x_{ic} (i = 1, 2,...s) and $\frac{x}{Y} - 1$ by computer. After obtaining $\frac{x}{Y}$, π_j and x_{ic}, x_{ig} can be calculated by

$$\chi_{ig} = -y_{ig}\,[(g_i^0/RT)_g + \ln p + \ln (y_{ig}/Y)] + y_{ig}\,[(\tfrac{X}{Y})_g + \sum_{j=1}^{l} (A_{ij})_g]$$

$$(i = 1, 2, \ldots m) \qquad \text{(A1-10)}$$

Besmann[19] developed this program to involve condensed phase solutions in this program and made this program more useful.

Table A1-1 is an example of the output of a equilibrium Fe-CO system at 1 atom, 500°C.

An important advantage of SOLGASMIX program is its simplicity. All we need to run this program is a list of all species including reactants and possible products and their basic thermodynamical data g°.

There are two ways to express g°

$$\text{a)}\quad g^0/RT = \Delta_f G^0/RT \qquad \text{(A1-11)}$$

or

$$\text{b)}\quad g^0/RT = \frac{1}{R}\left(\frac{G^0-H^0_{298}}{T}\right) + \Delta_f H^0_{298}/RT \qquad \text{(A1-12)}$$

where $\Delta_f G$ —— Gibbs free energy of formation

$\frac{G^0-H^0_{298}}{T}$ —— free energy function

$\Delta_f H_{298}$ —— heat of formation at 298 K

Table A1-1. An Example of Output of an Equilibrium Fe-CO System.

CO Disintegration Calculation

T = 773.00 K
P = 1.000D+00 ATM

	X*/Mole	Y/Mole	P/ATM	Activity
CO	0.00000D+00	0.25258D-01	0.66591D-01	0.66591D-01
CO_2	0.00000D+00	0.35404D+00	0.93341D+00	0.93341D+00
O_2	0.50000D+00	0.63923D-27	0.16853D-26	0.16853D-26
		Mole Fraction		
Fe(S)	0.00000D+00	0.00000D+00	0.00000D+00	0.00000D+00
C(s)	0.00000D+00	0.00000D+00	0.00000D+00	0.00000D+00
Fe	0.20000D+00	0.00000D+00		
Fe_2O_3	0.00000D+00	0.00000D+00		
Fe_3O_4	0.00000D+00	0.66667D-01		
FeO	0.00000D+00	0.00000D+00		
Fe_2C	0.00000D+00	0.00000D+00		
Fe_3C	0.00000D+00	0.00000D+00		
C	0.10000D+01	0.62070D+00		

The vita has been removed from the scanned document